JOURNAL OF PETROLOGY | VOLUME 0 | NUMBER 0 | PAGES 1–53 | 2011 | doi:10.1093/petrology/egq088
Journal of Petrology Advance Access published January 12, 2011

Differentiation of Tholeiitic Basalt to A-Type Granite in the Sept Iles Layered Intrusion, Canada

OLIVIER NAMUR[1]*, BERNARD CHARLIER[1], MICHAEL J. TOPLIS[2], MICHAEL D. HIGGINS[3], VERONIQUE HOUNSELL[3], JEAN-PAUL LIÉGEOIS[4] AND JACQUELINE VANDER AUWERA[1]

[1]UR PÉTROLOGIE ET GÉOCHIMIE ENDOGÈNES, DÉPARTEMENT DE GÉOLOGIE, UNIVERSITÉ DE LIÈGE, LIÈGE, BELGIUM

[2]UMR 5277 – CNRS (IRAP), OBSERVATOIRE MIDI-PYRÉNÉES, PAUL SABATIER UNIVERSITY, 14 AVENUE E. BELIN, F-31400, TOULOUSE, FRANCE

[3]SCIENCES DE LA TERRE, UNIVERSITÉ DU QUÉBEC À CHICOUTIMI, CHICOUTIMI, QUEBEC G7H 2B1, CANADA

[4]ISOTOPE GEOLOGY, ROYAL MUSEUM FOR CENTRAL AFRICA, TERVUREN, BELGIUM

RECEIVED MARCH 18, 2010; ACCEPTED NOVEMBER 26, 2010

The undeformed 564 Ma Sept Iles layered intrusion (Quebec, Canada) is a large igneous body of c. *20 000 km^3. From the base to the top, it consists of a Layered Series dominated by troctolite and gabbro, an anorthositic Upper Border Series and a dominantly granitic Upper Series. The parent magma of the Layered Series is inferred to be an iron-rich tholeiitic basalt (48 wt % SiO_2; 15 wt % FeO_t). Whole-rock compositions from the chilled margin, dykes cross-cutting the Layered Series and silicic rocks from the Upper Series display continuous major and trace element geochemical trends ranging from basalts to ferroan metaluminous A-type granites (77 wt % SiO_2). Initial $^{143}Nd/^{144}Nd$ (0·51201–0·51207) and $^{87}Sr/^{86}Sr$ (0·70353–0·70548) indicate a juvenile-mantle source and minimal contamination by old crust (1–2%) during crystallization. Geochemical modeling, using the MELTS thermodynamic calculator combined with equations predicting mineral–melt equilibria from experiments on tholeiitic basalts, indicate that basaltic to monzonitic melt compositions are in equilibrium with the troctolites and gabbros of the Layered Series. Fe–Ti oxides saturate early in the Layered Series, after 14% fractionation of plagioclase–olivine cumulates. Further fractionation of Fe–Ti oxide-bearing gabbros drives the residual liquids toward silica enrichment and iron depletion. Major and trace element modeling indicates that the A-type granites from the Upper Series were produced by protracted fractional crystallization of an iron-rich basaltic parent magma, at a fraction of residual liquid of only 8%. The observed relative volumes of mafic cumulates and silicic rocks in the intrusion are in agreement with the calculations. Most of the intermediate compositions correspond to magmatic mafic enclave-bearing granitoids and display geochemical evidence of hybridization. Intermediate compositions produced by fractional crystallization are scarce and a Daly gap occurs from 57 to 67 wt % SiO_2. This gap could result either from the fractional crystallization process or from silicate–liquid immiscibility during that compositional interval.*

KEY WORDS: *liquid line of descent; fractional crystallization; tholeiitic magma; MELTS; least-squares modeling; ferroan (A-type) granitoid; layered intrusion*

INTRODUCTION

Tholeiitic basalts from many tectonic environments are commonly associated with silica-rich rocks (Fig. 1; e.g. Carmichael, 1964; Hildreth *et al.*, 1991; Geist *et al.*, 1995; Naumann *et al.*, 2002; McCurry *et al.*, 2008) that are usually interpreted as being the crystallization products of evolved residual liquids resulting from protracted fractionation of the parental basic magma. These high

*Corresponding author. E-mail: onamur@ulg.ac.be

© The Author 2011. Published by Oxford University Press. All rights reserved. For Permissions, please e-mail: journals.permissions@oup.com

Downloaded from petrology.oxfordjournals.org at Bibliotheque Fac de Medecine on January 12, 2011

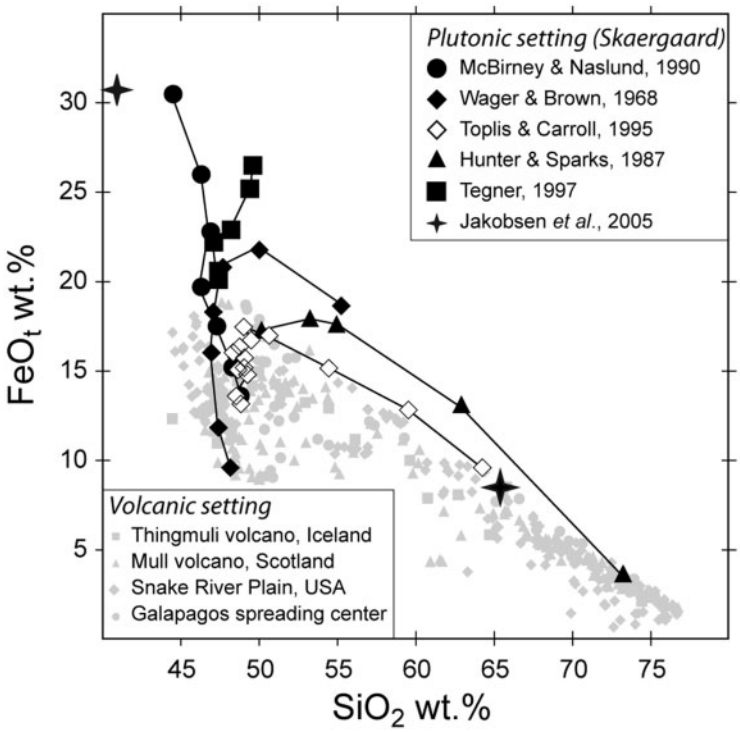

Fig. 1. FeO_t vs SiO_2 diagram showing proposed liquid lines of descent for the Skaergaard layered intrusion and for a number of tholeiitic volcanic suites. Stars represent the average composition of immiscible Fe-rich and Si-rich melt inclusions found in Skaergaard cumulus apatites by Jakobsen *et al.* (2005). Data sources are as follows: Snake River Plain: Tilley & Thompson (1970), Leeman *et al.* (1976), Leeman & Vitaliano (1976), Stout & Nicholls (1977), Honjo & Leeman (1987), Andrews *et al.* (2008), Bonnichsen *et al.* (2008), Brueseke *et al.* (2008), McCurry *et al.* (2008); Thingmuli: Carmichael (1964); Galapagos: Byerly *et al.* (1976), Byerly (1980); Mull: Walsh *et al.* (1979), Kerr *et al.* (1999).

Fe-number [molar FeO/(FeO + MgO)] silicic rocks, if rich in incompatible elements and K_2O, are referred to as A-type magmas (Loiselle & Wones, 1979; Turner *et al.*, 1992; Bonin, 2007). In plutonic settings, the liquid line of descent of tholeiitic basalts is more difficult to identify owing to the scarcity of samples representative of preserved melt compositions. It is thus inferred indirectly from experimental liquid compositions or from mass-balance calculations based on cumulate rock chemistry. These indirect approaches do not provide an unambiguous result, as exemplified by the lively discussions concerning the differentiation of the ferrobasaltic Skaergaard layered intrusion, East Greenland (Wager & Deer, 1939; Wager & Brown, 1968; Hunter & Sparks, 1987; McBirney & Naslund, 1990; Toplis & Carroll, 1996; Tegner, 1997; Thy *et al.*, 2006, 2009). The disagreement mostly concerns the evolution of Fe–Ti oxide saturated melts, for which two differentiation paths are proposed (Fig. 1). On the one hand, residual liquids are interpreted to show iron depletion and silica enrichment after the saturation of Fe–Ti oxide minerals (Wager & Brown, 1968; Hunter & Sparks, 1987; Morse, 1990; Toplis & Carroll, 1995, 1996). On the other hand, some workers have suggested that the iron content of the residual liquids increases continuously during differentiation with no significant silica enrichment, even after the saturation of Fe–Ti oxide minerals (Brooks & Nielsen, 1990; McBirney & Naslund, 1990; Tegner, 1997; Thy *et al.*, 2009). A part of the problem in the case of the Skaergaard is that there is no significant volume of silica-rich rocks, but the geometry of the intrusion does not exclude their former presence at a now eroded level.

The Sept Iles layered intrusion (Quebec, Canada) displays a well-preserved association of layered troctolites, gabbros, anorthosites and A-type granites (Higgins, 2005), which crystallized from a tholeiitic parent magma (Namur *et al.*, 2010). A detailed study of the Layered Series (see below) by Namur *et al.* (2010) has constrained the sequence of crystallization and the timing of cumulus phase saturation. This intrusion is thus appropriate to further document the liquid line of descent of tholeiitic basalts crystallizing in a plutonic environment.

In this study, we present new whole-rock major and trace element as well as Sr and Nd isotopic data on fine- to medium-grained rocks coming from the chilled margin of the intrusion, from dykes cross-cutting the Layered Series and from silicic rocks located in the upper part of the intrusion. Petrographic and geochemical data suggest

Downloaded from petrology.oxfordjournals.org at Bibliotheque Fac de Medecine on January 12, 2011

that these rocks represent liquids with compositions evolving from tholeiitic basalt to monzonite and A-type granite. These data are used to assess to what extent a single consistent liquid line of descent may be defined for the Sept Iles layered intrusion as a whole. We first review the most important results of previous studies of the Sept Iles layered intrusion. Then, the MELTS algorithm (Ghiorso & Sack, 1995) is used to show that liquid compositions ranging from 47 to 57 wt % SiO_2 are in equilibrium with the rocks of the Layered Series. Based on least-squares modeling, we also show that fractional crystallization is the dominant process in producing the most evolved lithologies. Finally, we show that intermediate compositions are scarce along the liquid line of descent, and we suggest that this paucity could result either from the fractional crystallization process itself or from silicate liquid immiscibility. All these results, combined with detailed field relationships, allow us to propose large-scale magma chamber processes that ultimately led to the development of silicic magmas. The silica enrichment of the tholeiitic parental magma that occurred after the saturation of Fe–Ti oxide minerals is also used to discuss the origin of silicic magmas in layered intrusions in general and their relation to the cumulate rocks.

THE SEPT ILES INTRUSIVE SUITE

The Sept Iles intrusive suite (SIIS) is located on the north shore of the St Lawrence River, about 500 km to the NE of Quebec City. It is unmetamorphosed and undeformed, and was emplaced at 564 ± 4 Ma (U–Pb on zircons; Higgins & van Breemen, 1998) into high-grade gneisses of the Grenville Province (Davidson, 1995; Rivers, 2008). It belongs to a widespread magmatic phase related to the formation of the St Lawrence rift system and corresponding to the initial stages of opening of the Iapetus ocean (Kumarapeli & Saull, 1966; Higgins & van Breemen, 1998). Higgins (2005) suggested that the igneous activity in the Sept Iles area started with the eruption of flood basalts, which are now completely eroded, and that the SIIS was emplaced at the unconformity between these basalts and the surface of the Canadian Shield.

The SIIS is a lopolith with a dinner plate-like shape and a diameter of *c.* 80 km, a maximum thickness of *c.* 6 km and an estimated magma volume of *c.* 20 000 km^3 (Loncarevic *et al.*, 1990). Most of the SIIS is hidden beneath the St Lawrence River and Paleozoic sedimentary rocks. The northwestern part of the intrusive suite crops out around the Sept Iles peninsula and on the islands of the Sept Iles archipelago (Fig. 2). Higgins (2005) considered that the SIIS is composed of a number of intrusive units, of which the Sept Iles layered intrusion is by far the largest. Other intrusive components are represented by a composite sill named Pointe du Criard and a series of dolerite dykes [referred to as diabase dykes by Higgins (2005)] that belongs to the Late Gabbro intrusion.

THE SEPT ILES LAYERED INTRUSION: PREVIOUS WORK

The Sept Iles layered intrusion is divided into three series: the Layered Series, the Upper Border Series and the Upper Series (Cimon, 1998; Higgins, 2005). A Border Zone of dolerite (at least 20 m thick) separates the Grenvillian country-rocks from the intrusion. Based on whole-rock compositions from the Border Zone, calculations with the MELTS thermodynamic calculator and by analogy with other well-studied mafic layered intrusions, Namur *et al.* (2010) concluded that this zone represents a chilled margin against the relatively cold country-rocks (Wager & Brown, 1968; Hoover, 1989). Based on these data, Namur *et al.* (2010) proposed that the Sept Iles parent magma was a tholeiitic basalt (48 wt % SiO_2; 15 wt % FeO_t; Table 1) similar to that of the Skaergaard intrusion, but slightly richer in FeO_t (Hoover, 1989; Nielsen, 2004).

The 4700 m thick Layered Series is made up of an alternation of troctolite (po-C; Table 2; classification following Irvine, 1982), Fe–Ti oxide-bearing troctolite (pomi-C), and layered gabbro (pomic-C; pmic-C; pomica-C; Fig. 3a). The sequence of crystallization in the Layered Series is plagioclase + olivine, followed by the successive appearance of magnetite and ilmenite, then Ca-rich pyroxene and finally apatite as cumulus phases. Cumulus olivine disappears in the most Ca-rich pyroxene-rich rocks (pmic-C cumulates). The Layered Series is subdivided into three megacyclic units (MCU; Table 2; Fig. 2b), the base of each corresponding to a compositional reversal to more primitive mineral compositions as a result of a significant influx of new undifferentiated magma (Namur *et al.*, 2010). Each megacyclic unit displays the same stratigraphic succession of liquidus assemblages and mineral compositions (Table 2). Based on the simultaneous appearance of cumulus magnetite and ilmenite and by comparison with the experimental data of Toplis & Carroll (1995), Namur *et al.* (2010) estimated that the Layered Series mostly crystallized under oxygen fugacity conditions (fO_2) close to the FMQ (Fayalite–Magnetite–Quartz) buffer. The Layered Series is cross-cut by many centimetre- to decimetre-scale dykes of basaltic to intermediate composition.

The *c.* 100–500 m thick Upper Border Series is composed of anorthosite with minor leucotroctolite and leucogabbro. Higgins (2005) suggested that it was formed by flotation of plagioclase from the Layered Series toward the top of the magma chamber. In contrast to the Upper Border Series unit in the Skaergaard intrusion, it is of note that these rocks are not interpreted to result from downward crystallization from the roof towards the center of the

Downloaded from petrology.oxfordjournals.org at Bibliotheque Fac de Medecine on January 12, 2011

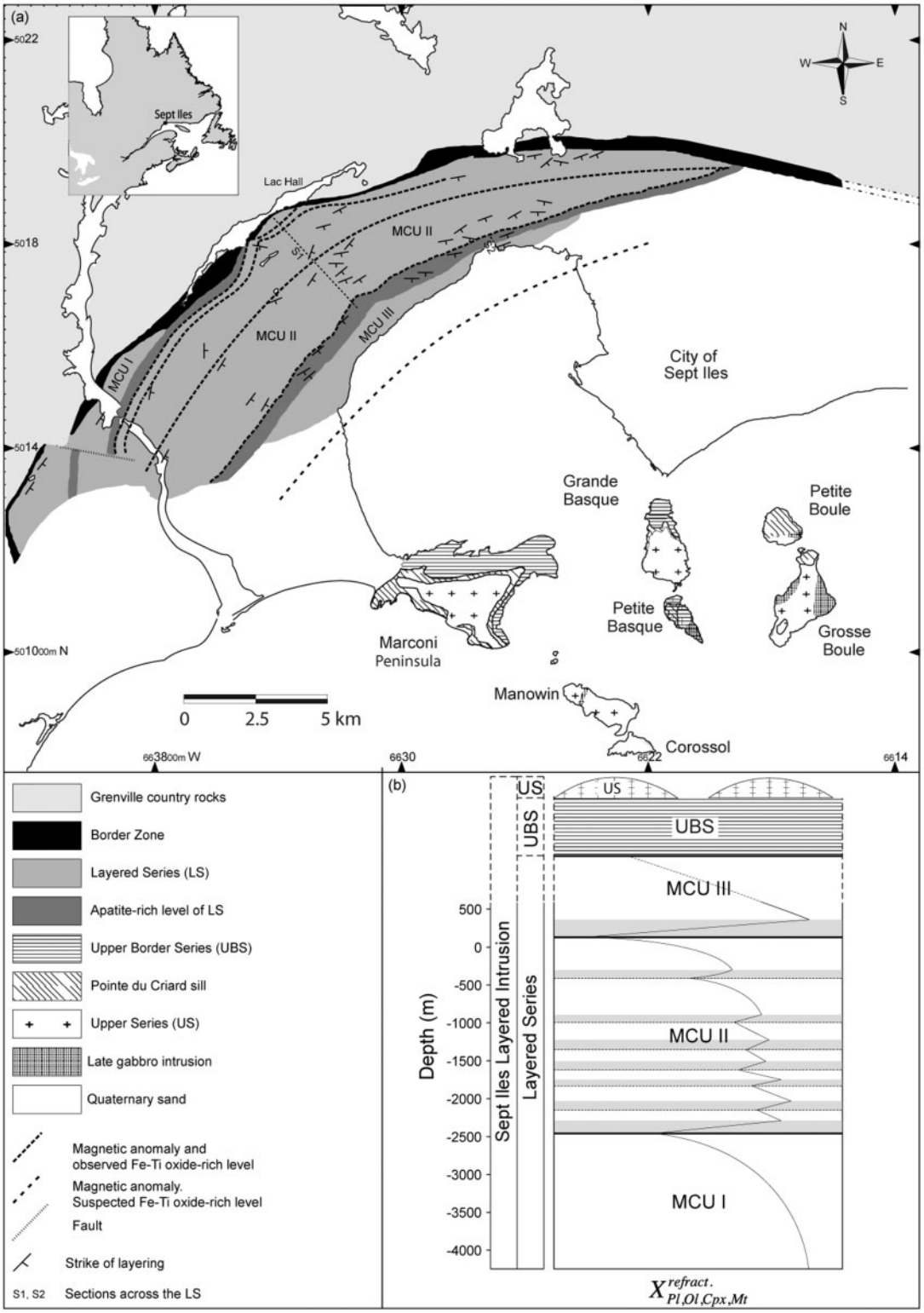

Fig. 2. (a) Geological map of the Sept Iles intrusive suite adapted from Higgins (2005). Inset map shows the location of the map area in the southeastern part of Canada. (b) Schematic stratigraphic column of the Sept Iles layered intrusion with evolution of mineral composition in the Layered Series ($X^{refract}$ is the An content of plagioclase, Fo content of olivine, Mg-number of clinopyroxene and Cr content of magnetite). Horizontal dashed lines in MCU II represent the end of successive small differentiation cycles. Horizontal grey bands in MCU II and at the bottom of MCU III represent stratigraphic intervals with reverse evolution of mineral compositions as a result of magma chamber replenishments by undifferentiated basaltic magma. MCU, megacyclic unit.

Downloaded from petrology.oxfordjournals.org at Bibliotheque Fac de Medecine on January 12, 2011

Table 1: Parent magma compositions of the Sept Iles Layered Series

Sample:	05-45	07-01	07-48	07-180	Average
Location:	Border Zone	Layered Series	Border Zone	Border Zone	
SiO_2 (wt %)	48·56	48·51	48·65	48·53	48·56
TiO_2	2·91	2·88	2·78	2·82	2·85
Al_2O_3	14·62	14·13	14·59	14·67	14·50
FeO_t	15·10	14·82	15·06	14·50	14·87
MnO	0·29	0·23	0·21	0·21	0·24
MgO	5·53	5·56	5·14	5·65	5·47
CaO	9·97	9·61	9·47	9·79	9·71
Na_2O	2·90	2·76	2·81	2·63	2·78
K_2O	0·83	0·60	0·90	0·77	0·78
P_2O_5	0·36	0·72	0·36	0·82	0·57
LOI	0·00	0·23	0·23	0·03	–
Total	101·07	100·05	100·20	100·42	100·33
Rb (ppm)	8·97	16·2	18·1	8·03	12·8
Sr	472	531	517	523	511
Ba	458	509	421	515	476
Zr	90·8	126	264	126	152
Hf	2·81	3·52	–	–	3·17
Th	0·741	0·957	–	–	0·849
La	32·4	42·2	–	–	37·3
Ce	72·1	86·3	–	–	79·2
Pr	10·5	11·8	–	–	11·2
Nd	42·4	52·2	–	–	47·3
Sm	9·31	10·5	–	–	9·91
Eu	2·92	3·10	–	–	3·01
Gd	9·61	11·4	–	–	10·5
Tb	1·42	–	–	–	1·42
Dy	8·49	10·7	–	–	9·60
Ho	1·82	2·12	–	–	1·97
Er	4·96	6·00	–	–	5·48
Tm	0·699	–	–	–	0·699
Yb	5·58	5·59	–	–	5·59
Lu	0·581	0·876	–	–	0·729

Data from Namur *et al.* (2010).

chamber. The anorthosite contains many centimetre- to decimetre-scale pods of granophyre (Fig. 3b), which are mainly syenitic to granitic in composition; one of these has been dated at 564 Ma (Higgins & van Breemen, 1998).

The Upper Series is made up of ferroan metaluminous syenite and granite with minor monzonite (Higgins & Doig, 1986). It is exposed as small separated cupolas (*c.* 2 km × 1 km) topping the central part of the intrusion and probably represents *c.* 10 vol. % of the total intrusion. The Upper Series is cross-cut by a composite dolerite–syenite–granite sill named the Pointe du Criard (Higgins, 1990) and by many centimetre- to decimetre-thick dolerite dykes.

SAMPLING STRATEGY

Sixty-two samples of fine-grained mafic rocks from the Border Zone were collected. In outcrops containing country-rock xenoliths, samples were taken at least 1 m from the xenoliths. No samples were collected from outcrops displaying large crystals that may have resulted from mineral accumulation. Eleven mafic to intermediate fine- to medium-grained samples were collected from dykes cross-cutting the Layered Series along two north–south transects (S1 and S2 in Fig. 2a). One sample (S9-106) was collected from a dyke intersected by a drill-core [1166-95-09 (S9) of Soquem Inc.] through the Critical Zone of the Layered Series. Seventy-six samples were taken from silicic and mafic rocks of the Upper Series. Among these samples, 12 come from the silicic part of the Pointe du Criard sill and 14 come from fine-grained dolerite dykes cross-cutting the Upper Series. Fourteen samples of layered gabbro from the Layered Series were selected for isotopic analysis. Sixteen samples of country-rocks were collected at the northern contact of the intrusion. Analytical methods, including all the preparation techniques and instrument protocols, are presented in the Appendix.

FIELD RELATIONSHIPS AND PETROGAPHY

The Sept Iles Border Zone

The exposed part of the Sept Iles intrusion is surrounded by a Border Zone (at least 20 m thick; Fig. 2) of massive fine-grained mafic rocks (dolerite), representing an abrupt textural discontinuity between the coarse-grained gabbros of the Layered Series and the gneisses of the Grenvillian country-rocks. The external part of the Border Zone locally contains centimetre- to metre-scale blocks of partially melted Grenvillian gneiss (Fig. 3c).

Rocks from the Border Zone are mostly composed of plagioclase, Ca-rich pyroxene and Fe–Ti oxides, with a granular texture and a grain size commonly between 0·1 and 0·5 mm (Fig. 4a). Plagioclase is the most abundant phase (50–60 vol. %; Table 3), forming small randomly oriented grains with a roughly tablet-shaped morphology. Plagioclase grains frequently display strong normal zoning and are locally antiperthitic. Ca-rich clinopyroxene is the dominant ferro-magnesian mineral with a modal proportion locally exceeding 25 vol. %. It occurs as anhedral to subhedral tabular grains. Iron–titanium oxides of both magnetite–ulvöspinel and ilmenite–hematite solid solutions occur in all the samples. Magnetite is usually more abundant than ilmenite. Orthopyroxene and olivine are subordinate phases observed only in very few

Downloaded from petrology.oxfordjournals.org at Bibliotheque Fac de Medecine on January 12, 2011

Table 2: Mineral assemblages and mineral compositions in the Sept Iles Layered Series

Unit	Thickness (m)	Average mineral proportions (wt %)						Range of silicate mineral compositions			Isotopic composition $(^{87}Sr/^{86}Sr)_{564}$
		Plagioclase	Olivine	Magnetite	Ilmenite	Cpx	Apatite	Plag (An%)	Olivine (Fo%)	Cpx (Mg-no. %)	
MCU I											
po-C	522	67	33	–	–	–	–	68–61	73–66	–	0·70372–0·70392
pomi-C	340	53	25	13	9	–	–	61–60	66–66	–	0·70376
pomic-C	326	47	12	12	10	19	–	60–57	66–65	75–73	0·70382
pmic-C	432	47	–	13	12	28	–	57–51		74–71	0·70382
pomica-C	165	47	21	9	6	12	5	51–47	60–55	71–68	0·70393–0·70405
MCU II											
pomi-C	543	56	20	17	7	–	–	62–60	70–68	–	0·70381–0·70389
pomic-C	1116	47	14	13	9	17	–	60–56	68–64	76–73	0·70444
pmic-C	722	46	–	14	11	29		56–52		74–70	0·70396–0·70462
pomica-C	171	43	19	12	6	14	6	52–34	57–21	70–57	0·70493
MCU III											
po-C	132	68	32	–	–	–	–	69–62	71–65	–	0·70360
pomi-C	120	56	27	12	8	–	–	62–60	67–65	–	0·70382–0·70383
pomic-C	144	52	12	14	7	15	–	60–39	65–45	76–66	–

Data from Namur *et al*. (2010); cumulate classification following Irvine (1982): p, plagioclase; o, olivine; m, magnetite; i, ilmenite; c, Ca-rich pyroxene; a, apatite.

samples, with a modal proportion less than 10 vol. %. Orthopyroxene is represented by tabular grains whereas olivine forms anhedral rounded grains. Apatite is a minor phase in all the samples and occurs as needle-shaped grains rarely exceeding 300 μm. Brown amphibole and biotite are widespread as rims around Ca-rich pyroxene and Fe–Ti oxides. Traces of quartz, alkali-feldspar and zircon have been observed in a few samples.

Dolerite dykes in the Layered, Upper Border and Upper Series

Dolerite dykes (0·1–1 m thick) are common in the Sept Iles layered intrusion. They have mineral assemblages similar to those observed in the mafic rocks from the Border Zone, but are generally finer-grained, particularly at their outer contacts. The grain size of minerals commonly decreases from the center toward the margin of the dykes, where glassy contacts are locally observed. In the Layered Series, they tend to cut the cumulus layering at a high angle and dip steeply to the south. In the Upper Border Series and the Upper Series, the dykes form dense swarms. Many samples have undergone extensive alteration, principally resulting in the hydrothermal replacement of Ca-rich pyroxene by amphibole and the crystallization of fibrous carbonate minerals.

Intermediate and silicic dykes in the Layered Series

Intermediate to silicic dykes and pods with fine- to medium-grained textures (1–5 mm) are frequently found in the apatite-rich gabbros of the Layered Series. They are dominated by zoned subhedral antiperthitic plagioclase (Fig. 4b). Some samples contain small subhedral grains of perthitic alkali-feldspar. Alkali-feldspar is also locally found as rims around plagioclase grains (Fig. 4b). Quartz is generally absent or present in amounts less than 5 vol. % (Table 3). Mafic minerals are dominated by Ca-rich pyroxene and Fe–Ti oxide minerals. Amphibole is much more abundant than in the dolerite dykes and has two different habits. The first is represented by a fibrous brown coronitic amphibole replacing primary Ca-rich pyroxene and orthopyroxene. Relict cores of pyroxene are frequently observed in the central part of the grains. The second type occurs as small, separated anhedral, brown to slightly green grains. Biotite, apatite and zircon are common accessory phases in the more silicic dykes.

The Upper Series and Pointe du Criard Sill

Mafic and silicic magma interaction

The Upper Series is composed of granites, syenites and monzonites, cropping out on the Marconi peninsula and

Downloaded from petrology.oxfordjournals.org at Bibliotheque Fac de Medecine on January 12, 2011

Fig. 3. Field relations in the Sept Iles layered intrusion. (a) Representative outcrop of the Layered Series showing decimetre-scale modal layering with an erosive channel in gabbroic rocks. (b) Matrix of silicic material invading anorthosite fragments from the Upper Border Series. Pen is 13 cm long. (c) Quartzite block from the country-rocks enclosed in fine-grained dolerite in the Border Zone. (d) Metre-scale dyke of intermediate (monzonite) composition cross-cutting Fe–Ti oxide-rich gabbros of the Layered Series.

on the islands (Fig. 2). Locally well-defined schlieren occur defining layering consisting of alternating centimetre-scale dark and felsic layers (Barbey, 2009).

In the Upper Series there are several components that have complex field relationships (Higgins, 2005). The most obvious subdivision distinguishes silicic rocks free of magmatic mafic enclaves (MME; Barbarin, 1988; Didier & Barbarin, 1991; Wiebe & Collins, 1998; Fig. 5a) and MME-rich silicic rocks (Fig. 5b). Most MME contain plagioclase megacrysts (up to 1 cm long) and petrographically resemble the abundant dolerite dykes of the Upper Series. The enclaves are invariably finer grained than the enclosing silicic rocks. Most MME are ovoid and 1–10 cm long, but some enclaves are highly elongated, up to more than 2 m long and a few centimetres wide. MME locally occur as aggregates, forming huge metre-scale masses or dyke-like swarms made up of mafic pillows separated by veins of felsic material. Continuity is observed between isolated blob-like MME to undisturbed mafic dykes through disjointed dykes made up of MME aggregates. Barbarin (2005) described similar structures in the Sierra Nevada batholith.

Downloaded from petrology.oxfordjournals.org at Bibliotheque Fac de Medecine on January 12, 2011

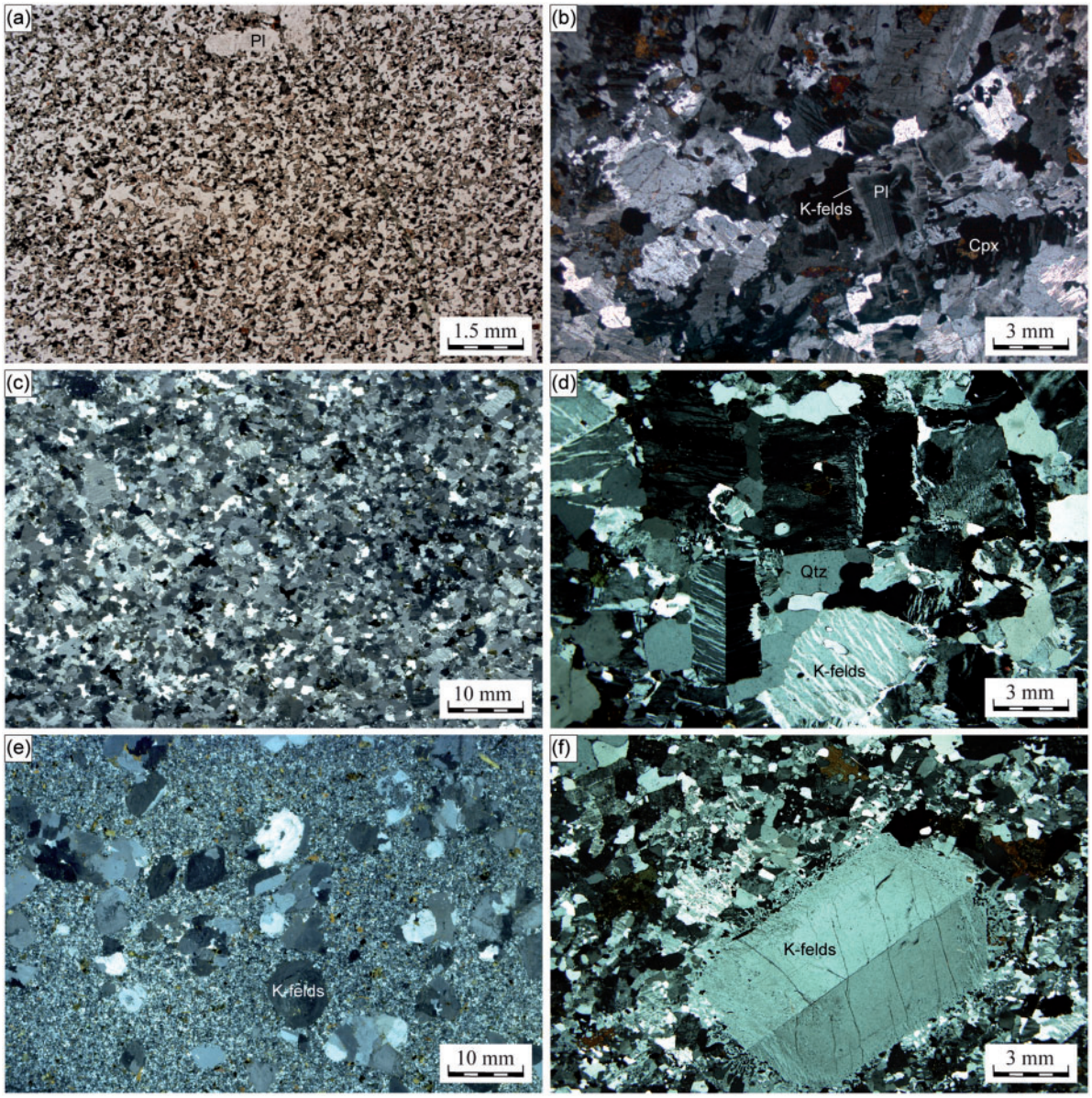

Fig. 4. Photomicrographs showing the main textures and mineral assemblages in rocks from the Border Zone, dykes in the Layered Series and the Upper Series. (a) Fine-grained mafic rock from the Border Zone mainly made up of plagioclase, Ca-rich pyroxene and Fe–Ti oxides. Sample 05-45, transmitted light. (b) Medium-grained intermediate rock from a dyke cross-cutting the Layered Series, dominated by antiperthitic plagioclase with local overgrowths of alkali-feldspar, Ca-rich pyroxene and Fe–Ti oxides. Sample 07-82, cross-polarized transmitted light. (c) Representative fine-grained granite from the Upper Series. Sample 03-01, cross-polarized transmitted light. (d) Coarse-grained granite from the Upper Series showing large alkali-feldspar and quartz grains. Sample 03-05, cross-polarized transmitted light. (e) Representative porphyritic granite from the Pointe du Criard sill showing large alkali-feldspar grains in a fine-grained matrix comprised of alkali-feldspar, quartz, plagioclase and amphibole. Sample 03-08, cross-polarized transmitted light. (f) Close-up of a large alkali-feldspar grain in a granite from the Pointe du Criard sill. Sample 03-08, cross-polarized transmitted light. Mineral abbreviations: Pl, plagioclase; K-felds, alkali-feldspar; Cpx, Ca-rich pyroxene; Qtz, quartz.

MME-free rocks are present as homogeneous 'pillows' 2–10 m long. The MME-rich units occur between the pillows (Fig. 5c). In vertical section of the Upper Series, the amount of pillows drastically decreases from base to top (Fig. 5d).

Petrography of the silicic rocks

Silicic rocks from the Upper Series are medium-grained (2–7 mm) and display intergranular textures (Fig. 4c and d). Alkali-feldspar, plagioclase, quartz and hornblende are the main rock-forming minerals, and Ca-rich pyroxene,

Downloaded from petrology.oxfordjournals.org at Bibliotheque Fac de Medecine on January 12, 2011

Table 3: Mineral modes in representative fine-grained and silicic samples of the Sept Iles Intrusive Suite

Sample	Rock-type	Location	Feldspars	Quartz	FeTiOx	Cpx	Opx	Ol	Amph	Ap
05-45	Dolerite	Border Zone	56·5	–	6·0	23·0	4·5	9·0	–	1·0
05-30	Dolerite	Border Zone	58·2	–	7·1	19·1	7·6	7·4	–	0·6
05-28	Dolerite	Border Zone	63·2	–	6·9	17·1	3·3	8·8	–	0·7
07-47	Dolerite	Border Zone	57·3	–	7·1	22·3	7·2	5·8	–	0·3
07-48	Dolerite	Border Zone	58·3	–	6·8	23·2	6·9	4·1	–	0·7
07-64	Dolerite	Border Zone	56·2	–	7·1	20·3	4·2	11·2	–	1·0
05-32	Dolerite	Border Zone	64·2	–	6·1	19·2	4·1	5·9	–	0·5
07-01	Dolerite	Layered Series	58·1	–	5·8	22·3	3·9	9·2	–	0·7
07-82	Monzonite	Layered Series	81·3	2·5	4·2	7·3	0·9	–	3·2	0·6
07-16	Monzonite	Border Zone	82·8	0·9	3·8	9·3	0·3	–	2·2	0·7
03-19	Monzonite	Upper Series	77·2	4·3	2·7	9·2	–	–	5·7	0·9
03-33	Monzonite	Upper Series	67·5	1·2	4·3	17·4	–	–	7·6	2·0
03-10	Syenite	Upper Series	75·1	8·7	1·5	–	–	–	14·3	0·4
03-43	Syenite	Upper Series	71·5	5·8	2·1	3·5	–	–	16·5	0·6
03-47	Syenite	Upper Series	74·2	7·6	1·7	1·2	–	–	14·7	0·6
03-02	Granite	Upper Series	64·6	32·8	0·3	–	–	–	3·0	0·3
03-04	Granite	Upper Series	63·8	27·6	0·8	–	–	–	7·6	0·2
03-20	Granite	Upper Series	61·2	33·6	0·6	–	–	–	14·2	0·3
03-38	Granite	Upper Series	65·5	19·4	1·2	0·3	–	–	12·7	0·4
03-45	Granite	Upper Series	64·5	21·4	0·9	–	–	–		0·5

Modal proportions determined by point counting on thin sections (at least 1000 points for each sample).

Fe–Ti oxides, biotite, apatite, zircon, titanite, allanite, chlorite and fluorite are subordinate phases (Fig. 4d). Perthitic alkali-feldspar is represented by anhedral to subhedral tabular grains with modal proportions generally in the range between 10 and 40 vol. %. Alkali-feldspar ($Ab_{31}An_1Or_{68}$–$Ab_8An_0Or_{92}$; Table 4) commonly contains small inclusions of plagioclase, quartz and amphibole. Antiperthitic zoned plagioclase ($An_{25–18}$; Table 4) is found as small anhedral to slightly tabular grains with a mode generally lower than 50 vol. %. Plagioclase grains commonly enclose inclusions of Fe–Ti oxide minerals and locally Ca-rich pyroxene. Quartz is found in most samples with a modal proportion of 10 vol. % on average but higher than 25 vol. % in some samples. It occurs as small (0·2–3 mm) rounded anhedral grains. Mafic minerals are dominated by 2–3 mm anhedral to subhedral dark green to brown ferro-edenitic, edenitic to ferro-richteritic amphibole (Leake *et al.*, 1997), with a modal proportion higher than 20 vol. % in some samples. The Mg-number of amphibole (Table 5) evolves from 54 to 13, and their F and Cl concentrations range from 0·70 to 2·40 wt % and 0·05 to 0·32 wt %, respectively. Some grains of amphibole contain relic cores of Ca-rich pyroxene with Mg-number ranging from 51 ($Ens_{25}Fs_{24}Wo_{51}$; Table 6) to 29 ($Ens_{18}Fs_{34}Wo_{48}$). A low amount (less than 3 vol. %) of subhedral to euhedral reddish biotite was observed in some samples. Fluorite is frequently closely associated with biotite. Fe–Ti oxide minerals are represented by both magnetite–ulvöspinel ($Usp_{17–3}$; Table 7) and ilmenite–hematite ($Hem_{1–0}$) solid-solutions. Oxide minerals occur as small (<2 mm) anhedral patches dominated by magnetite. Zircon shows a prismatic habit with multi-faceted terminations.

The Pointe du Criard sill

The Upper Series and Upper Border Series are cross-cut by the Pointe du Criard composite sill, the geology of which has been described in detail by Higgins (1990). The sill crops out over an area of 10 km by 23 km, including all the islands and the Marconi peninsula, and is up to 50 m thick. It is composed of three magmatic components: dolerite, leucogabbro and silicic rocks (Fig. 5e and f). The margins of the sill are composed of dolerite, which has fine-grained contacts with the host granite (Upper Series) or anorthosite (Upper Border Series). At the base of the sill this dolerite unit is 0·1–6 m thick and locally contains plagioclase megacrysts with a proportion that increases upwards. The dolerite is gradational into a leucogabbro unit over a few centimetres to decimetres. The latter is variable in thickness, generally in the range 0·3–10 m, and

Downloaded from petrology.oxfordjournals.org at Bibliotheque Fac de Medecine on January 12, 2011

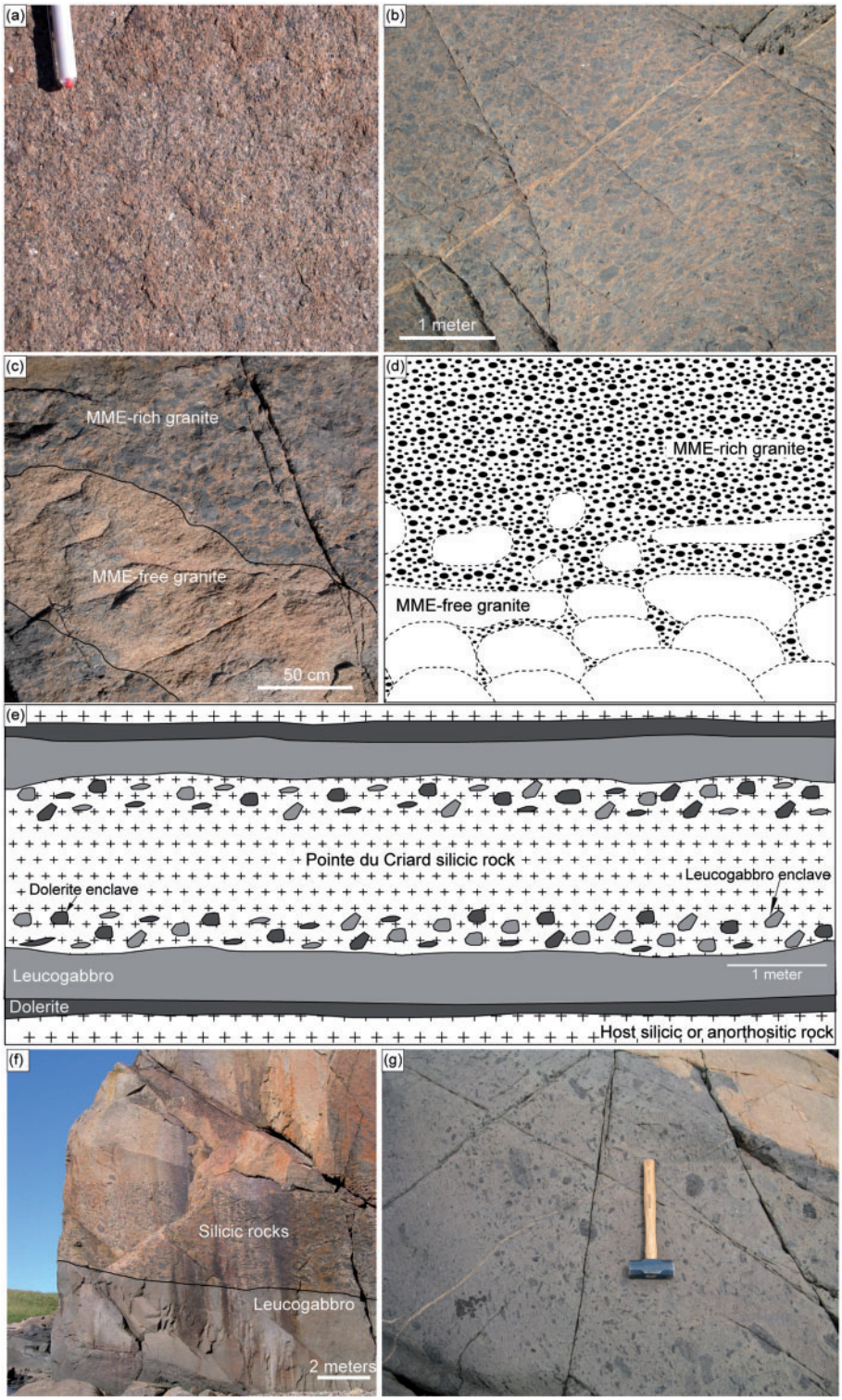

Fig. 5. Photographs and schematic sketches of field relations in the Sept Iles Upper Series and Pointe du Criard sill. (a) Representative outcrop of pinkish MME-free granite. (Note the presence of large whitish grains of alkali-feldspar.) (b) Typical outcrop of yellow–pink MME-bearing granite. MME are mainly composed of fine-grained dolerite. (c) Sharp contact between the MME-rich granite facies and a metre-scale pillow of MME-free granite. (d) Schematic relationships of MME-bearing rocks and MME-free rocks as observed on Corossol Island (after Higgins, 2005). (e) Schematic sketch of the Pointe du Criard sill displaying the succession of the three magmatic components: dolerite, leucogabbro and felsic rocks (after Higgins, 2005). Enclaves of dolerite and leucogabbro are abundantly found in the lower and upper part of the felsic component. (f) Typical outcrop of the Pointe du Criard sill showing the succession of two different magmatic components: leucogabbro and silicic rocks. It should be noted that the external part of the silicic rocks contains abundant MME and mafic xenoliths. Size and abundance of MME and xenoliths decrease progressively toward the central part of the sill. The first dolerite component of the Pointe du Criard sill is not observed on this outcrop. (g) Close-up of the leucogabbro component of the Pointe du Criard sill. It is made up of fine-grained dolerite containing abundant centimetre-scale plagioclase phenocrysts. Plagioclase crystals larger than 20 cm have been observed in some outcrops.

Downloaded from petrology.oxfordjournals.org at Bibliotheque Fac de Medecine on January 12, 2011

Table 4: Major (wt %) element compositions of feldspars from the Sept Iles Upper Series and the Pointe du Criard Sill (microprobe analyses)

Sample	Rock-type	Location	*n*	SiO_2	Al_2O_3	FeO_t	CaO	Na_2O	K_2O	Total	An*	An†	Ab‡	Or§
Plagioclase														
03-01	Granite	Upper Series	1	68·50	19·80	0·44	0·00	10·90	1·47	101·11	0·0	0·0	91·9	8·2
03-08	Syenite	Pointe du Criard	7	67·60	20·64	0·13	0·88	11·11	0·28	100·64	4·2	4·1	94·3	1·6
03-09	Granite	Pointe du Criard	7	67·47	20·49	0·30	1·01	10·74	0·53	100·54	4·9	4·8	92·3	3·0
03-11	Granite	Pointe du Criard	4	67·53	20·31	0·02	0·26	10·29	1·51	99·92	1·4	1·3	90·1	8·7
03-15	Granite	Pointe du Criard	7	68·20	20·32	0·12	0·56	11·33	0·13	100·66	2·6	2·6	96·7	0·7
03-22	Granite	Upper Series	5	68·80	19·83	0·23	0·01	11·30	0·47	100·64	0·0	0·0	97·3	2·7
03-28	Granite	Upper Series	2	67·80	19·15	0·74	0·14	10·75	0·58	99·16	0·7	0·7	96·0	3·4
03-35	Granite	Upper Series	2	68·75	19·60	0·44	0·01	11·10	1·10	101·00	0·0	0·0	93·9	6·1
03-37	Syenite	Upper Series	4	67·97	20·23	0·14	0·69	10·93	0·67	100·63	3·4	3·2	93·0	3·8
03-42	Monzonite	Upper Series	6	61·94	24·29	0·11	5·36	8·66	0·19	100·55	25·5	25·3	73·7	1·0
03-48	Syenite	Upper Series	4	64·38	22·96	0·26	3·74	9·22	0·46	101·02	18·3	17·8	79·6	2·6
Alkali-feldspar														
03-01	Granite	Upper Series	1	65·20	18·60	0·37	0·01	1·20	14·99	100·37	0·5	0·1	10·8	89·1
03-08	Syenite	Pointe du Criard	6	64·87	18·81	0·08	0·01	1·71	14·18	99·66	0·6	0·1	9·1	90·9
03-09	Granite	Pointe du Criard	7	64·94	18·93	0·02	0·05	1·66	14·23	99·83	1·8	0·3	15·0	84·7
03-11	Granite	Pointe du Criard	4	64·95	18·87	0·00	0·13	1·35	14·55	99·85	5·0	0·6	12·2	87·1
03-15	Granite	Pointe du Criard	6	65·00	18·62	0·10	0·01	1·18	14·94	99·85	0·3	0·0	10·7	89·3
03-22	Granite	Upper Series	5	64·82	18·56	0·17	0·00	0·88	15·35	99·78	0·3	0·0	8·0	92·0
03-28	Granite	Upper Series	2	65·45	18·10	0·65	0·00	1·70	13·67	99·57	0·0	0·0	15·9	84·1
03-35	Granite	Upper Series	2	65·10	18·35	0·46	0·01	0·85	15·44	100·21	0·3	0·0	7·7	92·3
03-37	Syenite	Upper Series	4	64·90	18·70	0·05	0·02	1·05	15·13	99·85	1·0	0·1	9·5	90·4
03-42	Monzonite	Upper Series	3	63·80	18·85	0·32	0·05	1·30	14·47	98·79	1·9	0·2	12·0	87·8
03-48	Syenite	Upper Series	5	66·30	18·94	0·08	0·19	3·44	11·31	100·26	2·9	0·9	31·3	67·8

n, number of microprobe analyses.
*An = 100[Ca/(Ca + Na)].
†An = 100[Ca/(Ca + Na + K)].
‡Ab = 100[Na/(Ca + Na + K)].
§Or = 100[K/(Ca + Na + K)].

is composed of large plagioclase crystals (Fig. 5g). The silicic unit generally constitutes the bulk of the sill. At the base the leucogabbro is gradational to the silicic rocks over a few centimetres. The lower 1–3 m of the silicic rocks contain abundant MME and xenoliths of dolerite and leucogabbro, in approximately equal amounts.

Silicic rocks from the Pointe du Criard sill display mineralogical features similar to those of silicic rocks from the Upper Series. They have a distinctive porphyritic texture (Fig. 4e and f) with large zoned and rounded crystals (up to 1 cm; 40–70 vol. %) of alkali-feldspar ($Ab_{15}An_0Or_{85}$–$Ab_9An_0Or_{91}$) in a relatively fine-grained equigranular matrix (<1 mm) mainly made up of perthitic alkali-feldspar, with plagioclase exsolution lamellae of An_{5-1}, amphibole (Mg-number 22–18), Fe–Ti oxides (Usp_{14-3} and Hem_1), ± quartz. Relict cores of Ca-rich pyroxene (Mg-number 30–29; $Ens_{16}Fs_{38}Wo_{46}$–$Ens_{15}Fs_{38}Wo_{47}$) are also locally included in the central part of amphibole grains.

WHOLE-ROCK GEOCHEMISTRY

General assumption and classification

Whole-rock major and trace element compositions of fine-grained samples from the Border Zone and dykes cross-cutting the Layered Series, as well as silicic samples from the Upper Zone and Pointe du Criard Sill, are listed in Table 8. These samples are the main focus of this study as their petrographic characteristics indicate that they could potentially represent liquid compositions. Owing to their high degree of alteration, the compositions of samples from dolerite dykes cross-cutting the Upper

Downloaded from petrology.oxfordjournals.org at Bibliotheque Fac de Medecine on January 12, 2011

Table 5: Major (wt %) element compositions of amphibole from the Sept Iles Upper Series and the Pointe du Criard Sill (microprobe analyses)

Sample	Rock-type	Location	*n*	SiO_2	TiO_2	Al_2O_3	FeO_t	MnO	MgO	CaO	Na_2O	K_2O	F	Cl	Total	O = F, Cl	H_2O*	Total	Mg-no.†
03-01	Granite	Upper Series	2	48·40	1·25	2·00	31·15	1·34	2·67	5·34	4·62	1·26	1·24	0·07	99·33	−0·53	1·28	100·08	13·2
03-08	Syenite	Pointe du Criard	2	43·85	1·36	5·34	28·65	0·81	4·41	9·97	2·15	1·02	1·23	0·19	98·98	−0·56	1·25	99·67	21·5
03-09	Granite	Pointe du Criard	2	43·96	1·38	5·29	30·12	1·02	4·13	9·69	2·21	1·03	1·51	0·16	100·48	−0·67	1·13	100·94	19·6
03-11	Granite	Pointe du Criard	1	43·71	1·50	5·27	30·06	0·91	3·61	9·72	2·34	1·03	1·37	0·21	99·73	−0·62	1·17	100·28	17·6
03-15	Granite	Pointe du Criard	2	43·70	1·22	5·48	29·40	1·08	4·20	9·74	2·20	1·05	1·16	0·17	99·39	−0·52	1·29	100·16	20·3
03-22	Granite	Upper Series	2	46·45	0·95	3·59	27·45	1·22	5·33	9·39	2·47	0·98	1·17	0·08	99·06	−0·51	1·33	99·88	25·7
03-35	Granite	Upper Series	6	48·95	1·03	2·02	27·63	1·12	5·28	6·79	4·20	1·17	1·85	0·05	100·09	−0·79	1·03	100·33	25·4
03-37	Syenite	Upper Series	3	44·43	1·11	5·56	27·33	0·91	5·34	10·31	1·94	0·96	1·36	0·20	99·45	−0·62	1·20	100·03	25·8
03-42	Monzonite	Upper Series	3	42·60	1·90	7·26	27·57	0·62	5·06	10·32	1·86	1·01	0·70	0·32	99·22	−0·37	1·48	100·33	24·7
03-48	Syenite	Upper Series	3	46·93	1·22	5·52	18·67	0·60	12·11	10·83	2·00	0·94	2·40	0·21	101·43	−1·06	0·81	101·18	53·6

n, number of microprobe analyses.
*Water calculated to fill up the (OH, F, Cl) group.
†Mg-number = 100[Mg/(Mg + Fe)].

Table 6: Major (wt %) element compositions of Ca-rich pyroxene from the Sept Iles Upper Series and the Pointe du Criard Sill (microprobe analyses)

Sample	Rock-type	Location	*n*	SiO_2	TiO_2	Al_2O_3	FeO_t	MnO	MgO	CaO	Na_2O	Total	Wo*	Ens†	Fs‡	Mg-no.§
03-08	Syenite	Pointe du Criard	2	49·30	0·33	0·72	24·26	1·15	5·45	19·09	0·49	100·79	46·7	15·2	38·1	28·6
03-11	Granite	Pointe du Criard	1	49·17	0·29	0·55	23·98	1·16	5·63	18·95	0·42	100·15	46·5	15·8	37·7	29·5
03-42	Monzonite	Upper Series	3	49·80	0·15	0·45	21·38	1·00	6·64	19·93	0·33	99·67	48·3	18·4	33·3	35·6
03-48	Syenite	Upper Series	3	51·67	0·07	0·32	16·48	1·24	9·51	21·71	0·41	101·41	50·3	25·2	24·5	50·7

n, number of microprobe analyses.
*Wo = 100[Ca/(Mg + Fe + Ca)].
†Ens = 100[Mg/(Mg + Fe + Ca)].
‡Fs = 100[Fe/(Mg + Fe + Ca)].
§Mg-number = 100[Mg/(Mg + Fe)].

Series are not considered but their occurrence is used in the subsequent discussion to constrain the crystallization history of the SIIS.

The samples display a range of compositions from basalt (gabbro) to rhyolite (granite), with intermediate trachyandesite (monzonite) and trachyte (syenite) straddling the boundary between subalkaline and alkaline fields (Fig. 6a). Following Liégeois & Black (1987), the mafic to intermediate rocks are thus sub-alkaline, whereas the silicic rocks are mildly alkaline. In a plot of K_2O vs SiO_2, the mafic samples lie in the medium-K field, whereas the intermediate and silicic samples plot in the high-K and shoshonitic fields (Fig. 6b). All the samples, including the silicic rocks, have high Fe-number [0·63–0·99; Fe-number $= FeO_t/(FeO_t + MgO)$] and thus plot in the tholeiitic field on an AFM diagram (Fig. 6c).

The silicic samples have strong geochemical affinities with A-type granitoids (Loiselle & Wones, 1979; Clemens *et al.*, 1986; Eby, 1990; Frost *et al.*, 2001; Bonin, 2007), plotting within the ferroan alkalic to alkali-calcic A-type granitoid fields (Fig. 7a and b). They have high contents of incompatible trace elements [$10000 \times (Ga/Al) > 3{\cdot}1$; $(Zr + Nb + Ce + Y) > 956$ ppm), well above the A-type granite discriminating values suggested by Whalen *et al.* (1987), and in alkalis, above the A-type lower limit of Eby (1990). The presence of abundant small grains of fluorite and the

Downloaded from petrology.oxfordjournals.org at Bibliotheque Fac de Medecine on January 12, 2011

Table 7: Major (wt %) element compositions of Fe–Ti oxide minerals from the Sept Iles Upper Series and the Pointe du Criard Sill (microprobe analyses)

Sample	Rock-type	Location	*n*	SiO_2	TiO_2	Al_2O_3	FeO	Fe_2O_3	MnO	MgO	Total	X_{Mt}/X_{Ilm}	X_{Usp}/X_{Hem}
Magnetite													
03-01	Granite	Upper Series	2	0·12	6·46	0·02	36·09	56·08	0·75	0·01	99·53	0·82	0·18
03-08	Syenite	Pointe du Criard	9	0·07	1·50	0·07	32·71	66·88	0·07	0·03	101·33	0·96	0·04
03-09	Granite	Pointe du Criard	6	0·10	5·34	0·19	35·20	58·34	0·77	0·00	99·94	0·86	0·14
03-11	Granite	Pointe du Criard	8	0·08	1·13	0·12	31·18	68·23	0·13	0·84	101·71	0·97	0·03
03-15	Granite	Pointe du Criard	5	0·11	2·74	0·25	33·30	63·72	0·47	0·00	100·59	0·93	0·07
03-22	Granite	Upper Series	5	0·05	5·54	0·08	35·68	58·40	0·61	0·00	100·35	0·85	0·15
03-28	Granite	Upper Series	4	0·14	0·98	0·06	31·96	67·37	0·03	0·07	100·60	0·97	0·03
03-35	Granite	Upper Series	8	0·09	0·95	0·04	32·46	68·53	0·09	0·01	102·17	0·97	0·03
03-37	Syenite	Upper Series	9	0·10	2·37	0·18	33·17	64·43	0·20	0·00	100·45	0·93	0·07
03-42	Monzonite	Upper Series	3	0·12	2·20	0·26	33·07	64·55	0·09	0·01	100·30	0·94	0·06
03-48	Syenite	Upper Series	4	0·10	2·06	0·40	33·12	65·45	0·15	0·09	101·37	0·94	0·06
Ilmenite													
03-15	Granite	Pointe du Criard	6	–	52·34	0·01	41·92	0·75	5·06	0·01	100·10	0·99	0·01
03-35	Granite	Upper Series	5	–	52·87	0·29	42·92	0·75	4·48	0·05	101·36	0·99	0·01
03-42	Monzonite	Upper Series	4	–	53·28	0·03	45·87	0·04	1·86	0·09	101·16	1·00	0·00
03-48	Syenite	Upper Series	5	–	52·88	0·03	45·51	1·13	1·86	0·09	101·49	0·99	0·01

n, number of microprobe analyses. FeO and Fe_2O_3 recalculated from FeO_{tot} by charge balance. Molar fractions of magnetite, ulvöspinel, hematite and ilmenite (X_{Mt}, X_{Usp}, X_{Hem}, X_{Ilm}) calculated following QUILF algorithm (Andersen *et al.*, 1993).

high F concentration of amphibole clearly suggest a high F content for these samples (Table 5).

Geochemical trends

Major elements

Major element variations are plotted relative to SiO_2 (44–77 wt %) in Fig. 8; all the samples define coherent trends. TiO_2 first increases from *c.* 2·5 to 5 wt %, whereas SiO_2 decreases slightly from *c.* 49 to 46 wt %, and TiO_2 then continuously decreases to 0·5 wt % with increasing SiO_2 content. The Sept Iles parent magma contains *c.* 14–15 wt % FeO_t (Table 1; Namur *et al.*, 2010). FeO_t first increases from *c.* 14 to 17 wt %, a common feature of tholeiitic magma series, before decreasing continuously to *c.* 2 wt % in the silica-rich rocks. Al_2O_3 scatters around 14 wt % in samples with less than *c.* 60 wt % SiO_2 and then decreases continuously to *c.* 11 wt % in the SiO_2-rich rocks. With increasing SiO_2, CaO and MgO decrease continuously, from *c.* 10 to 0 wt % and from *c.* 6 to 0 wt %, respectively. Na_2O increases continuously from *c.* 2·5 to 4·5 wt % in the SiO_2-poor samples (<60 wt % SiO_2) and then decreases to *c.* 3·5 wt % in the more silicic rocks. K_2O increases sharply to *c.* 70 wt % SiO_2, where it reaches *c.* 5 wt %, and then stabilizes around this value or slightly decreases in the most SiO_2-rich samples. P_2O_5 first increases from *c.* 0·4 to 1·5 wt % in liquids with less than 52 wt % SiO_2 and then decreases continuously to 0 wt % P_2O_5.

Trace elements

Incompatible elements (e.g. La; not shown) increase continuously with increasing SiO_2. Rb shows the same evolutionary trend up to 70 wt % SiO_2 and then flattens at *c.* 100 ppm (Fig. 9). Sr contents are rather variable up to 55 wt % SiO_2 and then decrease to *c.* 20 ppm, with increasing SiO_2. A few samples have very high Sr concentrations (>800 ppm), which probably results from plagioclase accumulation. Zr and Ba display bell-shaped trends with the highest values, 3265 ppm and 1350 ppm respectively, observed at *c.* 60 wt % SiO_2. Some samples display very high Ba and Zr concentrations, and large ranges of Ba and Zr are observed at constant SiO_2 values; this could result from biotite and zircon accumulation, in a similar way to what has been reported by Vander Auwera *et al.* (2003) for the Holum granite and by Bogaerts *et al.* (2003) for the Lyngdal granodiorite. Cr and V display half-bell-shaped curves with the highest concentrations, of *c.* 100 ppm and *c.* 300 ppm respectively, observed at

Downloaded from petrology.oxfordjournals.org at Bibliotheque Fac de Medecine on January 12, 2011

Table 8: Whole-rock major (wt %) and trace (ppm) element compositions of Sept Iles Samples

Sample:	05-10	05-28	05-29	05-30	05-31	05-32	05-33	05-45	07-04	07-05	07-06	07-15	07-16	07-42
Rock-type:	Doler.	Doler.	Monz.	Doler.	Doler.	Doler.	Doler.	Doler.	Doler.	Doler.	Doler.	Monz.	Monz.	Doler.
Location:	BZ	BZ	BZ	BZ	BZ	BZ	BZ	BZ	BZ	BZ	BZ	BZ	BZ	BZ
Xenoliths:														
East WGS84:	03·63·012	03·81·926	03·81·926	03·81·879	03·81·918	03·78·396	03·78·396	03·71·996	03·63·009	03·63·010	03·63·011	03·65·175	03·65·175	03·72·003
North WGS84:	55·63·216	55·74·691	55·74·691	55·74·699	55·74·657	55·74·571	55·74·571	55·72·424	55·63·213	55·63·214	55·63·215	55·66·033	55·66·033	55·72·448
SiO_2	46·14	50·03	56·78	46·94	50·79	49·02	50·91	48·56	46·33	45·55	47·27	57·27	56·54	48·75
TiO_2	4·51	4·15	2·39	3·38	3·12	2·79	3·54	2·91	4·29	4·22	3·52	2·15	2·59	3·03
Al_2O_3	14·21	12·17	15·29	14·13	11·04	15·26	15·75	14·62	13·91	14·02	14·40	13·79	13·45	13·53
FeO_t	16·64	17·08	10·18	16·06	13·51	14·13	14·14	15·10	16·21	16·79	15·89	11·27	11·33	14·87
MnO	0·33	0·20	0·15	0·40	0·24	0·16	0·14	0·29	0·31	0·26	0·26	0·18	0·16	0·28
MgO	5·64	3·68	2·06	5·07	8·02	5·36	4·01	5·53	5·26	5·42	5·44	2·62	2·98	5·04
CaO	8·76	6·47	5·46	8·64	9·72	9·37	7·10	9·97	8·82	8·69	8·83	5·42	5·38	9·19
Na_2O	2·19	4·22	4·26	3·42	2·43	2·78	3·42	2·90	2·85	2·92	2·97	3·78	3·77	3·19
K_2O	0·21	1·17	2·17	0·52	1·28	0·91	1·16	0·83	0·36	0·15	0·26	2·50	2·87	0·75
P_2O_5	1·11	0·62	0·54	0·34	0·39	0·39	0·39	0·36	0·92	0·63	0·45	0·68	0·77	1·27
LOI	0·23	0·13	0·47	0·11	0·19	0·12	0·13	0·00	0·32	0·87	0·54	0·28	0·13	0·02
Total	99·97	99·92	99·75	99·01	100·73	100·29	100·09	101·07	99·58	99·52	99·83	99·94	99·97	99·92
Fe-no.	0·75	0·82	0·83	0·76	0·63	0·76	0·78	0·73	0·76	0·76	0·73	0·81	0·79	0·75
Rb	16·1	11·2	16·2	8·77	32·0	9·51	13·4	8·97	15·5	21·1	19·2	29·2	31·4	8·63
Sr	398	788	996	751	677	506	848	472	452	505	429	490	387	542
Ba	244	1006	1154	356	668	479	601	458	245	149	237	1246	1148	546
V	245	232	51·8	398	166	234	91·5	233	259	278	298	83·2	99·0	170
Cr	47·3	59·2	31·3	58·7	65·9	43·2	40·1	41·6	43·6	114	136	33·5	45·1	47·8
Co	53·3	40·9	36·0	34·1	42·5	48·3	42·6	49·6	51·1	56·5	52·4	10·5	23·1	43·4
Ni	21·4	29·2	35·1	4·85	155	38·4	40·2	30·2	26·3	137	147	7·17	6·62	25·1
Cu	70·5	28·7	20·8	20·1	29·4	36·2	34·8	37·1	78·6	134	148	20·6	16·3	30·1
Zn	135	202	134	190	166	142	128	133	184	181	169	143	181	209
Ga	20·5	27·9	26·2	27·8	17·1	27·3	25·4	23·6	21·1	22·2	24·3	33·5	27·6	24·9
Zr	88·9	178	128	101	182	99·3	114	90·8	45·1	81·9	77·7	651	670	118
Hf	–	4·76	7·74	2·88	5·29	3·72	2·95	2·81	1·46	–	–	10·9	9·34	3·30
Nb	18·6	28·5	49·4	19·8	27·2	22·3	18·5	12·2	15·9	26·4	11·1	40·5	39·7	8·23
Ta	–	1·43	3·05	1·47	2·41	1·99	1·88	0·995	1·57	–	–	2·23	1·38	0·577
U	–	0·692	0·986	0·472	0·675	0·618	0·501	0·465	3·03	–	–	1·52	1·67	0·228
Th	–	1·03	2·46	0·549	1·45	1·39	0·519	0·741	6·21	–	–	5·79	10·3	0·453
Pb	26·1	25·7	27·9	22·6	23·4	29·5	40·1	24·5	7·72	3·13	4·81	16·2	12·1	8·32
Y	33·4	23·1	30·6	73·8	44·1	10·7	9·72	45·7	38·5	26·1	20·9	72·5	79·8	58·8
La	–	57·7	57·0	29·5	37·0	51·9	48·3	32·4	27·0	–	–	62·1	71·4	52·7
Ce	–	114	122	74·9	82·8	123	113	72·1	56·3	–	–	107	142	103
Pr	–	15·1	18·3	12·0	12·1	14·5	14·0	10·5	9·45	–	–	12·9	17·2	14·3
Nd	–	63·9	80·1	53·9	56·3	48·2	54·5	42·4	45·5	–	–	50·7	71·0	61·5
Sm	–	13·6	19·0	13·8	12·2	13·30	11·8	9·31	10·8	–	–	11·4	19·1	13·2
Eu	–	3·89	7·44	4·77	3·38	4·81	4·76	2·92	3·38	–	–	3·29	4·49	3·80
Gd	–	13·1	17·4	14·6	12·1	11·6	10·2	9·61	11·5	–	–	10·9	13·2	13·3
Tb	–	2·65	2·69	2·25	1·79	1·65	1·31	1·42	–	–	–	–	–	–
Dy	–	11·2	13·9	13·5	10·2	6·88	7·70	8·49	8·22	–	–	8·11	10·2	11·3
Ho	–	2·53	2·80	2·97	2·11	1·12	1·41	1·82	1·63	–	–	1·89	2·19	2·50
Er	–	5·66	6·63	7·88	5·39	2·91	2·65	4·96	3·80	–	–	5·52	6·06	6·57
Tm	–	0·987	0·983	1·12	0·789	0·402	0·324	0·699	–	–	–	–	–	–
Yb	–	4·73	5·77	7·78	4·50	2·61	2·37	5·58	2·76	–	–	5·79	5·58	5·74
Lu	–	1·01	0·965	1·12	0·683	0·354	0·265	0·581	0·396	–	–	0·980	0·964	0·839
Eu/Eu*	–	0·90	1·26	1·04	0·86	1·20	1·34	0·95	0·94	–	–	0·91	0·87	0·88
$(La/Yb)_n$	–	7·89	6·39	2·46	5·33	12·88	13·19	4·58	6·34	–	–	6·94	8·28	5·94

(continued)

Downloaded from petrology.oxfordjournals.org at Bibliotheque Fac de Medecine on January 12, 2011

Table 8: Continued

Sample:	07-43	07-44	07-45	07-46	07-47	07-48	07-49	07-52	07-53	07-54	07-64	07-65	07-66	07-67
Rock-type:	Doler.	Doler.	Doler.	Doler.	Doler.	Doler.	Doler.	Monz.	Doler.	Monz.	Doler.	Monz.	Doler.	Doler.
Location:	BZ	BZ	BZ	BZ	BZ	BZ	BZ	BZ	BZ	BZ	BZ	BZ	BZ	BZ
Xenoliths:														
East WGS84:	03·82·063	03·82·040	03·82·022	03·81·931	03·79·517	03·79·479	03·79·409	03·68·097	03·68·131	03·68·383	03·61·251	–	03·61·247	03·61·129
North WGS84:	55·74·721	55·74·762	55·74·735	55·74·689	55·74·194	55·74·224	55·74·132	55·69·522	55·69·663	55·70·089	55·59·838	–	55·60·659	55·60·976
SiO_2	50·22	48·89	49·34	52·38	48·43	48·65	49·45	54·46	46·97	53·95	48·25	55·05	46·56	47·83
TiO_2	3·87	3·07	3·63	2·97	2·98	2·78	3·55	2·53	4·24	2·19	3·41	1·98	3·89	3·65
Al_2O_3	15·39	14·34	14·06	14·31	14·13	14·59	13·76	14·01	14·48	14·51	14·56	14·61	14·58	13·84
FeO_t	14·17	15·10	15·05	13·70	14·92	15·06	15·08	12·01	16·48	12·61	14·93	12·76	16·08	15·94
MnO	0·15	0·16	0·15	0·19	0·22	0·21	0·16	0·18	0·24	0·18	0·22	0·13	0·22	0·28
MgO	4·00	5·31	4·01	3·61	5·34	5·14	4·31	2·53	4·56	2·65	5·55	2·23	5·28	6·05
CaO	6·53	9·27	7·16	6·76	9·71	9·47	8·01	5·89	9·34	6·49	8·88	5·99	8·59	8·58
Na_2O	3·90	2·83	3·75	3·42	2·79	2·81	3·48	4·39	2·92	3·45	3·42	4·14	2·99	2·56
K_2O	1·05	0·73	1·35	1·73	1·08	0·90	0·89	2·68	0·42	3·07	0·78	2·02	0·94	1·03
P_2O_5	0·63	0·48	1·38	1·27	0·76	0·36	1·46	0·61	0·58	0·73	0·37	0·72	0·59	0·61
LOI	0·24	0·11	0·13	0·25	0·03	0·23	0·03	0·42	0·08	0·21	0·00	0·24	0·13	0·02
Total	100·15	100·29	100·01	100·59	100·39	100·20	100·18	99·71	100·31	100·04	100·37	99·87	99·85	100·39
Fe-no.	0·78	0·74	0·79	0·79	0·74	0·75	0·78	0·83	0·78	0·83	0·73	0·85	0·75	0·73
Rb	9·82	9·32	10·7	16·7	7·37	18·1	11·2	22·5	6·74	27·4	9·93	30·9	9·63	10·6
Sr	437	484	547	466	465	517	515	554	468	549	509	546	346	453
Ba	521	418	870	806	347	421	432	820	490	897	255	953	342	513
V	253	35·8	127	142	162	257	241	118	106	170	174	105	194	165
Cr	58·2	40·3	46·2	31·3	34·6	41·3	44·2	39·0	46·3	43·3	51·2	26·1	54·2	66·5
Co	36·2	44·4	43·2	34·4	49·1	49·5	29·8	26·4	48·3	32·6	51·5	32·1	51·6	46·2
Ni	44·8	12·6	44·3	42·5	37·7	44·5	26·3	23·6	43·1	33·4	36·4	9·62	36·2	70·9
Cu	43·4	51·8	49·1	7·13	51·5	45·6	18·5	46·2	42·8	14·9	192	7·32	80·9	56·6
Zn	188	237	204	105	614	334	272	109	144	143	137	51·5	150	185
Ga	32·4	34·3	31·3	19·4	25·6	35·4	35·1	26·4	21·3	19·9	19·2	38·4	25·3	24·4
Zr	231	106	104	167	83·6	264	152	493	97·8	520	118	658	102	99·6
Hf	4·77	–	3·55	4·66	2·55	–	14·8	7·59	–	6·50	–	20·4	–	3·16
Nb	22·7	32·9	25·1	27·6	12·0	13·6	25·1	36·1	13·7	42·7	36·8	41·4	11·3	25·3
Ta	1·29	–	1·33	1·33	0·728	–	1·26	1·90	–	1·79	–	1·45	–	1·53
U	0·376	–	0·228	0·207	0·227	–	0·990	0·599	–	0·461	–	3·84	–	0·244
Th	0·991	–	0·446	1·54	0·645	–	1·50	3·51	–	3·41	–	12·4	–	1·15
Pb	9·83	10·9	7·21	12·2	6·85	7·56	14·5	9·33	8·31	12·9	6·82	11·8	15·7	3·51
Y	48·5	47·6	48·3	52·2	44·6	54·1	34·6	71·2	47·9	77·8	54·7	94·2	56·6	51·7
La	37·5	–	39·9	55·8	27·9	–	49·2	54·9	–	42·4	–	82·5	–	39·9
Ce	72·1	–	73·7	122	57·6	–	96·3	105	–	64·8	–	162	–	73·7
Pr	10·4	–	10·6	16·0	7·85	–	13·3	14·3	–	9·34	–	21·3	–	10·6
Nd	45·3	–	45·3	64·2	32·7	–	58·5	59·7	–	38·2	–	85·3	–	45·3
Sm	9·77	–	10·1	15·9	7·58	–	13·0	13·2	–	8·96	–	18·5	–	10·1
Eu	3·40	–	2·94	4·87	2·25	–	4·06	2·76	–	1·84	–	4·26	–	2·94
Gd	10·1	–	10·3	15·1	8·04	–	14·3	13·6	–	9·02	–	14·2	–	10·3
Tb	–	–	–	–	–	–	–	–	–	–	–	–	–	–
Dy	8·70	–	9·01	14·0	7·07	–	10·2	13·4	–	8·66	–	14·5	–	9·02
Ho	1·82	–	2·01	2·97	1·53	–	2·17	3·070	–	1·96	–	3·23	–	2·01
Er	4·87	–	5·35	8·50	4·25	–	5·56	8·64	–	5·08	–	9·10	–	5·35
Tm	–	–	–	–	–	–	–	–	–	–	–	–	–	–
Yb	4·26	–	4·75	7·88	3·62	–	4·30	8·32	–	5·37	–	9·81	–	4·75
Lu	0·615	–	0·737	1·20	0·455	–	0·715	1·25	–	0·792	–	1·33	–	0·736
Eu/Eu*	1·06	–	0·89	0·97	0·89	–	0·92	0·63	–	0·63	–	0·70	–	0·89
$(La/Yb)_n$	5·71	–	5·44	4·58	4·99	–	7·38	4·27	–	5·12	–	4·91	–	4·99

(continued)

Downloaded from petrology.oxfordjournals.org at Bibliotheque Fac de Medecine on January 12, 2011

Table 8: Continued

Sample:	07-70	07-139	07-141	07-142	07-144	07-145	07-146	07-147	07-162	07-164	07-165	07-167	07-168	07-171
Rock-type:	Doler.	Doler.	Doler.	Doler.	Doler.	Doler.	Doler.	Doler.	Doler.	Doler.	Doler.	Doler.	Doler.	Doler.
Location:	BZ	BZ	BZ	BZ	BZ	BZ	BZ	BZ	BZ	BZ	BZ	BZ	BZ	BZ
Xenoliths:														
East WGS84:	03·61·359	03·61·451	03·87·339	03·86·333	03·81·951	03·81·875	03·81·931	03·81·952	03·61·723	03·61·654	03·63·212	03·81·923	03·81·883	03·81·876
North WGS84:	55·60·887	55·59·745	55·74·945	557·50·93	55·74·694	55·74·683	55·74·696	55·74·687	55·62·216	55·62·423	55·63·418	55·74·678	55·74·693	55·74·672
SiO_2	49·19	47·01	51·94	46·31	47·08	47·31	47·98	47·62	50·66	49·19	45·86	49·08	46·80	49·03
TiO_2	2·76	3·98	3·04	4·26	3·45	3·63	2·86	3·54	3·02	3·11	4·62	3·45	3·52	4·04
Al_2O_3	14·51	13·52	13·95	14·38	13·63	12·92	13·88	14·04	14·39	13·57	13·03	13·89	15·70	14·50
FeO_t	15·17	16·50	13·85	16·28	16·05	16·12	14·97	15·39	14·18	15·39	17·06	15·01	15·30	15·54
MnO	0·22	0·29	0·23	0·19	0·25	0·24	0·12	0·24	0·28	0·21	0·31	0·23	0·21	0·21
MgO	5·74	4·84	3·98	4·07	5·31	5·39	6·29	4·79	3·91	4·06	5·88	4·57	5·00	4·56
CaO	9·02	8·79	6·72	8·87	9·31	9·48	8·68	9·26	6·42	8·64	9·72	8·10	9·39	7·14
Na_2O	2·72	2·71	3·41	2·92	3·13	3·20	2·83	2·79	2·92	2·87	2·17	3·08	2·56	3·14
K_2O	0·88	0·99	1·81	0·87	0·79	0·76	1·08	1·11	2·01	0·94	0·56	1·36	0·64	0·91
P_2O_5	0·30	0·70	0·91	1·06	0·78	1·17	1·36	0·88	1·07	1·05	0·85	0·87	0·78	0·96
LOI	0·03	0·13	0·12	0·09	0·24	0·18	0·13	0·33	0·23	0·45	0·09	0·08	0·14	0·03
Total	100·54	99·26	99·96	99·30	100·02	100·40	100·18	99·99	99·09	99·48	100·15	99·72	100·04	100·06
Fe-no.	0·73	0·77	0·78	0·80	0·75	0·75	0·70	0·76	0·78	0·79	0·74	0·77	0·75	0·72
Rb	9·66	10·4	12·8	10·2	9·92	9·74	9·43	10·1	14·7	18·4	9·52	17·1	7·41	16·9
Sr	577	429	630	617	501	517	484	412	625	583	519	522	437	515
Ba	403	523	721	345	379	319	379	410	580	521	349	472	373	778
V	225	272	170	286	331	315	355	298	–	165	264	216	301	339
Cr	48·0	49·5	45·6	64·3	93·2	79·0	81·5	68·8	–	42·8	147	59·5	59·5	79·9
Co	60·7	55·7	40·2	46·5	52·3	49·1	61·5	51·4	56·1	51·4	37·8	40·3	50·1	58·8
Ni	44·4	31·5	28·6	93·9	35·8	48·1	157	36·1	31·8	47·8	33·2	44·6	34·1	96·8
Cu	62·5	137	58·4	224	95·8	108	131	117	9·42	3·93	46·6	63·1	120	79·7
Zn	144	185	156	178	214	173	67·8	193	170·2	120	199	180	138	73·2
Ga	25·7	25·2	23·6	28·1	28·5	26·2	28·8	29·4	20·2	17·9	31·3	30·9	28·6	28·8
Zr	156	107	305	131	104	104	139	96·6	296	173	86·2	108	92·3	221
Hf	–	3·44	6·09	–	–	–	–	3·79	4·68	–	1·92	3·92	7·23	8·37
Nb	6·82	38·1	24·2	16·6	17·8	15·2	14·2	16·4	23·9	10·6	19·5	17·8	16·2	15·2
Ta	–	1·93	1·53	–	–	–	–	1·08	1·48	–	1·13	1·08	1·41	1·67
U	–	0·299	3·31	–	–	–	–	0·957	0·242	–	0·215	1·08	0·773	0·879
Th	–	0·918	2·50	–	–	–	–	1·33	1·58	–	0·891	1·78	2·72	3·20
Pb	6·60	9·11	8·72	9·70	11·3	9·16	6·72	6·13	9·82	13·6	1·71	5·52	7·61	5·32
Y	47·5	61·4	52·5	46·3	39·6	44·5	46·3	51·6	49·4	61·3	46·8	53·3	40·8	57·6
La	–	37·3	35·6	–	–	–	–	43·1	47·9	–	37·1	48·3	40·1	42·9
Ce	–	81·6	60·3	–	–	–	–	91·2	101	–	70·6	96·6	76·1	90·8
Pr	–	11·3	8·27	–	–	–	–	13·3	14·8	–	11·3	13·8	11·0	13·2
Nd	–	50·2	33·7	–	–	–	–	58·9	63·5	–	52·7	59·1	48·2	57·1
Sm	–	11·5	7·07	–	–	–	–	13·5	12·9	–	12·5	13·60	11·0	14·2
Eu	–	3·42	2·09	–	–	–	–	3·98	3·18	–	4·01	3·94	3·52	3·64
Gd	–	11·3	7·45	–	–	–	–	13·5	12·5	–	13·2	13·8	11·1	14·6
Tb	–	–	–	–	–	–	–	–	–	–	–	–	–	–
Dy	–	9·96	6·05	–	–	–	–	10·8	9·41	–	9·52	10·7	8·78	13·1
Ho	–	2·17	1·42	–	–	–	–	2·19	1·99	–	1·91	2·24	1·75	2·64
Er	–	5·85	4·00	–	–	–	–	5·32	4·71	–	4·39	5·39	4·40	6·71
Tm	–	–	–	–	–	–	–	–	–	–	–	–	–	–
Yb	–	5·39	4·28	–	–	–	–	4·60	4·15	–	3·51	4·49	3·57	5·54
Lu	–	0·871	0·709	–	–	–	–	0·669	0·599	–	0·511	0·632	0·513	0·809
Eu/Eu*	–	0·92	0·89	–	–	–	–	0·91	0·77	–	0·96	0·89	0·98	0·78
$(La/Yb)_n$	–	4·48	5·39	–	–	–	–	6·05	7·46	–	6·84	6·95	7·26	5·01

(continued)

Downloaded from petrology.oxfordjournals.org at Bibliotheque Fac de Medecine on January 12, 2011

Table 8: Continued

Sample:	07-179	07-180	07-183	07-185	07-186	07-187	07-188	07-189	07-190	07-191	07-192	07-193	07-194	07-195
Rock-type:	Doler.	Doler.	Doler.	Doler.	Doler.	Doler.	Doler.	Doler.	Doler.	Doler.	Doler.	Doler.	Doler.	Doler.
Location:	BZ	BZ	BZ	BZ	BZ	BZ	BZ	BZ	BZ	BZ	BZ	BZ	BZ	BZ
Xenoliths:														
East WGS84:	03·79·430	03·79·541	03·79·467	03·79·451	03·79·319	03·79·412	03·79·513	03·79·652	03·79·444	03·79·357	03·79·218	03·79·387	03·79·421	03·79·349
North WGS84:	55·74·139	55·74·218	55·74·317	55·74·239	55·74·146	55·74·232	55·74·323	55·74·234	55·74·344	55·74·125	55·74·356	55·74·347	55·74·248	55·74·149
SiO_2	47·77	48·53	48·46	47·86	48·97	49·89	49·29	47·71	48·53	49·06	51·94	48·55	48·92	48·54
TiO_2	3·40	2·82	3·05	3·91	3·18	2·68	2·83	3·78	3·31	3·66	3·27	3·17	3·12	3·26
Al_2O_3	14·05	14·67	14·40	14·53	14·09	14·19	14·32	13·10	14·29	14·07	14·02	13·78	14·34	13·99
FeO_t	15·55	14·50	15·48	14·70	14·82	15·19	15·15	15·19	14·83	14·87	13·19	15·01	15·22	15·22
MnO	0·30	0·21	0·18	0·23	0·23	0·19	0·13	0·23	0·22	0·22	0·23	0·23	0·22	0·24
MgO	5·15	5·65	5·39	5·64	5·13	5·52	5·47	5·54	4·88	5·29	4·36	5·27	5·14	5·08
CaO	9·35	9·79	9·39	8·99	9·07	8·75	8·81	9·56	9·19	8·73	7·09	8·99	8·65	9·12
Na_2O	2·80	2·63	2·50	2·59	3·50	2·80	2·69	3·08	3·19	2·88	3·45	2·97	2·74	2·89
K_2O	0·90	0·77	0·61	0·73	0·86	0·49	0·88	1·07	1·37	0·53	0·89	1·15	0·93	0·92
P_2O_5	0·55	0·82	0·33	0·83	0·63	0·61	0·62	0·66	0·81	0·74	1·26	0·76	0·70	0·69
LOI	0·35	0·03	0·18	0·02	0·00	0·12	0·00	0·05	0·04	0·24	0·22	0·21	0·07	0·03
Total	100·17	100·42	99·97	100·03	100·48	100·43	100·19	99·97	100·66	100·29	99·92	100·09	100·05	99·98
Fe-no.	0·75	0·72	0·74	0·72	0·74	0·73	0·74	0·73	0·75	0·74	0·75	0·74	0·75	0·75
Rb	9·62	8·03	6·71	8·84	10·8	17·3	17·2	8·32	5·59	8·22	17·1	8·56	6·75	7·21
Sr	452	523	468	612	513	579	509	498	478	569	604	488	504	498
Ba	487	515	548	391	288	624	599	743	576	602	633	490	601	652
V	249	214	287	246	212	199	115	196	228	213	163	215	254	248
Cr	45·2	56·5	48·0	72·6	47·0	45·2	51·4	67·2	63·3	54·9	62·3	45·3	47·9	60·2
Co	51·6	53·3	49·1	54·8	51·1	48·5	42·6	41·3	48·6	48·9	46·0	50·2	48·9	51·6
Ni	33·8	40·7	176	42·3	36·9	20·8	24·5	41·7	56·2	55·7	30·9	30·2	32·8	56·6
Cu	64·2	123	176	64·3	76·9	81·5	63·5	48·5	59·8	62·8	61·5	58·9	53·7	115
Zn	552	326	170	498	371	275	325	449	621	630	466	533	486	526
Ga	24·2	54·2	31·3	34·7	29·0	24·1	21·2	31·5	28·7	36·6	34·9	37·8	49·0	24·8
Zr	97·1	126	110	98·5	131	75·1	94·9	89·0	121	130	186	93·4	86·4	126
Hf	3·05	–	–	–	–	–	–	–	–	–	–	–	–	–
Nb	15·0	21·8	13·8	15·3	17·2	16·5	14·6	17·9	15·8	18·8	14·9	13·5	14·2	16·5
Ta	0·998	–	–	–	–	–	–	–	–	–	–	–	–	–
U	0·679	–	–	–	–	–	–	–	–	–	–	–	–	–
Th	0·841	–	–	–	–	–	–	–	–	–	–	–	–	–
Pb	9·52	6·12	8·43	9·41	6·34	8·45	6·18	7·54	6·98	4·12	7·63	7·41	6·85	4·98
Y	47·9	49·0	43·8	63·2	47·2	36·6	41·2	54·6	52·9	46·3	47·9	39·9	36·5	44·8
La	34·9	–	–	–	–	–	–	–	–	–	–	–	–	–
Ce	77·2	–	–	–	–	–	–	–	–	–	–	–	–	–
Pr	11·1	–	–	–	–	–	–	–	–	–	–	–	–	–
Nd	47·9	–	–	–	–	–	–	–	–	–	–	–	–	–
Sm	10·2	–	–	–	–	–	–	–	–	–	–	–	–	–
Eu	3·13	–	–	–	–	–	–	–	–	–	–	–	–	–
Gd	10·5	–	–	–	–	–	–	–	–	–	–	–	–	–
Tb	–	–	–	–	–	–	–	–	–	–	–	–	–	–
Dy	9·91	–	–	–	–	–	–	–	–	–	–	–	–	–
Ho	2·20	–	–	–	–	–	–	–	–	–	–	–	–	–
Er	5·64	–	–	–	–	–	–	–	–	–	–	–	–	–
Tm	–	–	–	–	–	–	–	–	–	–	–	–	–	–
Yb	5·05	–	–	–	–	–	–	–	–	–	–	–	–	–
Lu	0·898	–	–	–	–	–	–	–	–	–	–	–	–	–
Eu/Eu*	0·93	–	–	–	–	–	–	–	–	–	–	–	–	–
$(La/Yb)_n$	4·46	–	–	–	–	–	–	–	–	–	–	–	–	–

(continued)

Downloaded from petrology.oxfordjournals.org at Bibliotheque Fac de Medecine on January 12, 2011

Table 8: Continued

Sample:	07-196	07-197	07-198	07-199	07-10	07-11	07-82	07-21	07-25	07-56	07-57	07-58	07-59	07-174
Rock-type:	Doler.	Doler.	Doler.	Doler.	Monz.	Doler.	Monz.	Doler.	Doler.	Doler.	Doler.	Doler.	Doler.	Doler.
Location:	BZ	BZ	BZ	BZ	LS	LS	LS	LS	LS	LS	LS	LS	LS	LS
Xenoliths:														
East WGS84:	03·79·318	03·79·463	03·79·564	03·81·918	03·65·400	03·65·400	03·79·421	03·78·430	03·78·027	03·76·622	03·76·622	03·76·657	03·76·725	03·78·341
North WGS84:	55·74·267	55·74·189	55·74·156	55·74·683	55·64·900	55·64·900	55·70·609	55·58·278	55·58·200	55·57·933	55·57·933	55·57·932	55·57·925	55·58·550
SiO_2	48·37	49·09	48·77	50·36	52·66	51·14	56·97	46·99	47·66	47·21	46·91	47·62	47·59	44·04
TiO_2	3·58	2·71	2·72	3·26	3·22	3·15	1·47	4·34	4·32	4·11	4·22	4·38	4·19	5·00
Al_2O_3	13·77	15·49	14·34	14·01	14·11	13·45	15·80	13·69	13·54	14·10	13·12	13·47	13·65	12·61
FeO_t	15·37	15·14	15·11	14·45	13·21	14·07	9·39	15·53	14·89	15·05	14·84	14·81	14·26	16·96
MnO	0·20	0·13	0·19	0·21	0·17	0·25	0·22	0·21	0·21	0·23	0·22	0·22	0·19	0·25
MgO	5·16	5·11	4·44	4·88	3·77	4·04	2·01	5·34	5·11	5·07	4·98	5·15	4·75	5·53
CaO	9·18	6·92	9·39	7·55	6·98	7·26	4·81	8·26	8·99	8·62	8·88	9·02	8·54	9·97
Na_2O	3·11	2·27	2·61	2·82	4·18	3·27	5·26	3·26	3·11	3·44	3·14	3·13	3·45	2·77
K_2O	0·77	1·07	1·52	1·40	1·54	1·54	3·08	0·61	0·66	1·23	1·18	0·63	1·49	0·66
P_2O_5	0·64	0·62	0·78	1·02	0·71	0·99	0·75	0·83	0·78	0·94	0·73	0·77	0·90	0·84
LOI	0·11	1·12	0·23	0·04	0·11	0·47	0·11	0·13	0·32	0·06	0·78	0·23	0·26	0·65
Total	100·26	99·67	100·10	100·00	100·66	99·63	99·87	99·19	99·59	100·06	99·00	99·43	99·27	99·28
Fe-no.	0·75	0·75	0·77	0·75	0·78	0·78	0·82	0·74	0·74	0·75	0·75	0·74	0·75	0·75
Rb	7·06	15·6	9·31	20·2	16·1	19·8	38·3	10·5	12·4	12·4	12·8	13·6	11·7	9·01
Sr	524	612	518	568	1006	431	524	427	428	435	422	429	390	442
Ba	542	589	513	649	815	738	1294	396	355	420	408	375	423	337
V	255	313	259	184	128	191	47·7	264	283	225	285	300	244	338
Cr	57·5	95·6	61·2	56·3	39·8	57·3	34·2	63·0	60·4	74·2	55·3	57·8	86·1	116
Co	54·3	70·3	40·7	50·0	19·5	26·1	18·2	50·6	49·6	46·4	43·7	42·9	42·3	48·9
Ni	51·6	39·1	51·0	48·4	7·21	13·1	42·8	64·9	57·9	47	56·3	52·3	35·2	54·9
Cu	89·3	120	78·4	155	8·01	29·1	30·1	76·5	117	91·3	111	111	63·2	123
Zn	475	203	351	561	118	192	114	168	174	160	160	160	202	168
Ga	23·6	27·6	24·9	42·2	26·5	30·6	34·8	29·5	24·4	27·3	27·1	27·4	29·1	27·1
Zr	105	203	91·5	201	172	211	1278	84·2	121	109	126	128	152	143
Hf	–	–	–	–	–	4·71	–	3·41	3·04	3·39	3·87	3·20	3·45	3·51
Nb	19·0	16·5	17·8	19·6	35·4	25·7	35·7	12·2	13·3	14·2	11·7	13·3	17·2	15·6
Ta	–	–	–	–	–	1·23	–	0·997	1·11	0·781	0·994	0·783	1·14	1·37
U	–	–	–	–	–	0·287	–	0·856	0·813	0·826	0·858	0·834	0·992	0·507
Th	–	–	–	–	–	1·52	–	1·18	0·946	1·09	1·35	1·17	0·863	0·816
Pb	5·81	6·74	7·63	8·16	9·12	9·51	8·23	3·31	7·13	7·62	6·93	4·61	8·72	6·93
Y	59·8	63·2	67·3	49·6	21·3	54·5	49·1	43·1	44·6	43·6	43·6	45	52·7	46·6
La	–	–	–	–	–	42·2	–	42·4	41·8	43·1	43·8	45·2	48·0	39·3
Ce	–	–	–	–	–	78·7	–	81·9	82·2	89·2	89·7	88·0	99·2	73·2
Pr	–	–	–	–	–	11·1	–	12·0	11·8	13·0	13·1	12·9	14·2	10·0
Nd	–	–	–	–	–	48·9	–	51·8	51·6	56·2	56·5	55·7	62·0	40·6
Sm	–	–	–	–	–	11·4	–	11·9	11·9	12·8	12·9	12·7	15·1	9·33
Eu	–	–	–	–	–	3·03	–	3·68	3·66	3·93	3·91	3·86	4·27	2·44
Gd	–	–	–	–	–	11·0	–	12·3	12·1	13·1	13·0	13·1	14·7	9·5
Tb	–	–	–	–	–	–	–	–	–	–	–	–	–	–
Dy	–	–	–	–	–	7·07	–	9·47	9·49	9·82	10·2	9·99	11·5	8·42
Ho	–	–	–	–	–	1·41	–	1·87	1·94	1·99	2·00	2·03	2·37	1·80
Er	–	–	–	–	–	3·43	–	4·35	4·72	4·73	4·87	4·7695	5·51	4·91
Tm	–	–	–	–	–	–	–	–	–	–	–	–	–	–
Yb	–	–	–	–	–	2·85	–	3·67	3·81	3·98	4·20	3·91	4·53	4·83
Lu	–	–	–	–	–	0·431	–	0·512	0·557	0·540	0·588	0·563	0·655	0·765
Eu/Eu*	–	–	–	–	–	0·83	–	0·94	0·94	0·94	0·93	0·92	0·88	0·80
$(La/Yb)_n$	–	–	–	–	–	9·57	–	7·47	7·09	7·01	6·75	7·49	6·86	5·26

(continued)

Downloaded from petrology.oxfordjournals.org at Bibliotheque Fac de Medecine on January 12, 2011

Table 8: Continued

Sample:	S9-106	03-01	03-02	03-03	03-04	03-06	03-08	03-09	03-10	03-11	03-12	03-13	03-14	03-15
Rock-type:	Monz.	Granite	Granite	Syenite	Granite	Granite	Syenite	Granite	Syenite	Granite	Monz.	Syenite	Gabbro	Granite
Location:	LS	US	US	US	US	US	PC	PC	PC	PC	US	PC	US	PC
Xenoliths:						X							X	
East WGS84:	03·74·973	03·79·750	03·79·748	03·79·740	03·79·736	03·79·750	03·86·177	03·86·177	03·86·175	03·85·745	03·90·616	03·90·723	03·90·525	03·91·000
North WGS84:	55·68·623	55·58·400	55·58·330	55·58·317	55·58·256	55·58·220	55·59·866	55·59·866	55·59·860	55·60·008	55·58·810	55·58·808	55·58·816	55·58·900
SiO_2	61·68	74·07	76·43	65·88	72·92	76·61	68·44	70·60	67·87	69·87	55·04	67·98	50·46	71·14
TiO_2	0·83	0·35	0·08	0·42	0·43	0·27	0·49	0·44	0·67	0·49	2·34	0·64	2·70	0·44
Al_2O_3	16·36	11·65	11·42	13·21	11·48	11·40	13·32	13·06	12·78	12·85	14·62	12·61	18·89	12·71
FeO_t	6·02	3·50	1·36	7·65	4·04	2·77	5·79	5·03	5·90	5·60	9·39	5·53	11·45	5·11
MnO	0·12	0·07	0·01	0·10	0·11	0·03	0·15	0·11	0·13	0·13	0·16	0·07	0·13	0·11
MgO	0·98	0·30	0·01	0·88	0·20	0·23	0·34	0·28	0·46	0·29	2·76	0·42	2·48	0·32
CaO	2·73	0·51	0·27	3·12	0·73	0·26	1·70	1·39	1·76	1·34	5·63	1·43	7·70	1·27
Na_2O	5·53	4·09	4·19	4·60	4·39	3·99	4·86	4·60	4·74	4·54	3·84	4·62	4·02	4·36
K_2O	4·94	4·79	4·47	3·79	4·63	4·87	4·51	4·60	4·46	4·55	2·99	4·53	1·06	4·56
P_2O_5	0·10	0·09	0·04	0·14	0·09	0·04	0·12	0·10	0·18	0·12	0·72	0·17	1·33	0·10
LOI	0·53	0·07	1·50	0·46	0·47	0·10	0·02	0·06	0·44	0·10	1·59	1·56	0·16	0·07
Total	99·82	99·45	99·78	100·17	99·46	100·54	99·71	100·24	99·37	99·85	99·05	99·54	100·28	100·16
Fe-no.	0·86	0·92	1·00	0·90	0·95	0·92	0·94	0·95	0·93	0·95	0·77	0·93	0·82	0·94
Rb	39·4	118	146	120	120	126	70·2	96·2	96·0	99·1	42·9	79·3	16·4	84·3
Sr	245	47·2	12·3	51·8	50·0	19·3	151	132	134	130	330	85·0	601	119
Ba	953	324	78·0	502	316	126	813	705	579	701	1052	513	234	638
V	47·2	9·22	8·93	2·68	4·67	6·38	1·36	2·59	13·0	1·18	28·4	2·42	141	5·68
Cr	34	10·8	23·4	13·6	12·2	5·32	17·3	16·4	13·5	15·1	21·8	23·6	23·2	3·92
Co	8·23	1·21	1·12	1·18	2·34	0·980	2·43	2·05	2·51	2·53	17·3	2·65	48·6	2·25
Ni	10·2	4·95	0·713	7·02	8·07	2·13	3·17	16·7	8·45	13·2	4·05	2·61	17·3	9·73
Cu	22	7·27	4·45	6·67	7·05	1·83	12·62	11·2	12·0	11·2	29·8	10·1	41·2	10·1
Zn	154	99·8	30·1	166	212	91·1	199	165	218	186	85·4	99·1	127	93·4
Ga	31·2	30·1	34·7	37·1	35·7	39·9	31·7	30·6	33·4	28·2	28·5	35·1	28·7	30·5
Zr	1154	815	245	874	1017	637	1081	1058	1099	982	537	1220	222	1098
Hf	–	25·1	–	–	–	21·9	28·8	32·9	–	28·7	–	–	–	30·4
Nb	68·2	89·9	155	104	110	83·6	64·3	80·9	95·0	74·9	42·2	69·9	37·3	86·6
Ta	–	3·17	–	–	–	2·27	5·16	4·87	–	4·62	–	–	–	4·62
U	–	3·35	–	–	–	3·03	1·37	2·76	–	2·33	–	–	–	2·29
Th	–	14·0	–	–	–	13·3	6·72	12·0	–	10·3	–	–	–	11·4
Pb	11·3	14·3	6·93	11·8	10·5	11·1	12·3	11·7	5·89	14·5	6·76	6·22	7·46	12·1
Y	81·5	87·7	42·0	107	112	77·6	85·0	88·1	101	85·4	68·4	82·4	41·6	97·9
La	–	80·0	–	–	–	146	64·2	82·9	–	73·2	–	–	–	82·7
Ce	–	168	–	–	–	227	142	175	–	160	–	–	–	166
Pr	–	–	–	–	–	–	–	–	–	–	–	–	–	–
Nd	–	81·6	–	–	–	105	73·8	83·4	–	78·5	–	–	–	86·0
Sm	–	16·3	–	–	–	22·1	14·9	18·5	–	18·0	–	–	–	18·5
Eu	–	2·36	–	–	–	2·43	3·45	3·50	–	3·70	–	–	–	3·15
Gd	–	16·5	–	–	–	19·0	12·5	14·6	–	15·9	–	–	–	18·4
Tb	–	2·63	–	–	–	2·74	1·68	2·10	–	2·26	–	–	–	2·65
Dy	–	–	–	–	–	–	–	–	–	–	–	–	–	–
Ho	–	2·93	–	–	–	3·33	1·89	2·43	–	2·73	–	–	–	3·03
Er	–	–	–	–	–	–	–	–	–	–	–	–	–	–
Tm	–	–	–	–	–	–	–	–	–	–	–	–	–	–
Yb	–	7·98	–	–	–	8·26	4·26	6·06	–	7·18	–	–	–	7·98
Lu	–	1·05	–	–	–	1·20	0·610	0·860	–	1·05	–	–	–	1·01
Eu/Eu*	–	0·44	–	–	–	0·37	0·78	0·66	–	0·67	–	–	–	0·53
$(La/Yb)_n$	–	6·49	–	–	–	11·47	9·75	8·85	–	6·59	–	–	–	6·71

(continued)

Downloaded from petrology.oxfordjournals.org at Bibliotheque Fac de Medecine on January 12, 2011

Table 8: Continued

Sample:	03-16	03-17	03-18	03-19	03-20	03-21	03-23	03-24	03-25	03-26	03-27	03-28	03-29	03-30
Rock-type:	Syenite	Syenite	Granite	Monz.	Granite	Granite	Granite	Syenite	Granite	Monz.	Granite	Granite	Syenite	Granite
Location:	US	US	US	US	US	US	US	US	US	US	US	US	US	US
Xenoliths:	X	X	X	X			X	X		X	X			
East WGS84:	03·90·025	03·90·025	03·91·200	03·91·207	03·82·200	03·82·007	03·82·020	03·82·066	03·82·500	03·85·807	03·85·410	03·85·200	03·86·100	03·86·100
North WGS84:	55·58·820	55·58·820	55·58·400	55·58·403	55·52·287	55·52·101	55·51·955	55·51·902	55·52·300	55·58·200	55·58·185	55·58·200	55·57·400	55·57·400
SiO_2	66·95	66·92	69·31	60·28	76·04	72·72	76·29	63·98	76·34	58·80	72·66	76·39	68·14	72·59
TiO_2	0·75	0·75	0·72	1·23	0·23	0·43	0·25	1·01	0·25	1·47	0·29	0·27	0·74	0·42
Al_2O_3	14·71	14·28	12·60	15·84	11·13	11·74	11·60	12·52	11·17	12·24	12·21	10·99	12·91	13·13
FeO_t	5·73	6·20	4·79	7·07	2·35	3·80	2·36	9·09	2·44	13·36	3·56	2·84	7·06	3·98
MnO	0·09	0·11	0·02	0·13	0·05	0·09	0·04	0·18	0·01	0·24	0·02	0·04	0·08	0·03
MgO	0·97	0·77	0·43	1·22	0·01	0·09	0·07	0·73	0·37	1·12	0·05	0·07	0·70	0·42
CaO	1·68	1·07	2·23	3·46	0·26	0·55	0·39	1·83	0·06	3·11	0·43	0·28	0·94	0·57
Na_2O	5·10	4·69	4·14	5·72	4·39	4·43	4·36	4·87	3·96	4·66	4·37	3·59	4·34	4·48
K_2O	4·29	4·93	4·63	3·13	4·54	4·76	4·64	4·09	4·58	3·41	4·54	4·44	4·49	4·95
P_2O_5	0·19	0·15	0·17	0·43	0·06	0·09	0·04	0·28	0·05	0·46	0·04	0·04	0·19	0·10
LOI	0·16	0·08	0·26	0·90	0·54	0·58	0·64	0·58	0·13	0·79	0·53	0·16	0·12	0·11
Total	100·59	99·92	99·27	99·37	99·55	99·25	100·64	99·13	99·33	99·64	98·67	99·08	99·68	100·75
Fe-no.	0·86	0·89	0·92	0·85	1·00	0·98	0·97	0·93	0·87	0·92	0·99	0·98	0·91	0·90
Rb	59·2	80·6	88·8	41·6	98·8	121	101	76·3	98·7	74·0	98·7	108	89·9	97·9
Sr	154	108	94·9	270	20·0	41·4	21·5	116	27·3	174	52·0	15·2	86·4	77·4
Ba	994	672	421	1216	186	344	247	557	210	600	398	167	495	499
V	11·8	2·18	2·26	1·12	5·50	2·00	2·64	6·81	4·71	11·8	5·06	8·42	6·01	11·0
Cr	8·29	14·8	6·12	16·5	18·7	12·9	15·7	15·2	10·2	13·0	15·9	5·91	6·12	4·57
Co	4·13	3·58	3·78	10·2	1·21	2·43	1·06	4·34	1·28	13·1	2·24	1·19	3·77	2·66
Ni	12·1	8·97	5·67	1·33	0·737	5·72	0·723	5·40	9·45	13·7	0·601	1·63	5·81	6·72
Cu	9·99	12·3	10·4	13·5	2·78	11·2	3·77	18·5	3·99	35·1	6·27	13·9	13·6	118
Zn	270	234	370	133	86·4	170	72·2	201	143	171	66·0	37·5	147	190
Ga	27·0	32·3	28·1	33·0	35·9	36·1	36·0	40·3	29·4	37·5	34·4	26·2	28·1	30·4
Zr	998	960	1431	1241	479	964	567	1328	683	2043	428	674	1448	1018
Hf	26·4	25·7	37·9	–	–	–	–	–	23·8	–	–	18·5	36·9	28·6
Nb	54·3	57·6	77·2	48·7	77·6	99·3	77·2	82·1	225	70·7	84·4	74·4	67·3	70·6
Ta	7·27	4·62	5·91	–	–	–	–	–	2·00	–	–	1·94	5·87	3·95
U	1·09	1·82	2·20	–	–	–	–	–	10·9	–	–	2·34	2·09	2·66
Th	5·26	7·37	8·80	–	–	–	–	–	20·7	–	–	10·3	8·50	9·71
Pb	9·61	11·6	9·90	6·04	8·13	7·36	5·08	9·85	7·86	8·37	8·78	11·2	7·17	19·2
Y	72·7	73·3	92·5	70·8	56·4	102	73·4	117	105	127	71·8	62·8	94·8	77·9
La	55·8	63·6	67·8	–	–	–	–	–	112	–	–	69·9	86·4	79·9
Ce	130	139	162	–	–	–	–	–	255	–	–	145	195	169
Pr	–	–	–	–	–	–	–	–	–	–	–	–	–	–
Nd	69·0	82·7	91·1	–	–	–	–	–	125	–	–	71·4	110	88·8
Sm	14·8	18·2	20·9	–	–	–	–	–	30·5	–	–	14·4	34·6	19·0
Eu	4·12	4·42	3·55	–	–	–	–	–	3·68	–	–	1·82	3·73	3·60
Gd	14·7	16·3	19·2	–	–	–	–	–	27·9	–	–	12·8	20·5	16·7
Tb	2·13	2·32	2·71	–	–	–	–	–	4·11	–	–	1·77	2·86	2·35
Dy	–	–	–	–	–	–	–	–	–	–	–	–	–	–
Ho	2·30	2·49	3·05	–	–	–	–	–	4·40	–	–	2·11	3·19	2·69
Er	–	–	–	–	–	–	–	–	–	–	–	–	–	–
Tm	–	–	–	–	–	–	–	–	–	–	–	–	–	–
Yb	5·57	5·95	7·21	–	–	–	–	–	7·75	–	–	5·74	7·59	7·17
Lu	0·770	0·840	1·03	–	–	–	–	–	0·970	–	–	0·810	1·05	1·02
Eu/Eu*	0·86	0·79	0·55	–	–	–	–	–	0·39	–	–	0·41	0·43	0·62
$(La/Yb)_n$	6·48	6·91	6·09	–	–	–	–	–	9·32	–	–	7·88	7·37	7·21

(continued)

Downloaded from petrology.oxfordjournals.org at Bibliotheque Fac de Medecine on January 12, 2011

Table 8: Continued

Sample:	03-31	03-32	03-33	03-34	03-35	03-36	03-37	03-39	03-40	03-41	03-42	03-43	03-44	03-45
Rock-type:	Syenite	Monz.	Monz.	Granite	Granite	Granite	Syenite	Syenite	Granite	Monz.	Monz.	Syenite	Granite	Granite
Location:	US	US	US	US	US	US	US	US	US	US	US	US	US	US
Xenoliths:	X	X	X	X		X	X	X	X					
East WGS84:	03·86·124	03·86·110	03·86·102	03·85·807	03·85·807	03·76·100	03·76·100	03·76·142	03·76·200	03·76·300	03·76·300	03·76·315	03·78·250	03·76·100
North WGS84:	55·58·763	55·58·783	55·58·778	55·58·797	55·58·797	55·56·800	55·56·800	55·56·790	55·56·500	55·56·450	55·56·450	55·56·454	55·57·300	55·57·312
SiO_2	63·25	60·50	53·19	70·08	72·68	74·87	65·26	62·11	75·69	56·17	61·09	63·39	74·71	71·13
TiO_2	1·29	1·52	2·58	0·69	0·48	0·29	0·62	1·16	0·27	2·21	1·27	1·20	0·34	0·41
Al_2O_3	12·61	13·56	13·98	12·54	12·07	12·26	14·60	13·78	12·10	14·09	14·49	13·31	11·95	12·63
FeO_t	8·43	9·27	10·81	6·40	4·46	2·98	6·99	8·80	2·28	11·65	9·52	8·52	3·42	5·26
MnO	0·15	0·19	0·17	0·16	0·09	0·05	0·16	0·21	0·04	0·20	0·23	0·19	0·08	0·10
MgO	1·07	1·29	2·77	0·36	0·29	0·09	0·60	0·60	0·18	2·70	0·96	0·80	0·20	0·17
CaO	2·79	3·96	5·13	1·28	0·85	0·73	1·80	3·27	0·53	5·36	3·63	3·01	0·63	0·64
Na_2O	4·92	4·86	5·47	4·43	4·23	3·71	5·02	5·13	3·88	3·92	4·61	4·87	3·99	4·53
K_2O	4·07	3·02	2·24	4·52	4·60	5·07	4·87	3·57	5·12	2·54	3·40	3·69	4·68	4·32
P_2O_5	0·40	0·59	1·32	0·15	0·11	0·04	0·19	0·29	0·04	0·85	0·30	0·31	0·07	0·09
LOI	0·77	0·87	1·96	0·04	0·07	0·08	0·04	0·29	0·09	0·11	0·04	0·38	0·05	0·32
Total	99·72	99·58	99·59	100·62	99·90	100·14	100·12	99·20	100·19	99·77	99·51	99·64	100·09	99·57
Fe-no.	0·89	0·88	0·80	0·95	0·94	0·97	0·92	0·94	0·93	0·81	0·91	0·91	0·94	0·97
Rb	72·8	50·7	24·8	107	99·9	104	65·9	61·2	96·4	48·1	51·8	48·9	114	119
Sr	144	297	352	87·1	66·1	56·7	99·8	265	16·6	362	330	294	54·0	45·4
Ba	501	652	556	385	405	379	526	1055	135	797	1010	869	339	302
V	37·4	3·93	76·8	4·47	6·17	5·45	11·0	1·14	7·45	45·6	44·5	30·3	7·19	4·53
Cr	19·8	17·6	21·9	20·5	7·12	6·32	33·2	12·7	3·57	34·7	34·8	20·8	4·12	14·8
Co	4·65	9·88	27·3	3·62	2·49	1·48	3·91	3·56	0·870	18·8	7·92	4·32	2·23	1·24
Ni	11·8	3·04	15·1	9·44	9·44	1·25	5·43	5·04	2·33	41·3	9·34	19·0	32·5	3·59
Cu	13·0	16·7	23·5	11·2	5·93	40·7	15·0	21·6	4·28	80·8	20·9	30·6	10·0	7·28
Zn	139	230	187	327	175	94·9	91·7	234	78·4	202	147	294	172	163
Ga	35·7	37·8	29·1	28·7	25·2	24·2	24·9	35·8	22·7	27·6	30·4	33·9	27·3	35·4
Zr	1133	700	625	1121	1013	780	1142	1353	672	786	1264	1390	699	878
Hf	–	–	–	30·9	27·7	26·1	29·5	–	19·1	21·5	30·4	–	20·9	–
Nb	81·0	89·8	59·1	88·7	86·9	86·4	64·2	88·6	56·3	73·8	67·1	82·2	70·9	96·8
Ta	–	–	–	4·97	3·97	2·95	5·55	–	1·80	11·5	8·94	–	2·77	–
U	–	–	–	2·50	2·92	4·36	1·87	–	1·53	1·62	1·40	–	2·77	–
Th	–	–	–	11·3	12·3	18·2	6·83	–	8·01	5·69	5·43	–	10·4	–
Pb	5·25	7·10	21·9	17·5	13·8	16·4	14·1	3·65	4·46	13·2	10·1	2·61	11·1	9·09
Y	107	112	84·2	109	108	91·7	86·4	91·6	57·6	103	80·5	111	77·4	104
La	–	–	–	94·2	83·3	105	71·8	–	117	61·4	66·2	–	71·9	–
Ce	–	–	–	210	187	220	171	–	255	165	147	–	163	–
Pr	–	–	–	–	–	–	–	–	–	–	–	–	–	–
Nd	–	–	–	109	95·0	94·0	98·9	–	120·99	95·6	82·6	–	78·4	–
Sm	–	–	–	24·6	21·1	19·2	22·9	–	23·9	24·1	17·7	–	16·4	–
Eu	–	–	–	3·84	3·37	2·17	3·74	–	1·54	5·10	5·91	–	2·27	–
Gd	–	–	–	22·4	19·7	17·4	19·9	–	18·9	23·4	17·9	–	16·9	–
Tb	–	–	–	3·04	2·94	2·59	2·76	–	2·46	3·4	2·68	–	2·21	–
Dy	–	–	–	–	–	–	–	–	–	–	–	–	–	–
Ho	–	–	–	3·60	3·59	3·18	3·15	–	2·44	3·58	2·69	–	2·66	–
Er	–	–	–	–	–	–	–	–	–	–	–	–	–	–
Tm	–	–	–	–	–	–	–	–	–	–	–	–	–	–
Yb	–	–	–	8·95	8·98	8·53	7·26	–	5·81	7·74	6·50	–	6·48	–
Lu	–	–	–	1·26	1·20	1·23	1·12	–	0·900	0·970	0·920	–	0·840	–
Eu/Eu*	–	–	–	0·50	0·51	0·37	0·54	–	0·22	0·66	1·02	–	0·42	–
$(La/Yb)_n$	–	–	–	6·81	6·00	8·04	6·40	–	13·04	5·13	6·59	–	7·18	–

(continued)

Downloaded from petrology.oxfordjournals.org at Bibliotheque Fac de Medecine on January 12, 2011

Table 8: Continued

Sample:	03-46	03-47	03-48	03-49	03-50	03-51	03-52	04-53	04-55	04-56	04-57	07-59	07-60	07-61
Rock-type:	Syenite	Syenite	Syenite	Monz.	Syenite	Syenite	Syenite	Granite	Granite	Monz.	Monz.	Syenite	Syenite	Granite
Location:	US	US	US	US	US	US	US	US	PC	US	US	PC	PC	PC
Xenoliths:	X	X		X	X	X	X			X	X			
East WGS84:	03·78·500	03·76·108	03·78·200	03·77·525	03·77·512	03·91·100	03·91·100	03·82·200	03·83·000	03·83·100	03·83·100	03·85·310	03·85·309	03·91·200
North WGS84:	55·57·600	55·57·300	55·55·250	55·55·920	55·55·912	55·58·220	55·58·220	55·50·500	55·50·500	55·50·700	55·50·700	55·59·700	55·59·304	55·58·400
SiO_2	67·51	65·85	63·97	56·94	65·15	63·21	66·33	75·12	69·67	56·27	57·32	67·45	67·97	70·15
TiO_2	0·93	0·91	1·40	2·89	1·34	1·01	0·61	0·20	0·46	2·03	1·45	0·50	0·43	0·35
Al_2O_3	12·26	12·68	13·35	13·56	12·75	13·63	15·01	12·05	12·96	15·06	15·29	13·49	13·13	12·98
FeO_t	7·77	7·87	8·54	10·25	6·81	9·25	5·91	2·04	4·44	11·13	9·53	5·44	4·80	2·46
MnO	0·18	0·17	0·18	0·13	0·18	0·22	0·13	0·02	0·10	0·21	0·25	0·13	0·06	0·04
MgO	0·76	0·61	1·38	2·67	1·41	0·75	0·53	0·09	0·28	1·12	1·54	0·37	0·54	0·27
CaO	1·91	1·73	3·62	5·34	2·01	2·19	1·61	0·17	1·38	3·34	4·48	1·70	1·17	1·61
Na_2O	4·16	4·88	4·28	4·33	4·25	4·60	5·25	4·30	4·68	4·78	5·18	4·72	4·61	4·65
K_2O	4·21	4·25	3·35	2·24	3·94	4·55	4·65	4·89	4·78	3·96	3·28	4·84	4·87	4·92
P_2O_5	0·20	0·24	0·30	0·52	0·29	0·23	0·14	0·04	0·10	0·49	0·46	0·12	0·10	0·08
LOI	0·05	0·22	0·09	1·10	0·71	0·04	0·04	0·50	0·33	0·14	0·13	0·32	1·10	1·22
Total	99·91	99·38	100·43	99·94	98·82	99·65	100·18	99·39	99·15	98·30	98·78	99·05	98·75	98·70
Fe-no.	0·91	0·93	0·86	0·79	0·83	0·93	0·92	0·96	0·94	0·91	0·86	0·94	0·90	0·90
Rb	96·2	78·0	61·4	40·8	81·5	70·2	61·1	94·1	107	56·1	49·7	81·2	101	106
Sr	96·5	108	218	298	166	122	95·4	103	75·7	358	347	94·3	93·2	73·7
Ba	450	520	454	356	469	556	697	133	427	795	746	493	479	353
V	17·5	5·96	61·5	93·1	63·5	27·9	14·2	4·32	5·43	93·2	88·3	7·24	8·13	5·32
Cr	4·59	9·46	20·6	44·3	26·0	29·7	11·5	4·23	23·3	38·2	41·3	8·23	6·74	5·43
Co	5·11	3·47	12·0	17·8	3·8	5·26	3·29	2·18	1·98	6·42	6·96	1·53	1·57	2·46
Ni	11·3	6·19	18·1	35·9	18·7	17·3	15·3	2·23	4·12	13·2	21·3	7·13	8·25	5·43
Cu	12·1	15·3	21·4	33·3	26·8	15·4	7·33	9·87	15·4	22·3	24·4	9·76	8·67	8·74
Zn	200	294	228	230	129	147	199	289	162	166	187	166	49·8	45·7
Ga	32·1	39·1	34·2	31·5	33·5	25·3	28·1	29·4	36·5	26·7	31·7	32·8	34·9	36·5
Zr	1458	1549	1239	635	951	1827	793	565	1048	2383	3265	1224	1268	1038
Hf	39·3	–	31·5	–	–	44·9	20·3	13·7	24·3	46·1	63·4	26·4	27·9	22·7
Nb	103	81·3	83·2	67·0	75·9	55·0	45·8	72·3	92·5	71·6	73·9	86·4	83·2	91·9
Ta	6·65	–	7·31	–	–	7·72	5·07	6·12	6·94	3·71	8·78	4·30	6·42	6·07
U	2·94	–	2·40	–	–	1·75	1·15	2·25	2·89	2·25	2·43	2·11	2·71	2·49
Th	12·6	–	8·55	–	–	6·67	5·24	9·69	12·9	8·25	5·80	9·39	12·3	12·2
Pb	18·7	8·30	11·6	5·53	8·30	7·48	22·1	4·53	6·12	12·7	13·3	8·34	7·89	6·32
Y	113	111	101	81·4	89·5	66·0	63·3	78·5	114	82·3	83·7	101	105	109
La	84·7	–	74·0	–	–	72·7	50·5	61·3	105	80·9	85·2	89·7	97·0	101
Ce	198	–	187	–	–	192	113	164	240	236	239	216	233	239
Pr	–	–	–	–	–	–	–	–	–	–	–	–	–	–
Nd	115	–	92·8	–	–	116	69·2	76·4	116	125	140	107	106	107
Sm	23·9	–	22·1	–	–	26·9	13·3	15·6	22·1	27·5	33·7	21·3	21·4	20·4
Eu	3·87	–	4·59	–	–	4·28	4·28	2·19	3·78	7·25	7·87	4·77	4·41	3·97
Gd	23·4	–	19·9	–	–	25·5	12·3	–	–	–	–	–	–	–
Tb	3·22	–	3·33	–	–	3·65	2·01	2·46	3·35	4·30	5·55	3·26	3·28	3·06
Dy	–	–	–	–	–	–	–	–	–	–	–	–	–	–
Ho	3·67	–	3·56	–	–	3·43	2·36	0·460	0·640	0·720	0·940	0·530	0·560	0·550
Er	–	–	–	–	–	–	–	–	–	–	–	–	–	–
Tm	–	–	–	–	–	–	–	–	–	–	–	–	–	–
Yb	9·11	–	8·34	–	–	8·34	5·71	5·47	9·14	10·56	14·27	8·14	8·84	8·56
Lu	1·1	–	1·07	–	–	1·12	0·810	1·230	1·32	1·53	2·15	1·22	1·29	1·20
Eu/Eu*	0·51	–	0·68	–	–	0·50	1·03	0·43	0·53	0·81	0·71	0·69	0·64	0·60
$(La/Yb)_n$	6·01	–	5·74	–	–	5·64	5·72	7·25	7·40	4·95	3·86	7·13	7·10	7·62

(continued)

Downloaded from petrology.oxfordjournals.org at Bibliotheque Fac de Medecine on January 12, 2011

Table 8: Continued

Sample:	07-62	02-01	02-03	02-04	02-05	02-07	02-08	02-09	02-10	P4	P6	P7	P8	P18
Rock-type:	Granite	Doler.	Doler.	Doler.	Doler.	Doler.	Doler.	Doler.	Doler.	Doler.	Doler.	Doler.	Doler.	Doler.
Location:	US	US	US	US	US	US	US	US	US	US	US	US	US	US
Xenoliths:														
East WGS84:	03·81·200	03·81·620	03·80·730	03·81·810	03·81·640	03·77·525	03·77·505	03·77·460	03·77·320	03·91·420	03·91·120	03·91·820	03·76·130	03·86·220
North WGS84:	55·52·600	55·52·210	55·54·110	55·53·720	55·53·620	55·55·920	55·55·900	55·56·030	55·56·110	55·59·720	55·59·130	55·57·960	55·57·130	55·60·110
SiO_2	72·70	46·10	49·00	48·30	46·00	47·22	47·12	48·12	46·12	46·70	46·21	46·54	46·80	47·41
TiO_2	0·35	3·60	4·40	3·60	4·70	3·59	3·98	4·02	4·13	4·50	3·98	4·13	4·80	3·87
Al_2O_3	12·13	14·90	13·50	15·00	14·90	14·21	13·58	13·12	13·67	14·60	13·69	14·12	13·20	13·86
FeO_t	3·24	11·90	14·70	13·40	14·90	14·67	14·98	14·24	14·98	14·90	14·87	14·42	16·00	14·62
MnO	0·08	0·10	0·20	0·20	0·20	0·21	0·19	0·19	0·19	0·20	0·24	0·21	0·20	0·2
MgO	0·33	4·90	4·80	5·90	5·50	4·98	5·23	5·18	5·13	5·50	5·67	5·21	4·80	5·31
CaO	0·51	9·50	8·20	8·60	8·80	8·76	8·92	8·61	8·97	8·40	8·76	8·63	8·90	8·48
Na_2O	4·40	3·10	3·50	3·40	3·60	3·65	3·21	3·86	3·52	3·70	3·24	3·45	3·30	3·87
K_2O	5·08	1·50	1·40	1·20	1·10	1·22	1·06	1·22	1·21	1·40	1·31	1·21	1·30	0·86
P_2O_5	0·08	0·60	0·70	0·60	0·70	0·62	0·53	0·59	0·63	0·60	0·64	0·68	0·90	0·42
LOI	0·48	3·50	0·30	1·20	0·30	1·23	0·86	0·75	1·12	0·30	1·26	0·59	0·10	0·63
Total	99·35	99·70	100·70	101·40	100·70	100·36	99·66	99·90	99·67	100·80	99·87	99·19	100·30	99·53
Fe-no.	0·91	0·71	0·75	0·69	0·73	0·75	0·74	0·73	0·74	0·73	0·72	0·73	0·77	0·73
Rb	119	25·6	38·0	27·3	28·3	35·6	31·2	31·1	38·6	20·8	31·4	31·1	29·4	10·8
Sr	65·3	435	418	457	398	453	478	409	479	432	468	454	443	467
Ba	402	705	445	687	455	503	447	407	443	427	486	412	542	532
V	2·67	212	254	258	215	267	198	213	256	234	256	211	239	221
Cr	5·37	96·9	42·6	90·9	94·0	20·2	61·6	62·6	56·8	64·5	64·7	43·4	40·7	57·8
Co	3·09	49·1	50·0	48·4	58·7	48·6	48·9	45·9	50·1	54·3	49·1	49·5	50·6	51·1
Ni	4·22	39·1	48·3	20·8	141	56·1	55·7	30·9	80·2	51·6	57·7	54·4	83·8	96·9
Cu	9·53	53·3	42·7	51·8	39·7	60·2	50·8	48·7	37·6	44·6	43·5	44·7	53·8	48·7
Zn	70·2	–	113	59·9	51·6	43·5	65·4	61·0	48·3	48·6	44·5	42·2	35·91	59·6
Ga	29·8	–	–	–	–	–	–	–	–	–	–	–	–	–
Zr	983	203	223	168	143	217	247	231	257	228	304	157	216	164
Hf	25·4	7·06	12·3	7·41	8·99	11·1	9·99	9·76	10·1	9·91	10·0	8·82	11·7	10·1
Nb	88·6	12·7	15·8	21·8	17·9	15·6	13·8	14·9	22·8	13·4	18·7	17·5	13·2	15·1
Ta	6·59	2·93	3·62	2·42	3·41	3·87	3·32	4·51	4·22	3·99	3·68	3·90	4·42	3·33
U	3·10	0·574	0·985	0·575	0·793	1·19	0·701	0·647	0·741	0·987	0·958	1·02	0·999	1·20
Th	13·5	2·65	4·88	2·40	3·16	3·96	3·44	3·35	3·53	3·97	3·62	3·10	3·94	4·22
Pb	11·20	5·23	4·78	6·12	5·89	3·78	5·76	4·98	3·78	3·64	3·89	5·76	4·85	4·18
Y	89·8	43·7	47·8	41·4	53·8	51·5	49·7	47·6	52·9	36·8	33·2	48·7	47·9	52·6
La	103	38·2	49·2	35·4	37·1	45·4	41·8	48·9	41·5	37·4	40·6	40·8	46·9	38·6
Ce	250	118	135	95·7	106	126	114	136	112	97·4	105	105	134	96·8
Pr	–	–	–	–	–	–	–	–	–	–	–	–	–	–
Nd	99·9	47·7	62·7	44·9	51·2	62·0	60·4	69·2	57·3	52·4	57·6	58·4	69·6	54·6
Sm	20·8	11·3	14·5	10·5	12·4	14·5	12·9	15·7	13·9	11·7	13·4	13·2	16·1	12·0
Eu	3·82	4·56	4·88	4·26	4·36	5·04	4·66	4·60	4·63	4·11	4·47	4·33	5·22	4·34
Gd	–	–	–	–	–	–	–	–	–	–	–	–	–	–
Tb	3·32	2·72	2·28	1·55	1·97	2·26	2·01	2·45	2·25	1·85	2·46	2·09	2·58	1·89
Dy	–	–	–	–	–	–	–	–	–	–	–	–	–	–
Ho	0·570	–	–	–	–	–	–	–	–	–	–	–	–	–
Er	–	–	–	–	–	–	–	–	–	–	–	–	–	–
Tm	–	–	–	–	–	–	–	–	–	–	–	–	–	–
Yb	8·69	3·14	5·38	3·01	4·09	4·83	4·61	5·43	4·66	4·27	4·41	4·45	5·24	4·19
Lu	1·21	0·471	0·763	0·423	0·612	0·742	0·693	0·794	0·684	0·643	0·656	0·670	0·789	0·562
Eu/Eu*	0·56	1·10	1·03	1·26	1·08	1·07	1·11	0·90	1·01	1·08	0·98	1·00	0·99	1·11
$(La/Yb)_n$	7·68	7·87	5·92	7·61	5·87	6·08	5·87	5·83	5·76	5·67	5·96	5·93	5·79	5·96

(continued)

Downloaded from petrology.oxfordjournals.org at Bibliotheque Fac de Medecine on January 12, 2011

Table 8: Continued

Sample:	05-05	05-14	05-20	05-21	05-22	05-23	05-24	05-25	05-51	07-68	05-15	05-16	05-17	05-18	05-19
Rock-type:	Gneiss	Gneiss	Gneiss	Gneiss	Gneiss	Gneiss	Gneiss	Gneiss	Gneiss	Gneiss	Gabbro	Gabbro	Gabbro	Gabbro	Gabbro
Location:	Grenv.	Grenv.	Grenv.	Grenv.	Grenv.	Grenv.	Grenv.	Grenv.	Grenv.	Grenv.	Grenv.	Grenv.	Grenv.	Grenv.	Grenv.
Xenoliths:															
East WGS84:	03·87·273	03·57·189	03·57·189	03·57·189	03·57·189	03·87·202	03·87·215	03·87·237	03·57·189	03·87·387	03·57·189	03·57·189	03·57·189	03·57·189	03·57·189
North WGS84:	55·74·918	55·74·950	55·74·950	55·74·950	55·74·950	55·74·923	55·74·910	55·74·848	55·74·950	55·74·758	55·74·950	55·74·950	55·74·950	55·74·950	55·74·950
SiO_2	59·40	58·90	58·06	52·08	57·74	57·98	57·92	58·86	59·18	58·14	46·81	46·15	46·94	44·90	45·94
TiO_2	0·98	0·96	0·94	1·37	1·05	0·96	1·00	0·85	0·93	0·77	3·29	3·31	3·15	3·56	3·22
Al_2O_3	17·15	17·38	18·07	18·77	17·96	17·80	17·42	17·08	16·93	17·38	16·48	15·88	16·88	16·07	15·51
FeO_t	9·29	9·12	9·61	13·46	10·12	9·69	9·84	10·03	9·41	9·30	14·81	15·05	14·36	15·48	14·75
MnO	0·26	0·25	0·26	0·37	0·27	0·26	0·27	0·24	0·26	0·23	0·26	0·28	0·22	0·25	0·25
MgO	0·76	0·74	0·71	1·17	0·83	0·75	0·79	0·62	0·74	0·63	6·06	6·00	5·88	6·55	5·98
CaO	3·71	3·57	3·66	5·59	3·79	3·69	3·77	3·29	3·56	3·49	7·60	7·66	8·18	8·93	8·07
Na_2O	5·37	5·29	5·23	5·25	4·80	5·74	5·01	4·94	4·70	4·98	3·33	3·42	3·46	3·18	3·31
K_2O	4·08	4·11	3·87	1·27	4·27	4·19	4·20	4·81	5·22	4·85	1·46	1·26	0·96	0·96	2·21
P_2O_5	0·14	0·13	0·11	0·07	0·13	0·13	0·14	0·11	0·14	0·30	0·24	0·29	0·24	0·34	0·36
LOI	0·00	0·12	0·08	0·15	0·00	0·02	0·12	0·06	0·04	0·07	0·12	0·51	0·67	0·77	0·55
Total	101·14	100·57	100·60	99·55	100·96	101·21	100·48	100·89	101·11	100·14	100·34	99·30	100·27	100·22	99·60
Fe-no.	0·92	0·93	0·93	0·92	0·92	0·93	0·93	0·94	0·93	0·94	0·71	0·72	0·71	0·70	0·71
Rb	29·8	26·0	26·2	9·52	31·8	27·0	29·7	30·8	38·5	12·7	31·9	24·8	17·1	13·6	42·9
Sr	233	267	273	407	279	290	278	260	278	230	231	246	246	290	257
Ba	1527	1755	1548	1434	1975	2009	2052	1833	2227	1745	365	427	301	284	467
V	2·32	3·45	3·12	0·413	2·21	2·13	2·36	2·23	3·41	4·12	149	139	172	165	143
Cr	66·7	11·3	13·5	9·92	9·63	17·7	13·4	11·6	12·5	12·4	73·9	83·8	81·8	98·4	84·9
Co	22·3	22·7	19·7	28·5	20·3	16·2	25·6	16·7	14·7	5·29	48·9	49·4	53·1	51·5	49·8
Ni	15·2	–	–	–	–	–	–	–	–	–	59·1	54·2	70·2	68·5	64·2
Cu	12·7	12·3	13·9	16·1	13·5	15·6	13·4	14·9	15·9	12·5	38·5	38·8	35·8	45·9	38·5
Zn	151	146	152	214	159	148	133	142	123	127	141	131	143	154	144
Ga	29·8	31·3	33·6	33·8	30·8	33·5	31·9	27·7	27·8	32·5	19·9	23·5	20·3	21·3	20·3
Zr	757	795	993	841	1011	988	851	898	827	1093	146	167	140	152	170
Hf	20·9	22·6	25·0	–	–	–	–	–	–	–	–	–	–	–	–
Nb	43·8	44·7	43·8	35·2	44·1	45·0	46·7	30·0	43·1	35·6	16·3	16·8	13·6	17·3	18·1
Ta	2·90	2·67	2·17	–	–	–	–	–	–	–	–	–	–	–	–
U	1·37	1·27	1·32	–	–	–	–	–	–	–	–	–	–	–	–
Th	2·22	1·83	2·29	–	–	–	–	–	–	–	–	–	–	–	–
Pb	23·9	26·7	25·3	24·1	25·2	27·3	24·4	24·2	21·7	10·3	23·4	24·4	23·5	24·8	26·5
Y	53·2	54·4	51·6	53·2	48·5	53·8	48·8	37·5	49·3	49·6	32·2	36·6	29·2	39·3	37·6
La	49·2	49·4	50·8	–	–	–	–	–	–	–	–	–	–	–	–
Ce	113	115	113	–	–	–	–	–	–	–	–	–	–	–	–
Pr	16·7	17·303	16·6	–	–	–	–	–	–	–	–	–	–	–	–
Nd	67·7	69·5	67·4	–	–	–	–	–	–	–	–	–	–	–	–
Sm	14·1	14·3	14·3	–	–	–	–	–	–	–	–	–	–	–	–
Eu	4·98	5·71	5·99	–	–	–	–	–	–	–	–	–	–	–	–
Gd	13·9	13·1	13·1	–	–	–	–	–	–	–	–	–	–	–	–
Tb	1·95	2·07	1·91	–	–	–	–	–	–	–	–	–	–	–	–
Dy	11·3	12·0	11·5	–	–	–	–	–	–	–	–	–	–	–	–
Ho	2·41	2·41	2·44	–	–	–	–	–	–	–	–	–	–	–	–
Er	6·25	6·71	6·45	–	–	–	–	–	–	–	–	–	–	–	–
Tm	1·09	0·972	0·888	–	–	–	–	–	–	–	–	–	–	–	–
Yb	6·62	6·14	6·29	–	–	–	–	–	–	–	–	–	–	–	–
Lu	0·995	0·943	0·913	–	–	–	–	–	–	–	–	–	–	–	–
Eu/Eu*	4·82	5·20	5·22	–	–	–	–	–	–	–	–	–	–	–	–
$(La/Yb)_n$	1·10	1·28	1·35	–	–	–	–	–	–	–	–	–	–	–	–

Fe-no., $FeO_t/(FeO_t + MgO)$; BZ, Border Zone; LS, Layered Series; US, Upper Series; PC, Pointe du Criard; Doler., dolerite; Monz., monzonite. Grenv., Grenvillian country-rock; LOI, loss on ignition.

Downloaded from petrology.oxfordjournals.org at Bibliotheque Fac de Medecine on January 12, 2011

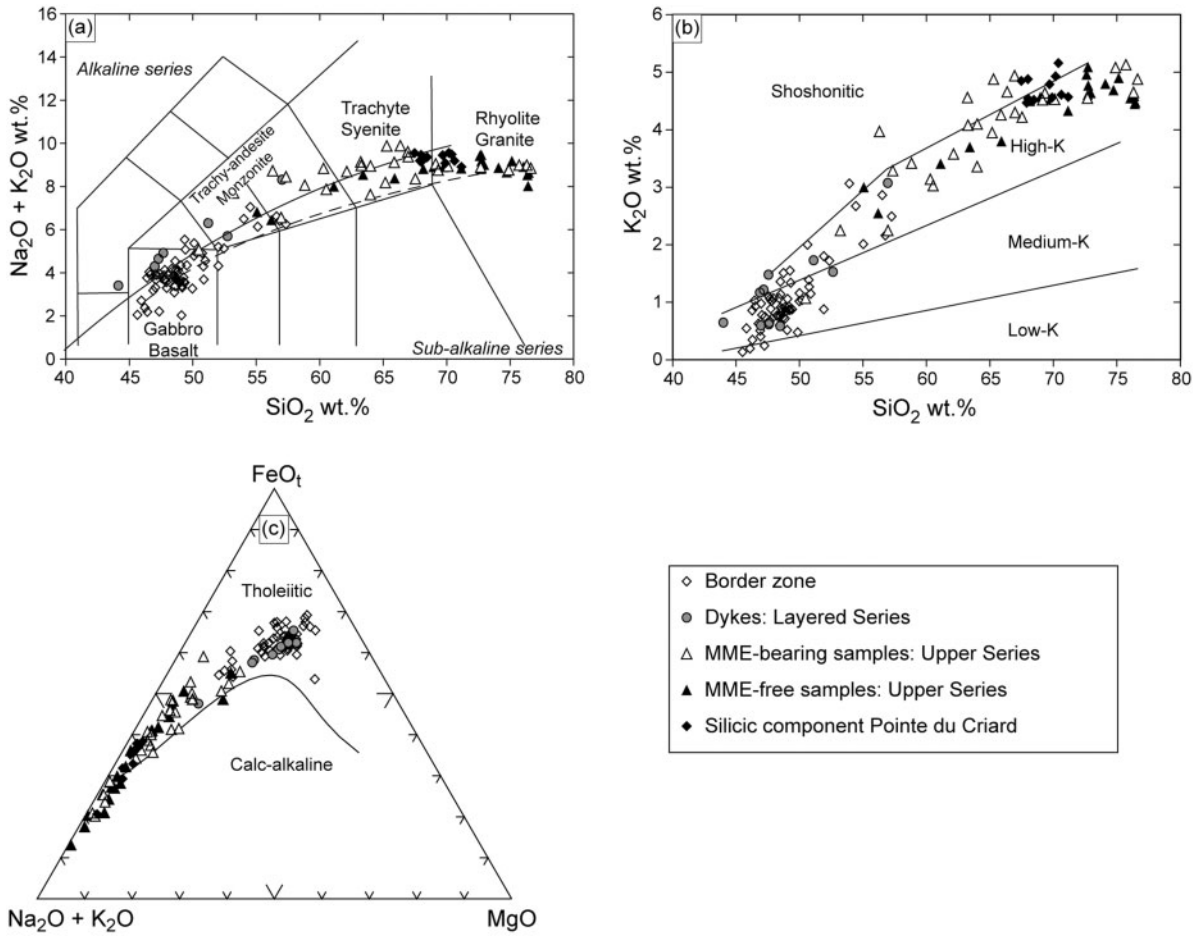

Fig. 6. Classification diagrams of fine-grained and silicic samples from the Sept Iles intrusive suite. (a) Nomenclature of the samples in the total alkalis–silica (TAS) diagram ($Na_2O + K_2O$) (wt %) vs SiO_2 (wt %) with field names from Cox *et al.* (1979) and subdivision between the alkaline and subalkaline series using the discrimination curves of Kuno (1966) and Irvine & Baragar (1971) (dashed curve). (b) K_2O (wt %) vs SiO_2 (wt %) diagram with dividing curves of Peccerillo & Taylor (1976). (c) AFM diagram. The limit between tholeiitic and calc-alkaline fields is from Irvine & Baragar (1971).

c. 47 wt % SiO_2. Accumulation of Fe–Ti oxide minerals is suspected in some samples with unusually high Cr (>100 ppm) and V (>350 ppm) concentrations.

Samples of basaltic composition (classified following Fig. 6a) show slightly fractionated rare earth element (REE) patterns [$(La/Yb)_n < 7$; Fig. 10a]. They have REE contents higher than those of enriched and normal mid-ocean ridge basalt (E-MORB and N-MORB) and similar to those of ocean island basalt (OIB). Europium anomalies (Eu/Eu*) range from 0·77 to 1·34. Two samples have Eu anomalies higher than 1·20 and also display abnormally high Sr concentrations (>800 ppm), probably resulting from plagioclase accumulation. Monzonitic samples show a large range of REE concentrations (Fig. 10b) that increase with increasing SiO_2 content. They have slightly fractionated REE patterns [$(La/Yb)_n$ 3·8–8·2] and moderate Eu/Eu* ratios (0·63–1·26); most samples have a significant negative Eu anomaly. Syenitic and granitic samples have the highest REE concentrations (Fig. 10c and d). They display fractionated REE patterns [$(La/Yb)_n$ 5·6–13·0] and strong negative Eu anomalies.

In N-MORB-normalized trace element variation diagrams (Fig. 11), the basaltic samples show trace element patterns highly enriched compared with those of N-MORB and E-MORB but similar to those of OIB (Fig. 11a). They have positive anomalies in Ba, Rb and K and negative anomalies in Nb, Ta, Sr, Zr and Hf. Some monzonitic samples are characterized by positive anomalies in Zr, Hf and Ta and small negative anomalies in Sr, P and Ti (Fig. 11b). Positive anomalies could result from the accumulation of accessory minerals such as zircon and titanite. Syenitic and granitic compositions show coherent patterns with significant negative anomalies in Sr, P and Ti (Fig. 11c and d).

Downloaded from petrology.oxfordjournals.org at Bibliotheque Fac de Medecine on January 12, 2011

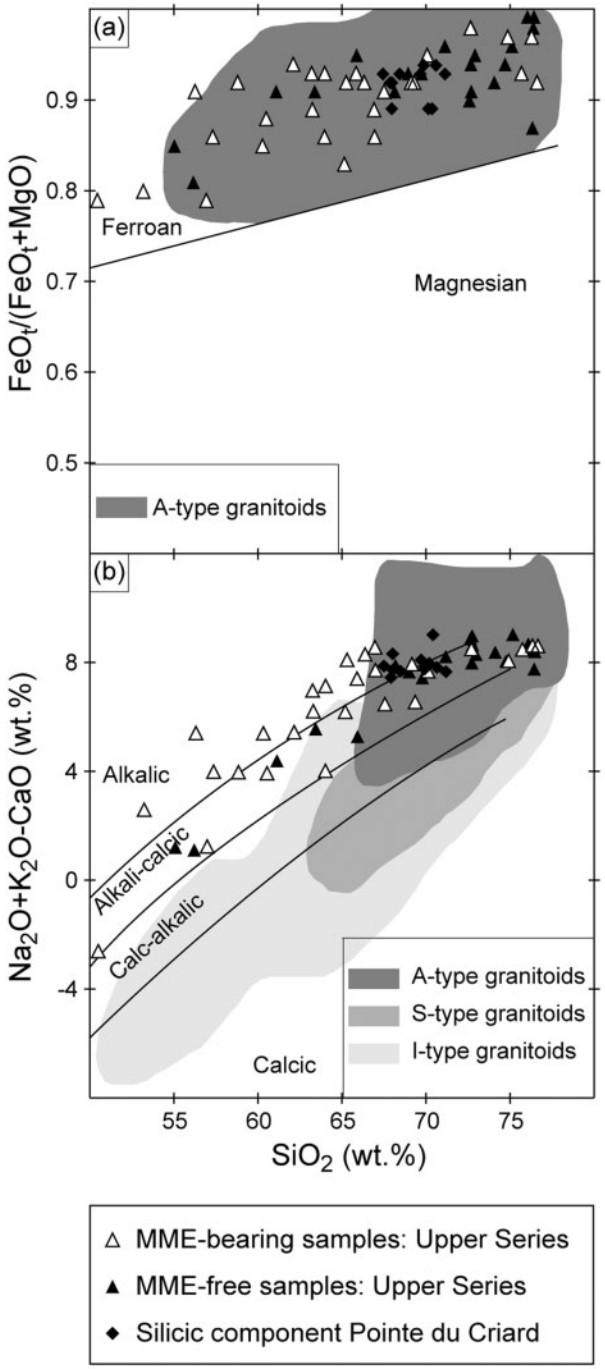

Fig. 7. Major element geochemical characteristics of silicic samples from the Upper Series and the Pointe du Criard sill. (a) $FeO_t/(FeO_t + MgO)$ vs SiO_2 (wt %) discriminant diagram of Frost *et al.* (2001). (b) $Na_2O + K_2O - CaO$ (wt %) vs SiO_2 (wt %) discriminant diagram of Frost *et al.* (2001).

Sr and Nd isotopes

Whole-rock Sr-isotopic ratios have been measured on 15 Sept Iles samples covering the compositional range from basalt (gabbro) to rhyolite (granite) and for 14 gabbroic samples from the Layered Series (Table 9). Nd-isotopic data have been acquired for 11 samples ranging from trachyandesite (monzonite) to rhyolite (granite) and for eight gabbroic samples from the Layered Series. All the isotopic data were recalculated for an age 564 Ma (Higgins & van Breemen, 1998). Except for sample 05-45 [$(^{87}Sr/^{86}Sr)_{564}$ 0·70621], which was collected in the Border Zone where significant country-rock contamination may have occurred, the Sept Iles samples display a narrow range of initial Sr isotopic compositions (0·70353–0·70548) with an overall increase of $(^{87}Sr/^{86}Sr)_{564}$ with increasing SiO_2 (Fig. 12a). This range of isotopic composition matches well that observed by Namur *et al.* (2010) in cumulates from the Layered Series (0·70360–0·70493; Table 1) and that obtained for gabbroic rocks as part of this study (0·70352–0·70530; Table 9). It also agrees with the data of Higgins & Doig (1981). It is worth noting that initial Sr isotopic ratios are higher in Upper Series MME-free silicic samples (0·70412–0·70548) than in MME-bearing silicic samples (0·70362–0·70369). A Rb–Sr isochron (Fig. 12b; calculations after Ludwig, 2001) gives an age of 576 ± 7 Ma and an initial $^{87}Sr/^{86}Sr$ ratio of 0·70353 (MSWD 0·62). The initial $^{87}Sr/^{86}Sr$ ratio is in perfect agreement with the less radiogenic value obtained for Sept Iles samples (0·70353). The $(^{143}Nd/^{144}Nd)_{564}$ compositions of the silicic samples are less variable and cluster around 0·51201–0·51207, with ε_{Nd} values ranging from 2·0 to 3·1 (Fig. 12c). No clear correlation is observed with the SiO_2 content of the samples. These Nd isotope ratios fall within the range of values obtained for the gabbroic rocks of the Layered Series (0·51195–0·51209).

LIQUID LINE OF DESCENT OF THE LAYERED SERIES

Geochemical modeling

Continuous whole-rock major and trace element variations (Figs 8–11) suggest that fractionation of the cumulus phases of the Layered Series (Table 2) could result in the genesis of intermediate and silicic liquids from parental mafic magmas. Sample compositions from 47 to 57 wt % SiO_2 are closely associated with the Layered Series, occurring in dykes cross-cutting this series and in the Border Zone in direct contact with it. Two independent methods have been employed to assess to what extent these samples represent liquid compositions that are able to crystallize the silicate minerals of the Layered Series with appropriate compositions. The first of these methods uses experimentally determined equations for mineral–melt equilibria proposed by Thy *et al.* (2006), whereas the second uses the MELTS algorithm of Ghiorso & Sack (1995).

The empirical equations of Thy *et al.* (2006) allow the estimation of the composition of silicate minerals in equilibrium with a given melt composition, based on linear

Downloaded from petrology.oxfordjournals.org at Bibliotheque Fac de Medecine on January 12, 2011

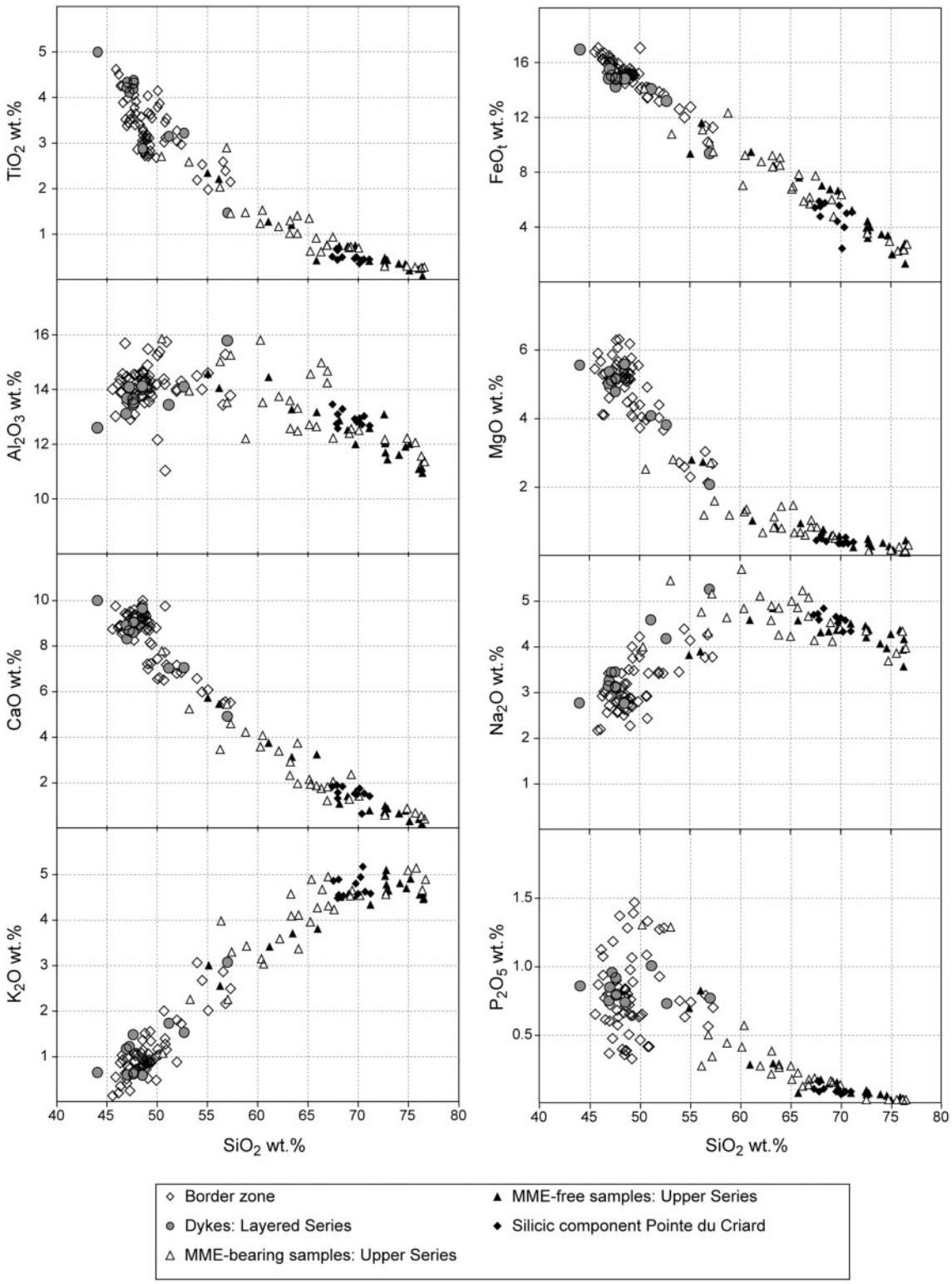

Fig. 8. Harker variation diagrams of major elements (wt %) vs SiO_2 (wt %).

Downloaded from petrology.oxfordjournals.org at Bibliotheque Fac de Medecine on January 12, 2011

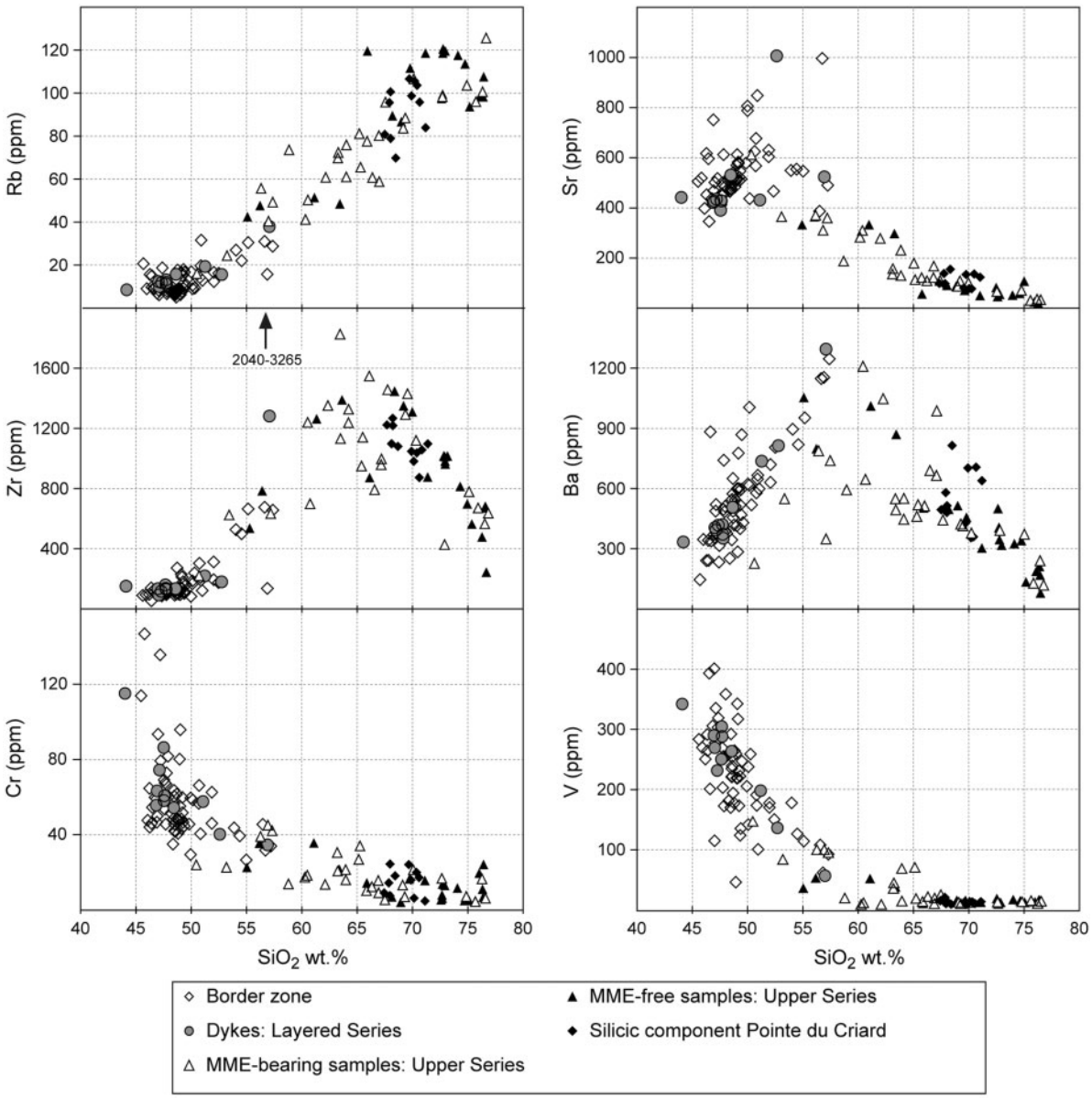

Fig. 9. Harker variation diagrams of selected trace elements (ppm) vs SiO_2 (wt %).

regression of melt components. The equations were derived from experiments on Skaergaard-related magmas similar to the Sept Iles parent magma composition. They are thus considered adequate for prediction of the composition of minerals crystallized from the Sept Iles magmas (see Appendix for the method of the calculation).

The MELTS algorithm is a well-known thermodynamic calculator, whose application to ferrobasaltic liquid lines of descent and mineral–melt equilibria has been assessed by comparison with experimental results on Skaergaard-related ferrobasalts carried out by Toplis & Carroll (1995) and Thy *et al.* (2006). Comparison of experimentally derived crystallization of the SCl ferrobasalt (Toplis & Carroll, 1995) at 1 atm, FMQ − 2 to FMQ + 1, and the sequence of crystallization predicted by MELTS for the same conditions (Appendix, Fig. A1), reveals that MELTS fails to predict appropriate Fe–Ti oxide equilibria, leading to erroneous liquid lines of descent for ferrobasaltic magmas (Appendix, Fig. A2; see also Toplis & Carroll, 1996). On the other hand, comparison of mineral compositions and liquidus temperatures calculated by MELTS and those obtained experimentally by Toplis & Carroll

Downloaded from petrology.oxfordjournals.org at Bibliotheque Fac de Medecine on January 12, 2011

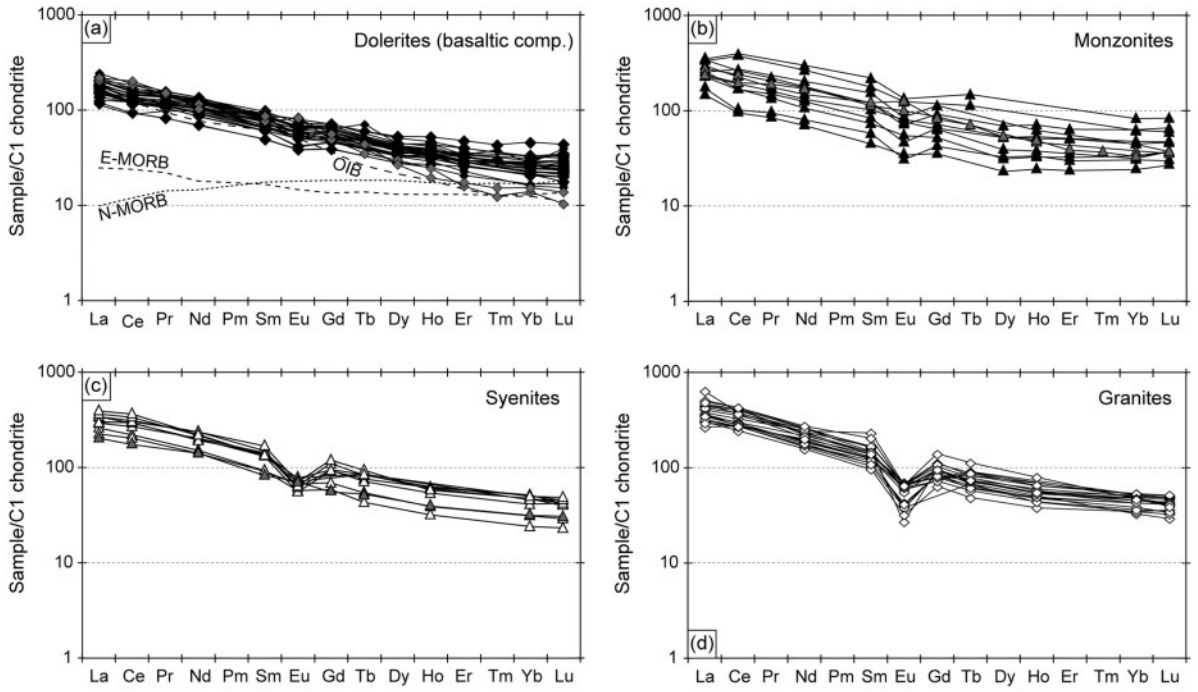

Fig. 10. Chondrite-normalized REE patterns of Sept Iles samples. (a) Dolerites (basaltic compositions) showing their comparison with N-MORB, E-MORB and OIB compositions. (b) Monzonites. (c) Syenites. (d) Granites. The four groups of samples were classified using Fig. 6a. Samples with positive Eu anomalies are represented with grey symbols. Chondrite, N-MORB, E-MORB and OIB values from Sun & McDonough (1989).

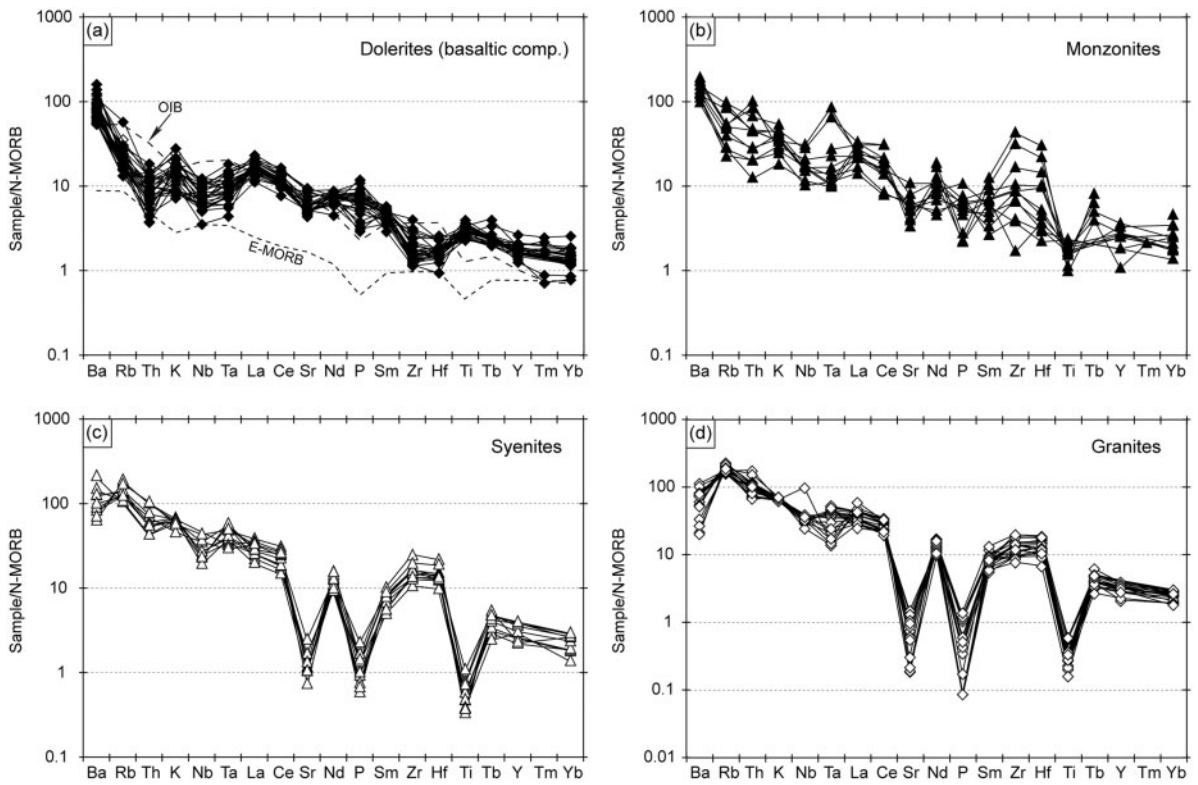

Fig. 11. N-MORB normalized trace element diagrams for Sept Iles samples. (a) Dolerite (basaltic compositions) and comparison with E-MORB and OIB compositions. (b) Monzonites. (c) Syenites. (d) Granites. N-MORB, E-MORB and OIB values from Sun & McDonough (1989).

Downloaded from petrology.oxfordjournals.org at Bibliotheque Fac de Medecine on January 12, 2011

Table 9: Sr and Nd isotopic data of the Sept Iles samples

Sample	Rock-type	Location	Rb (ppm)	Sr (ppm)	$^{87}Rb/^{86}Sr$	$^{87}Sr/^{86}Sr$	2σ	$(^{87}Sr/^{86}Sr)_{564}$	Sm (ppm)	Nd (ppm)	$^{147}Sm/^{144}Nd$	$^{143}Nd/^{144}Nd$	2σ	$(^{143}Nd/^{144}Nd)_{564}$	ε_{Nd}
Fine-grained and silicic samples															
05-45	Dolerite	Border Zone	9·0	472·3	0·05495	0·706648	0·000008	0·70621	–	–	–	–	–	–	–
07-01	Dolerite	Layered Series	16·2	530·9	0·08827	0·704243	0·000008	0·70353	–	–	–	–	–	–	–
07-82	Monzonite	Layered Series	36·7	543·1	0·195	0·705180	0·000007	0·70361	–	–	–	–	–	–	–
S9-106	Monzonite	Layered Series	40·1	262·6	0·441	0·707179	0·000008	0·70363	–	–	–	–	–	–	–
03-01	Granite	Upper Series	119·4	48·1	7·2	0·762398	0·000010	0·70434	16·3	82	0·1209	0·512508	0·000013	0·51206	2·9
03-08	Syenite	Pointe du Criard	70·2	150·9	1·347	0·714755	0·000008	0·70392	14·9	74	0·1221	0·512521	0·000018	0·51207	3·1
03-15	Granite	Pointe du Criard	84·3	118·8	2·05	0·720388	0·000007	0·70386	18·5	86	0·1299	0·512492	0·000015	0·51201	2·0
03-22	Granite	Upper Series	87·1	82·2	3·07	0·728826	0·000007	0·70412	21·9	97	0·1361	0·512539	0·000012	0·51204	2·4
03-28	Granite	Upper Series	108·4	15·3	20·9	0·873031	0·000010	0·70548	14·4	71	0·1222	0·512481	0·000012	0·51203	2·3
03-35	Granite	Upper Series	71·3	47·0	4·40	0·739700	0·000008	0·70429	21·1	95	0·1340	0·512530	0·000015	0·51204	2·4
03-37	Syenite	Upper Series	105·9	156·0	1·967	0·719507	0·000007	0·70369	22·9	99	0·1398	0·512558	0·000011	0·51204	2·5
03-42	Monzonite	Upper Series	53·4	327·1	0·473	0·707416	0·000010	0·70362	17·7	83	0·1294	0·512544	0·000011	0·51207	3·0
03-48	Syenite	Upper Series	61·4	217·7	0·816	0·710207	0·000008	0·70364	22·1	93	0·1438	0·512547	0·000012	0·51202	2·0
87-7	Granite	Upper Series	84·5	84·5	2·906	0·727510	0·000010	0·70444	14·2	66	0·1298	0·512507	0·000013	0·51203	2·3
87-6	Granite	Upper Series	100·5	18·6	16·1	0·831110	0·000008	0·70358	14·1	69	0·1232	0·512520	0·000018	0·51206	3·0
Cumulates															
86-78	Gabbro	Layered Series	1·0	530	0·005459	0·705340	0·000028	0·70530	3·45	13·8	0·1518	0·512551	–	0·51199	1·6
86-77	Gabbro	Layered Series	0·7	617	0·003282	0·704047	0·000030	0·70402	1·25	4·50	0·1683	0·512708	–	0·51209	3·4
86-76	Gabbro	Layered Series	1·0	500	0·005785	0·703570	0·000032	0·70352	–	–	–	–	–	–	–
86-74	Gabbro	Layered Series	0·5	406	0·003563	0·704140	0·000034	0·70411	2·47	6·95	0·2147	0·512845	–	0·51205	2·7
86-72	Gabbro	Layered Series	2·7	414	0·018866	0·704077	0·000036	0·70393	–	–	–	–	–	–	–
86-70	Gabbro	Layered Series	1·8	516	0·010091	0·703857	0·000038	0·70378	–	–	–	–	–	–	–
86-70	Gabbro	Layered Series	1·8	444	0·011727	0·703899	0·000040	0·70380	–	–	–	–	–	–	–
86-69	Gabbro	Layered Series	5·5	843	0·018873	0·703968	0·000042	0·70382	–	–	–	–	–	–	–
86-68	Gabbro	Layered Series	1·7	548	0·008975	0·705300	0·000044	0·70523	0·630	2·31	0·1650	0·512562	–	0·51195	0·8
86-67	Gabbro	Layered Series	4·2	765	0·015882	0·704072	0·000046	0·70394	–	–	–	–	–	–	–
86-64	Gabbro	Layered Series	0·7	677	0·002991	0·703862	0·000049	0·70384	0·515	2·17	0·1437	0·512580	–	0·51205	2·7
86-62	Gabbro	Layered Series	0·9	424	0·006140	0·703960	0·000051	0·70391	1·26	4·09	0·1869	0·512740	–	0·51205	2·7
87-17	Gabbro	Layered Series	0·0	109	0·000000	0·704470	0·000053	0·70447	0·837	2·64	0·1921	0·512776	–	0·51207	3·0
87-18	Gabbro	Layered Series	1·1	88	0·036078	0·704180	0·000055	0·70389	2·43	7·13	0·2061	0·512800	–	0·51204	2·5
Country-rocks															
05-25	Gneissic monzonite	Grenville	30·8	260·0	0·084178	0·712194	0·000010	0·70944	–	–	–	–	–	–	–
07-68	Gneissic monzonite	Grenville	12·8	230·0	0·161245	0·720204	0·000008	0·71891	–	–	–	–	–	–	–
07-08	Cordierite gneiss	Grenville	49·3	96·7	1·486802	0·786549	0·000014	0·77459	–	–	–	–	–	–	–

(1995) and Thy *et al.* (2006) for ferrobasaltic residual liquids is much more satisfactory. Liquidus temperatures are predicted with an accuracy of *c.* 10–20°C (Appendix, Fig. A3). For mineral–melt equilibria, plagioclase, olivine and Ca-rich pyroxene compositions are predicted by MELTS relatively accurately, with errors generally lower than 10%.

For the geochemical modeling, MELTS calculations were performed at a pressure of 1 kbar for three reasons: (1) the Sept Iles intrusion was emplaced just below a

Downloaded from petrology.oxfordjournals.org at Bibliotheque Fac de Medecine on January 12, 2011

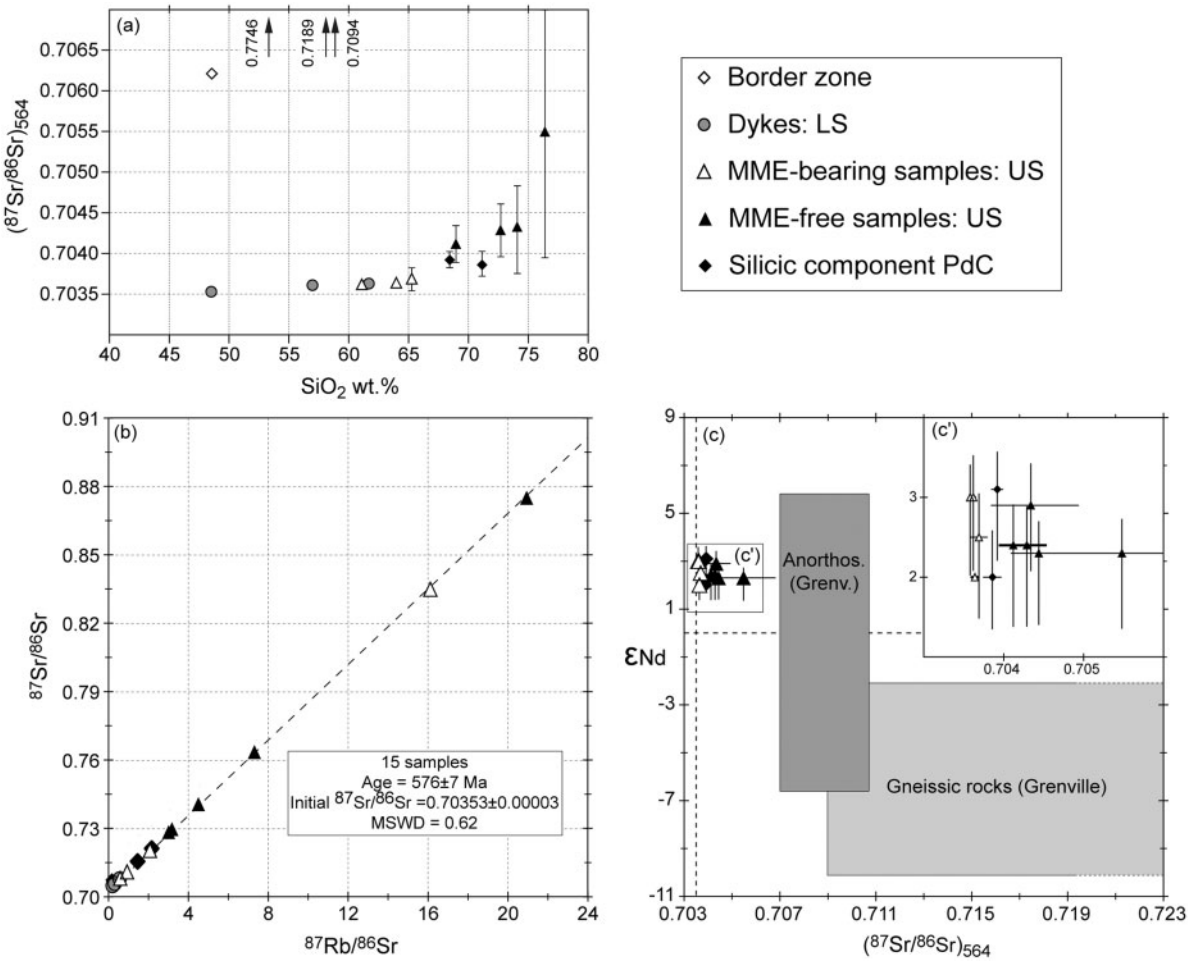

Fig. 12. (a) Initial Sr-isotopic ratios (calculated at 564 Ma) vs SiO_2 (wt %). Arrows are directed toward the isotopic compositions (given values) of country-rock samples. (b) Rb–Sr isochron of Sept Iles fine-grained and silicic samples. (c) Sr and Nd isotopic compositions of Sept Iles fine-grained and silicic samples (calculated at 564 Ma). The compositions of the country-rocks in the area of Sept Iles are also indicated (data from Wadleigh *et al.*, 1985; Ashwal *et al.*, 1986; Shaw *et al.*, 1986; Dickin & Higgins, 1992; Olive *et al.*, 1997; Dickin, 2000). (c') Close-up of variation in Sept Iles samples. Error bars for Sr and Nd isotopic ratios were calculated using expected errors in the determination of Rb (±5%), Sr (±2%), Sm and Nd (±5%; Vander Auwera *et al.*, 1998*a*).

sequence of continental flood basalts (Higgins, 2005); (2) autolith blocks in the Layered Series contain minerals indicative of low-temperature alteration (Higgins, 2005); (3) silicic rocks from the Upper Series contain miarolitic cavities, attesting to a shallow depth of intrusion.

Oxygen fugacity (fO_2) controls the oxidation state of iron in silicate liquids (Kilinc *et al.*, 1983), and thus influences Fe–Ti oxide equilibria (Juster *et al.*, 1989; Snyder *et al.*, 1993; Toplis & Carroll, 1995; Thy *et al.*, 2006) and the composition of ferro-magnesian minerals (Toplis & Carroll, 1995; Botcharnikov *et al.*, 2008). The range of fO_2 observed in most mafic layered intrusions is close to FMQ (Frost *et al.*, 1988; Carmichael, 1991; Thy *et al.*, 2009), in agreement with the estimate of Namur *et al.* (2010) for the Sept Iles Layered Series. MELTS calculations were thus performed at FMQ and FMQ − 1.

The composition of plagioclase, olivine and Ca-rich pyroxene in equilibrium with liquids ranging in composition from 47 to 57 wt % SiO_2 (Table 8; Fig. 13) were calculated using MELTS and the equations of Thy *et al.* (2006). These values were then compared with the range of mineral compositions observed in the Layered Series (Table 2). Liquids in equilibrium with plagioclase more calcic than An_{61} are not plotted in the Mg-number cpx vs An-plagioclase diagrams, as cumulus Ca-rich pyroxene is not considered to crystallize from such primitive melts (Table 2; Namur *et al.*, 2010). Scatter occurs in all the diagrams and probably results from both the inaccuracy of the two methods of calculation and the samples not being fully representative of liquid compositions. However, the compositional trends of the predicted minerals are close to those observed in the Layered Series. MELTS predicts

Downloaded from petrology.oxfordjournals.org at Bibliotheque Fac de Medecine on January 12, 2011

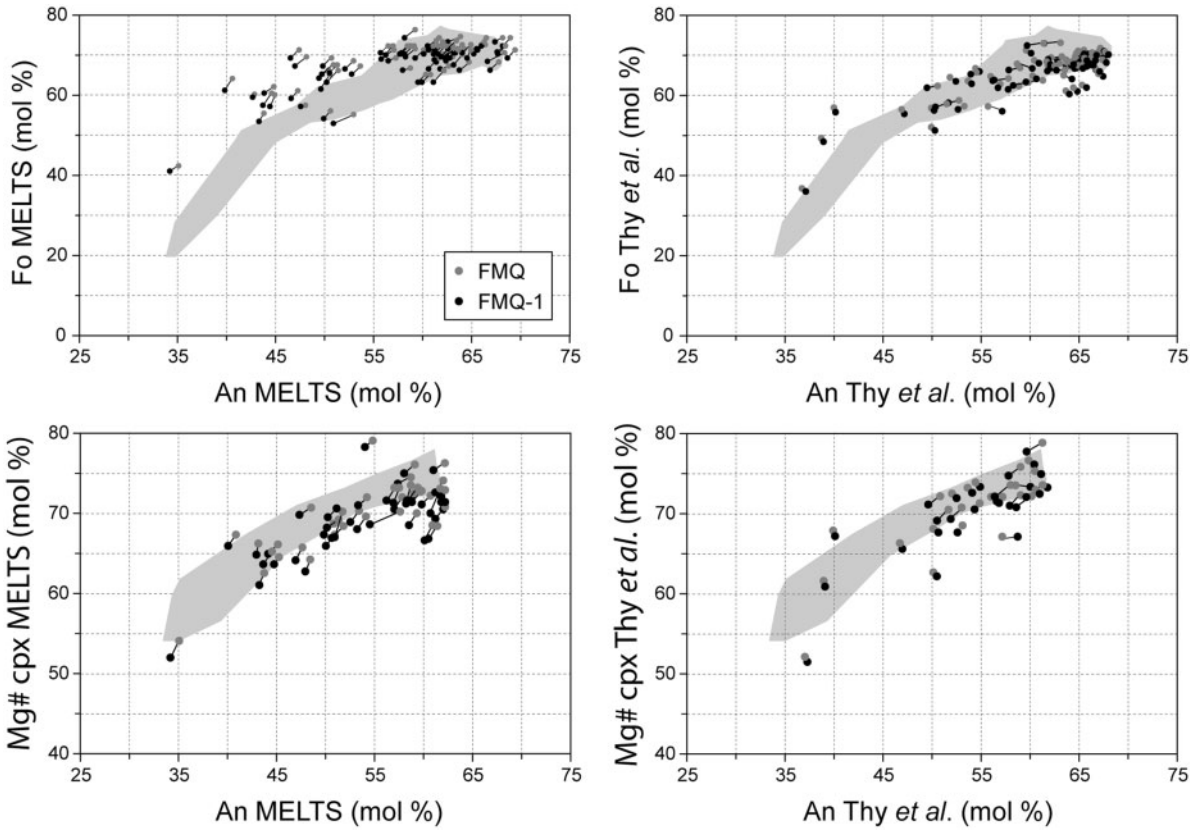

Fig. 13. Fo (mol %) vs An (mol %) and cpx-Mg-number (mol %) vs An (mol %) diagrams showing calculated mineral compositions in equilibrium with liquids of the Sept Iles intrusion. Mineral compositions were calculated using MELTS and the experimentally determined mineral–melt equilibria equations of Thy *et al.* (2006). The results for two oxidation states, FMQ and FMQ − 1, are linked by continuous lines. The evolution of calculated mineral compositions is compared with the mineral compositions of the Layered Series (grey fields).

liquidus temperatures ranging from *c.* 1170°C for basaltic compositions to *c.* 1080°C for monzonitic compositions, in excellent agreement with the experimental results of Toplis & Carroll (1995) for similar liquid compositions. Modeling thus indicates that liquids displaying geochemical trends from basalt to monzonite (47–57 wt % SiO_2) are able to crystallize minerals similar to those from the Layered Series and that these trends may thus be considered as a good estimate of the Layered Series liquid line of descent.

Saturation of Fe–Ti oxides and apatite

The point along the liquid line of descent at which Fe–Ti oxide minerals and apatite saturation occurs was modeled stepwise by least-squares mass regressions following the equations of Stormer & Nicholls (1978). For each step, the composition of a melt (parent) evolves to a more differentiated composition (daughter) by subtracting minerals with average compositions considered to be in equilibrium with liquids in the relevant interval of melt composition. Proportions of the subtracted minerals are calculated by error minimization represented by the sum of the squares of residuals ($\sum r^2$), which is considered to be relevant when $\sum r^2$ is lower than 1·0 (Geist *et al.*, 1995; Civetta *et al.*, 1998). Successful application of this method requires a minimum number of steps to capture first-order changes in phase relations (and thus bulk extract composition). On the other hand, step size cannot be too small because the compositions of the local bulk extract and the mineral compositions then become uncertain. From a trial and error approach we found that five steps was the minimum number to provide a self-consistent and meaningful set of liquid compositions for our data. Adding more steps is possible, but the results are fundamentally the same as those illustrated here.

Input parameters for this modeling are as follows. (1) The starting liquid composition. This is the parent magma of the Layered Series (Namur *et al.*, 2010), a FeO_t-rich tholeiitic basalt (*c.* 48 wt % SiO_2 and *c.* 15 wt % FeO_t). (2) The compositions of liquids at saturation of Fe–Ti oxides and apatite. These compositions were chosen based upon the maximum contents of FeO_t and TiO_2, and

Downloaded from petrology.oxfordjournals.org at Bibliotheque Fac de Medecine on January 12, 2011

P_2O_5 respectively. (3) Mineral compositions used in the model to calculate the bulk extract at each step of fractionation are from the Layered Series (Namur *et al.*, 2010; see ranges in Table 2). The fractionation path has been subdivided into five steps: two (FT1 and FT2 in Table 10) to reach Fe–Ti oxide saturation and three more (A1, A2 and A3 in Table 10) to reach apatite saturation.

Results of the least-squares modeling are presented in Table 10. Saturation of Fe–Ti oxide is reached when F (fraction of residual liquid) = 0·86, after fractionation of plagioclase and olivine (in proportions 77/23). Apatite saturation occurred when $F = 0{\cdot}52$, after fractionation of plagioclase and olivine, followed by fractionation of plagioclase, olivine, Ca-rich pyroxene, magnetite and ilmenite (in average proportions of 45/4/30/13/8; Table 10). The proportions of subtracted minerals are in good agreement with the average mineral modes of the Layered Series (see Table 2) where a relatively low proportion of minerals crystallized from the trapped interstitial liquid is expected (Namur *et al.*, 2010). In particular, the low proportion of olivine calculated by the model after the saturation of Fe–Ti oxides is clearly supported by the gabbros of the Layered Series (Table 2) and results from the well-known olivine hiatus owing to the destabilization of olivine in intermediate liquids (Morse, 1990).

Origin of Sept Iles silicic liquids

Silicic rocks occur in the Upper Series, as dykes and pods in the Upper Border Series and in apatite-rich gabbros, which are the most evolved cumulates of the Layered Series (Table 2). No silicic rocks have been identified in the troctolites and apatite-free gabbros of this series. Continuous trends in whole-rock major element, trace element and Sr isotopic composition (Figs 8, 9 and 12) from basaltic to granitic compositions indicate that all the liquids could be related by a process of fractional crystallization. Moreover, the similarity of ratios of compatible (e.g. Ni/Co) and incompatible (e.g. Th/U; Zr/Nb; Hf/Ta; Th/Nb; Th/La) trace elements between basaltic and silicic rocks also supports the idea of a common petrogenetic origin. Field relationships and geochemical data thus naturally suggest that the silicic melts are the result of protracted fractional crystallization of a parental tholeiitic basalt, a mechanism commonly proposed for the origin of A-type melts (Byerly *et al.*, 1976; Byerly, 1980; Turner *et al.*, 1992; Geist *et al.*, 1995; Mungall & Martin, 1995; Civetta *et al.*, 1998; Frost *et al.*, 2002; Anderson *et al.*, 2003; Macdonald *et al.*, 2008) and in agreement with the earlier studies of Sept Iles by Higgins & Doig (1986). This process is, however, controversial and an alternative process involving partial melting of underplated basalts or mafic cumulates in the crust has also been proposed and should be tested (Lightfoot *et al.*, 1987; Lowenstern & Mahood, 1991; Trua *et al.*, 1999; Tamura & Tatsumi, 2002). Partial melting of old upper crustal rocks (Patiño-Douce, 1997) is not tenable given the low initial Sr isotope ratios of the silicic rocks from Sept Iles (0·70353–0·70548), compared with the country-rocks (0·70944–0·77459).

Fractional crystallization of the parental basaltic magma

Geochemical modeling demonstrates that apatite saturation is reached when $F = 0{\cdot}52$. Major element modeling is used to test if silicic liquids can be derived by fractional crystallization from the first apatite-saturated melt of monzonitic composition. Modeling was performed in four steps to reach (1) the most evolved compositions closely associated with the Layered Series (monzonite; *c.* 55 wt % SiO_2; M1 in Table 10), (2) the most primitive syenitic compositions of the Upper Series (*c.* 64 wt % SiO_2; S1 in Table 10) and finally the granitic compositions of the Upper Series with (3) the highest K_2O content (*c.* 70 wt % SiO_2; 5 wt % K_2O; G1 in Table 10) and the lowest K_2O content (*c.* 76 wt % SiO_2; 4·4 wt % K_2O; G2 in Table 10). Mineral compositions used in the modeling are from the Critical Zone of the Layered Series (Namur *et al.*, 2010; Table 2) and from the Upper Series. A biotite composition was taken from the study of Vander Auwera *et al.* (1998*b*). Results are given in Table 10.

Monzonitic compositions can be reached when $F = 0{\cdot}32$. These compositions are obtained by removing an assemblage consisting of plagioclase (42%), olivine (25%), Ca-rich pyroxene (12%), Fe–Ti oxides (14%) and apatite (7%) from the first apatite-saturated melt. These mineral proportions are in good agreement with the average proportions in the apatite-bearing gabbros of the Layered Series (Table 2). Further fractionation ($F = 0{\cdot}17$) dominated by removal of plagioclase or alkali-feldspar (*c.* 50–70%), ferromagnesian minerals (Ca-rich pyroxene or amphibole + biotite; *c.* 7–30%), Fe–Ti oxides (*c.* 6–15%) and accessory apatite (*c.* 1%) drives the residual liquids towards more silicic compositions. The most evolved granitic compositions are reached when $F = 0{\cdot}08$. This amount of fractionation is in perfect agreement with other studies of basalt–rhyolite associations (e.g. Mungall & Martin, 1995; Civetta *et al.*, 1998; Peccerillo *et al.*, 2003). In their study of the Sherman batholith, Frost *et al.* (1999) indicated that A-type granites can theoretically be produced by protracted fractionation of a mafic parent magma, but rejected this hypothesis because of the low proportion of associated mafic cumulates. In the Sept Iles layered intrusion, small cupolas of granite occur above a *c.* 5·5 km thick pile of mafic troctolite, gabbro and anorthosite. Qualitatively, the relative volume of mafic cumulates and silicic rocks is thus in accordance with mass-balance calculations.

Fractional crystallization can also be tested using trace elements through application of the Rayleigh equation and appropriate partition coefficients (Table 11). Bulk partition coefficients were calculated using mineral proportions and the proportion of residual liquid obtained by

Downloaded from petrology.oxfordjournals.org at Bibliotheque Fac de Medecine on January 12, 2011

Table 10: Input data and results of least-squares modeling calculations for major elements

	Saturation of Fe–Ti oxides and apatite					Origin of silicic liquids			
	To Fe–Ti oxide saturation		To apatite saturation			Monzonite	Syenite	Granite	
Steps:	FT1	FT2	A1	A2	A3	M1	S1	G1	G2
Parent composition:	Parent magma	Medium Fe–Ti	High Fe–Ti	Int. P_2O_5 1	Int. P_2O_5 2	High P_2O_5	Monzonite	Syenite	High-K_2O granite
Sample:	05-45	07-179	07-139	07-167	07-11	07-46	07-65	03-48	04-54
SiO_2 (wt %):	48·56	47·77	47·01	49·08	51·14	52·38	55·05	63·97	70·37
Daughter composition:	Medium Fe–Ti	High Fe–Ti	Int. P_2O_5 1	Int. P_2O_5 2	High P_2O_5	Monzonite	Syenite	High-K_2O granite	Low-K_2O granite
Sample:	07-179	07-139	07-167	07-11	07-46	07-65	03-48	04-54	03-28
SiO_2 (wt %):	47·77	47·01	49·08	51·14	52·38	55·05	63·97	70·37	76·39
Composition of daughter (errors)*									
SiO_2	47·77 (−0·17)	47·01 (−0·35)	49·08 (−0·07)	51·14 (+0·07)	52·38 (−0·06)	55·05 (+0·11)	63·97 (+0·12)	70·37 (−0·08)	76·39 (+0·06)
TiO_2	3·40 (+0·30)	3·98 (+0·30)	3·45 (−0·05)	3·15 (+0·05)	2·97 (−0·04)	1·98 (+0·14)	1·40 (+0·09)	0·42 (−0·05)	0·27 (+0·07)
Al_2O_3	14·05 (+0·22)	13·52 (+0·35)	13·89 (−0·04)	13·45 (+0·02)	14·31 (+0·01)	14·61 (+0·04)	13·35 (+0·05)	12·75 (−0·12)	10·99 (+0·29)
FeO_t	15·55 (+0·03)	16·50 (+0·12)	15·01 (−0·04)	14·07 (+0·05)	13·70 (−0·03)	12·76 (−0·04)	8·54 (+0·08)	4·01 (−0·05)	2·84 (+0·05)
MnO	0·30 (+0·00)	0·29 (−0·02)	0·23 (−0·08)	0·25 (−0·01)	0·19 (−0·06)	0·13 (+0·04)	0·18 (−0·08)	0·08 (+0·02)	0·04 (−0·07)
MgO	5·15 (−0·06)	4·84 (−0·09)	4·57 (−0·01)	4·04 (+0·02)	3·61 (+0·00)	2·23 (+0·04)	1·38 (+0·00)	0·46 (−0·04)	0·07 (+0·04)
CaO	9·35 (−0·44)	8·79 (−0·40)	8·10 (+0·00)	7·26 (+0·01)	6·76 (+0·00)	5·99 (−0·09)	3·62 (+0·08)	0·49 (−0·01)	0·28 (+0·06)
Na_2O	2·80 (−0·07)	2·71 (−0·04)	3·08 (+0·11)	3·27 (+0·03)	3·42 (−0·07)	4·14 (−0·44)	4·28 (−0·07)	4·35 (+0·27)	3·59 (−0·21)
K_2O	0·90 (+0·03)	0·99 (+0·03)	1·36 (+0·16)	1·54 (−0·13)	1·73 (+0·06)	2·02 (+0·04)	3·35 (−0·35)	5·15 (+0·16)	4·44 (−0·12)
P_2O_5	0·55 (+0·16)	0·7 (+0·10)	0·87 (+0·02)	0·99 (−0·10)	1·27 (+0·19)	0·72 (+0·14)	0·30 (+0·08)	0·09 (−0·11)	0·04 (+0·06)
$\sum r^2$	0·397	0·512	0·052	0·037	0·052	0·230	0·178	0·141	0·161
Phase compositions									
Plagioclase	An_{68}	An_{64}	An_{61}	An_{54}	An_{52}	An_{42}	An_{25}	An_{18}	An_0
Olivine	Fo_{73}	Fo_{68}	Fo_{66}	Fo_{63}	Fo_{60}	Fo_{49}	–	–	–
Ca-rich pyroxene	–	–	Mg-no. 73	Mg-no. 72	Mg-no. 71	Mg-no. 61	Mg-no. 51	Mg-no. 51	–
Magnetite	–	–	$Mt_{70}Usp_{30}$	$Mt_{70}Usp_{30}$	$Mt_{70}Usp_{30}$	$Mt_{70}Usp_{30}$	$Mt_{85}Usp_{15}$	$Mt_{85}Usp_{15}$	$Mt_{85}Usp_{15}$
Ilmenite	–	–	$Ilm_{91}He_9$	$Ilm_{91}He_9$	$Ilm_{91}He_9$	$Ilm_{91}He_9$	Ilm_{100}	Ilm_{100}	Ilm_{100}
Amphibole	–	–	–	–	–	–	Mg-no. 54	Mg-no. 54	Mg-no. 25
FK	–	–	–	–	–	–	–	–	$Or_{92}Ab_8An_0$
Subtracted phases (%)									
Plagioclase	76·3	78·0	40·2	49·0	45·1	41·9	57·8	52·6	29·2
Olivine	23·7	22·0	6·2	7·8	0·0	25·2	–	–	–
Ca-rich pyroxene	–	–	32·7	24·4	35·0	11·5	4·4	7·2	–
Magnetite	–	–	12·8	11·6	11·3	10·3	13·4	14·2	6·5
Ilmenite	–	–	8·1	7·3	8·7	4·4	2·8	1·6	0·0
Apatite	–	–	–	–	–	6·8	2·4	0·5	0·6
Amphibole	–	–	–	–	–	–	18·2	21·4	5·9
Biotite	–	–	–	–	–	–	1·1	2·6	2·3
FK	–	–	–	–	–	–	–	–	55·5
*F***	0·933	0·860	0·717	0·557	0·521	0·324	0·172	0·114	0·077

*Error = observed composition − modeled composition.
***F*, proportion of residual liquid.

JOURNAL OF PETROLOGY VOLUME 0 NUMBER 0 MONTH 2011

Downloaded from petrology.oxfordjournals.org at Bibliotheque Fac de Medecine on January 12, 2011

Table 11: Trace element partition coefficients selected for geochemical modeling

	From basaltic to intermediate composition						From intermediate to granitic composition						
	Plagioclase	Olivine	Ca-rich pyr.	Magnetite	Ilmenite	Apatite	Plagioclase	Ca-rich pyr.	Magnetite	Ilmenite	Apatite	Amphibole	Biotite
Rb	0·1[1]	0·08[1]	0·05[1]				0·1[1]	0·03[19]			0·01[17]	0·15[24]	0·82[32]
Sr	2·12[1]	0·01[1]	0·14[1]			2·2[22]	3·5[17]	0·09[25]			1·4[22]	0·01[17]	0·12[1]
Ba	0·3[1]	0·02[1]	0·002[1]				1·08[24]	0·04[26]	0·11[24]	0·11[24]	0·1[1]	0·92[29]	30[32]
Zr	0·13[1]	0·12[1]	0·03[1]	0·12[14]	0·33[18]		0·3[24]	0·25[27]	0·12[14]	0·33[18]			0·31[1]
Th	0·001[1]	0·001[1]	0·001[1]	0·025[14]	0·09[19]	2[17]	0·16[24]	0·001[28]			23[19]	0·09[24]	0·2[32]
Hf	0·01[2]	0·04[6]	0·5[8]	0·16[15]	0·38[20]	0·01[17]	0·01[2]	0·29[17]	0·16[15]	0·38[20]		0·5[17]	0·1[32]
Co	0·05[3]	1·6[7]	1·2[11]	5[16]	9[20]		0·05[3]	1·2[11]	5[16]	9[20]		6·1[17]	36[32]
Cr	0·01[2]	0·3[8]	2·7[12]	30[17]	16[21]		0·01[3]	2·7[12]	30[17]	16[21]		40[17]	1·52[32]
V	0·1[4]	0·02[9]	0·74[4]	8[17]	11·2[8]		0·1[4]	0·74[4]	8[17]	11·2[8]		1·49[30]	79·5[33]
La	0·13[5]	0·012[10]	0·04[13]	0·006[5]	0·0023[5]	8·6[23]	0·13[5]	0·04[13]	0·006[5]	0·0023[5]	8·6[23]	0·56[31]	0·32[1]
Ce	0·11[5]	0·009[10]	0·075[13]	0·006[5]	0·0019[5]	11·2[23]	0·11[5]	0·075[13]	0·006[5]	0·0019[5]	11·2[23]	0·73[31]	0·04[1]
Pr	0·1[5]	0·005[10]	0·113[13]	0·006[5]	0·0016[5]	12·6[23]	0·1[5]	0·113[13]	0·006[5]	0·0016[5]	12·6[23]	0·7[31]	0·04[1]
Nd	0·09[5]	0·004[10]	0·15[13]	0·006[5]	0·0012[5]	14[23]	0·09[5]	0·15[13]	0·006[5]	0·0012[5]	14[23]	0·7[31]	0·04[1]
Sm	0·06[5]	0·003[10]	0·22[13]	0·006[5]	0·0023[5]	14·6[23]	0·06[5]	0·22[13]	0·006[5]	0·0023[5]	14·6[23]	1·2[31]	0·06[1]
Eu	0·75[5]	0·003[10]	0·2[13]	0·006[5]	0·009[5]	9·6[23]	0·75[5]	0·2[13]	0·006[5]	0·009[5]	9·6[23]	1·5[31]	0·15[1]
Gd	0·052[5]	0·004[10]	0·25[13]	0·006[5]	0·006[5]	15·8[23]	0·052[5]	0·25[13]	0·006[5]	0·006[5]	15·8[23]	1·5[31]	0·08[1]
Tb	0·05[5]	0·004[10]	0·258[13]	0·006[5]	0·009[5]	15·4[23]	0·05[5]	0·258[13]	0·006[5]	0·009[5]	15·4[23]	1·5[31]	0·09[1]
Dy	0·048[5]	0·007[10]	0·267[13]	0·006[5]	0·013[5]	14·35[23]	0·048[5]	0·267[13]	0·006[5]	0·013[5]	14·35[23]	1·7[31]	0·1[1]
Ho	0·046[5]	0·007[10]	0·275[13]	0·006[5]	0·022[5]	13·3[23]	0·046[5]	0·275[13]	0·006[5]	0·022[5]	13·3[23]	3·3[31]	0·13[1]
Er	0·044[5]	0·008[10]	0·283[13]	0·006[5]	0·031[5]	11·5[23]	0·044[5]	0·283[13]	0·006[5]	0·031[5]	11·5[23]	4·2[31]	0·16[1]
Tm	0·042[5]	0·009[10]	0·292[13]	0·006[5]	0·044[5]	9·7[23]	0·042[5]	0·292[13]	0·006[5]	0·044[5]	9·7[23]	4·2[31]	0·17[1]
Yb	0·04[5]	0·013[10]	0·3[13]	0·008[5]	0·057[5]	8·1[23]	0·04[5]	0·3[13]	0·008[5]	0·057[5]	8·1[23]	4·4[31]	0·18[1]
Lu	0·038[5]	0·018[10]	0·3[13]	0·008[5]	0·07[5]	6·4[23]	0·038[5]	0·3[13]	0·008[5]	0·07[5]	6·4[23]	4·4[31]	0·15[1]

(1) McKenzie & O'Nions (1991); (2) Phinney & Morrison (1990); (3) Vander Auwera *et al*. (1998*b*) from Duchesne *et al*. (1974) and Demaiffe & Hertogen (1981); (4) Bougault & Hekinian (1974); (5) Demaiffe & Hertogen (1981); (6) Villemant *et al*. (1981); (7) Seifert *et al*. (1988); (8) McBirney (2002); (9) Duke (1976); (10) Frey (1969); (11) Henderson (1982); (12) Vander Auwera *et al*. (1998*b*) calculated from Hart & Dunn (1993) and Hauri *et al*. (1994); (13) McKay (1989); (14) Nielsen *et al*. (1994); (15) Mahood & Hildreth (1983); (16) Horn *et al*. (1994); (17) Bacon & Druitt (1988); (18) McKay *et al*. (1986); (19) Vander Auwera *et al*. (1998*b*); (20) Zack & Brumm (1998); (21) Jensen *et al*. (1993); (22) Watson & Green (1981); (23) Paster *et al*. (1974); (24) Caroff *et al*. (1993); (25) Ray *et al*. (1983); (26) Chazot *et al*. (1996); (27) Johnson & Kinzler (1989); (28) Mahood & Stimac (1990); (29) Ewart & Griffin (1994); (30) Sisson (1994); (31) Luhr & Carmichael (1980); (32) Villemant (1988); (33) Bea *et al*. (1994). When the *D* value is not specified for a mineral, it is considered as being equal to zero.

mass-balance calculations for major elements (Table 10). The trace element composition of the Sept Iles parent magma (average in Table 1) was used as the starting composition (L0 SC in Table 12). Calculated trace element concentrations (calculated from L0 SC in Table 12) of liquids were then compared with natural samples of monzonitic, syenitic and granitic composition (Table 12; Fig. 14).

The trace element patterns of monzonitic, syenitic and granitic melts are well reproduced by fractional crystallization of the parent magma for $F = 0{\cdot}30$, 0·20 and 0·10, respectively. However, the calculated concentrations of Zr, Hf and Th in the monzonitic, syenitic and granitic melts are lower than those observed in the natural samples. These elements are highly incompatible in the minerals subtracted to reach these compositions, indicating that error in the proportions of subtracted minerals cannot be invoked to explain this discrepancy. As previously suggested, the high Zr, Hf and Th concentrations of the natural samples probably result from zircon accumulation.

Partial melting of underplated basalts

It has been experimentally shown that partial melting of a mafic source is a plausible mechanism for producing A-type silicic liquids (Beard & Lofgren, 1991; Rapp *et al.*,

Downloaded from petrology.oxfordjournals.org at Bibliotheque Fac de Medecine on January 12, 2011

Table 12: Modeling of trace element composition with fractional crystallization

Sample	Rb	Sr	Ba	Zr	Th	Hf	Co	Cr	V	La	Ce	Pr	Nd	Sm	Eu	Gd	Tb	Dy	Ho	Er	Tm	Yb	Lu
Starting composition (L0 SC)	12·8	511	476	152	0·849	3·17	52·9	48·4	241	37·3	79·2	11·2	47·3	9·91	3·01	10·5	1·42	9·60	1·97	5·48	0·699	5·59	0·729
Monzonite																							
Average[1]	28·3	496	974	607	8·74	12·4	27·2	36·7	107	69·6	136	17·6	72·0	16·9	3·84	13·7	–	12·7	2·83	7·92	–	7·89	1·18
Lowest[2]	22·5	554	1148	670	12·4	20·4	32·1	45·1	118	82·5	162	21·3	85·3	19·1	4·49	14·2	–	14·5	3·23	9·07	–	9·78	1·33
Highest[3]	31·4	387	820	493	3·51	7·59	23·1	26·1	99·0	54·9	105	14·3	59·7	13·2	2·76	13·2	–	10·2	2·19	6·06	–	5·58	0·964
Calculated from L0 SC[4]	31·6	462	1182	324	2·31	8·23	35·1	2·33	128	70·2	132	17·3	68·8	14·4	3·74	14·9	2·16	13·9	3·03	9·13	1·24	9·27	1·33
Syenite																							
Average[5]	80·1	163	580	1238	8·53	34·2	5·32	15·3	25·1	80·2	191	–	101	28·4	4·16	20·2	3·10	–	3·38	–	–	7·97	1·06
Lowest	48·9	294	869	1448	8·55	36·9	12·0	20·8	61·5	86·4	195	–	110	34·6	4·59	20·5	3·33	–	3·56	–	–	8·34	1·07
Highest	120	51·8	454	874	8·50	31·5	1·18	6·12	2·68	74·0	187	–	92·8	22·1	3·73	19·9	2·86	–	3·19	–	–	7·59	1·05
Calculated from L0 SC	56·1	236	855	533	2·84	14·2	13·51	0·002	45·9	95·1	184	23·8	95·9	18·4	3·86	17·5	2·63	16·9	3·09	8·65	1·32	9·03	1·13
Granite																							
Average[6]	105	44·2	308	742	12·5	21·8	1·79	7·12	8·11	79·2	177	–	86·9	18·7	2·65	18·2	2·59	–	2·54	–	–	6·77	0·903
Lowest	94·1	77·4	499	1018	20·7	28·6	2·66	10·8	11·0	112	255	–	125	30·5	3·68	27·9	4·11	–	4·40	–	–	7·98	1·05
Highest	118	15·2	167	565	9·69	13·7	1·19	4·12	4·71	61·3	145	–	71·4	14·4	1·82	12·8	1·77	–	0·460	–	–	5·47	0·730
Calculated from L0 SC	81·6	167	714	740	3·24	16·1	5·41	–	14·3	137	259	34·0	140	26·2	4·61	24·9	3·42	23·2	3·29	8·80	1·21	8·83	1·12

[1]Average of monzonite samples (07-65; 07-16; 07-52).
[2]Lowest concentration of the element in samples included in the average.
[3]Highest concentration of the element in samples included in the average.
[4]Calculated liquid composition using L0 SC as the starting composition (parent magma), mineral proportions obtained from major element least-squares calculations (Table 10) and appropriate mineral/liquid partition coefficients (Table 11). L0 SC starting composition is the average Sept Iles parent magma (see Table 1).
[5]Average of syenite samples (03-48; 03-03; 03-29; 03-43).
[6]Average of granite samples (03-01; 03-25; 03-28; 03-30; 04-53).

Downloaded from petrology.oxfordjournals.org at Bibliotheque Fac de Medecine on January 12, 2011

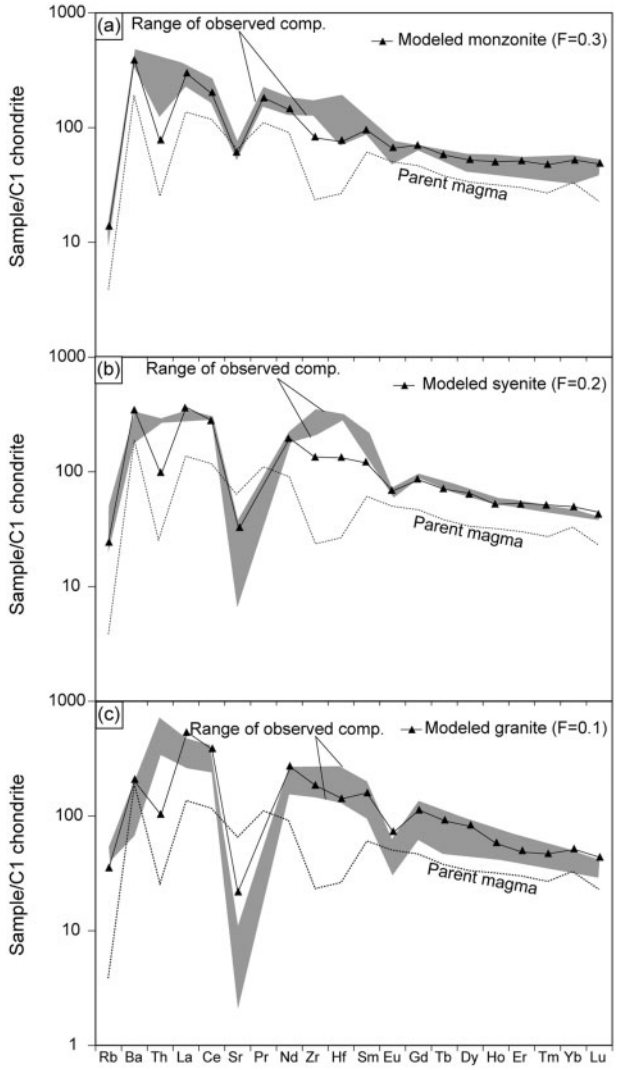

Fig. 14. Chondrite-normalized trace element variation diagrams comparing the composition of observed (a) monzonitic, (b) syenitic and (c) granitic liquids of the Upper Series (grey field indicates lowest to highest values for each element) with melts calculated assuming a fractional crystallization process. Mineral proportions and amounts of fractionation used in modeling are from the major-element mass-balance calculations (Table 10). Average of the parent magmas (Table 1) was used as the starting composition.

1991; Rushmer, 1991; Wolf & Wyllie, 1994; Rapp & Watson, 1995; Springer & Seck, 1997; Sisson *et al.*, 2005). In the following discussion, we test if partial melting of a mafic composition similar to the Sept Iles parent magma might produce liquids with trace element contents similar to those of the most primitive melts of the Upper Series. From a thermal point of view, such a hypothesis of partial melting is hardly tenable as it requires a significant heat input below the SIIS. However, it could be achieved by assuming repeated injection of mafic magma through sills in the lower to upper crust, the younger sills being responsible for local partial melting of the older sills.

Experiments by Beard & Lofgren (1991), Springer & Seck (1997) and Sisson *et al.* (2005) show that crystallization of a slightly hydrous basalt produces amphibolitic cumulates in the lower or the middle crust (>5 kbar) and anhydrous gabbros in the upper crust (<1 kbar). The presence of amphibole in the source is of critical importance, as dehydration melting of amphibole should occur during partial melting.

Partial melting of a basaltic source in the lower crust (amphibolite) was tested following the calculation method described by Vander Auwera *et al.* (2008) and using the experimental results of Beard & Lofgren (1991). As the partial melting process involves dehydration melting of amphibole (Beard & Lofgren, 1991; Rapp & Watson, 1995; Sisson *et al.*, 2005), we used the equations of Hertogen & Gijbels (1976), as they take into account incongruent melting processes and the fact that some phases, here amphibole, may be consumed during the melting process. We model the trace element composition of liquids produced for three amounts of partial melting ($F = 0{\cdot}115$, $0{\cdot}194$ and $0{\cdot}274$) of a source with trace element concentrations similar to that of the Sept Iles parent magma (average in Table 1). Results of the modeling are listed in Table 13 and presented in Fig. 15, where they are compared with the range of trace element concentrations of Sept Iles samples with *c.* 60 wt % SiO_2. Experiments by Beard & Lofgren (1991) show for $F = 0{\cdot}115$, partial melting of a mafic source produces liquids with *c.* 75 wt % SiO_2 and thus cannot produce the least evolved rocks of the Sept Iles Upper Series (*c.* 60 wt % SiO_2). Moreover, liquid produced at $F = 0{\cdot}115$ does not adequately reproduce the trace element patterns observed in the natural samples, particularly for light REE (LREE; mainly La), which are higher than those observed in the natural samples. When using $F = 0{\cdot}194$ and $F = 0{\cdot}274$, liquid compositions with 61–71 wt % SiO_2 are produced. The LREE concentrations are also better reproduced but the modeled heavy REE (HREE) contents become significantly higher than those of the natural samples.

Partial melting of basaltic rocks in the upper crust could also be responsible for the genesis of the SIIS silicic magmas. This hypothesis has been tested by trace element modeling using the experimental data of Toplis & Carroll (1995) on Skaergaard SC1 starting composition, which is closely similar to that of the Sept Iles parent magma. The concentrations of P_2O_5 and MnO (not incorporated in SC1) of the proposed Skaergaard parent magma KT-39 (Hoover, 1989) were used in the calculations. The proportions of the minerals contributing to the melt and left in the restite were calculated using the results of runs Fe-49 and Fe-52 of Toplis & Carroll (1995). Initial modal proportions in the source were determined by CIPW calculation

Downloaded from petrology.oxfordjournals.org at Bibliotheque Fac de Medecine on January 12, 2011

Table 13: Non-modal batch melting of a basaltic source in the lower and upper continental crusts

	Plag	Amph	Opx	Cpx	Oliv	Ilm	Mgt	Apat	Liq	Rb	Sr	Ba	Zr	Th	Hf	Cr	V	La	Ce	Pr	Nd	Sm	Eu	Gd	Tb	Dy	Ho	Er	Tm	Yb	Lu
Monzonite natural composition																															
Average*										28·3	496	974	607	8·74	12·4	36·7	107	69·6	136	17·6	72·0	16·9	3·84	13·7	–	12·7	2·83	7·92	–	7·89	1·18
Lowest†										22·5	387	820	493	3·51	7·59	26·1	99·0	54·9	105	14·3	59·7	13·2	2·76	13·2	–	10·2	2·19	6·06	–	5·58	0·964
Highest‡										31·4	554	1148	670	12·4	20·4	45·1	118	82·5	162	21·3	85·3	19·1	4·49	14·2	–	14·5	3·23	9·07	–	9·78	1·33
1. Non-modal batch melting of an amphibolite source (lower crust)																															
L0 SC (starting composition)	0·56	0·34				0·014	0·087			12·8	511	476	152	0·849	3·17	48·4	241	37·3	79·2	11·2	47·3	9·91	3·01	10·5	1·42	9·60	1·97	5·48	0·699	5·59	0·729
1.1. F = *0·115; non-modal batch melting with incongruent melting of amphibole*																															
p_i	0·53	0·47																													
t_i			0·23	0·61					0·16	64·4	466	1027	784	6·06	11·1	3·71	142	177	334	39·5	144	22·9	3·68	20·9	2·83	17·5	3·74	10·3	1·32	10·60	1·37
1.2. F = *0·194; non-modal batch melting*																															
X_i	0·56		0·09	0·23		0·02	0·10																								
p_i	0·44		0·24	0·19		0·14				50·2	394	1376	564	4·36	10·3	12·0	218	139	298	41·7	174	36·7	4·89	38·6	5·20	35·0	7·17	18·5	2·53	20·1	2·63
1.3. F = *0·274; non-modal batch melting*																															
X_i	0·57		0·07	0·23			0·13																								
p_i	0·53		0·35				0·12			38·7	408	1170	434	3·06	7·00	11·6	176	108	229	31·7	131	27·3	4·56	28·6	3·90	26·6	5·54	14·3	2·03	16·6	2·25
2. Non modal batch melting of a gabbroic anhydrous source (upper crust)																															
X_0	0·52		0·12	0·22	0·06	0·05	0·03	0·01																							
2.1. F = *0·236 Non-modal batch melting*																															
p_i	0·48		0·27		0·13	0·10		0·02		30·7	408	1269	291	3·08	7·15	18·0	244	105	231	32·8	130	27·7	5·94	28·1	4·14	24·6	5·20	13·2	2·01	16·1	1·67
2.2. F = *0·327 Non-modal batch melting*																															
X_i	0·40			0·44		0·01	0·15																								
p_i	0·30			0·15			0·54			23·1	418	1063	245	2·29	4·96	–	–	82·8	179	25	97·3	20·1	4·95	20·2	2·97	17·6	3·71	9·14	1·41	11·2	1·17

*Average of monzonite samples (07-65; 07-16; 07-52).
†Lowest concentration of the element in samples included in the average.
‡Highest concentration of the element in samples included in the average.
1. Trace element composition of the liquid produced by the non-modal batch melting of an amphibolite in the lower crust. The calculations follow equations of Hertogen & Gijbels (1976). Modal proportions of the initial amphibolite and incongruent melting reaction of the amphibole were estimated using experimental results (composition no. 466) of Beard & Lofgren (1991).
2. Trace element composition of the liquid produced by equilibrium non-modal batch melting of a tholeiitic source in the upper crust. Modal proportions of the source were estimated by CIPW calculation at FMQ conditions and 1160°C of the SC1 starting composition of Toplis & Carroll (1995). The melting reaction was determined using experimental results (runs Fe-49 and Fe-52) of Toplis & Carroll (1995).
p_i, fractional contribution of phase i to the melt; t_i, mass fractions of solid phases and liquid produced by the incongruent melting of amphibole; X_i, mass fraction of phase i.
L0 Sc (starting composition) is average Sept Iles parent magma (see Table 1).

Downloaded from petrology.oxfordjournals.org at Bibliotheque Fac de Medecine on January 12, 2011

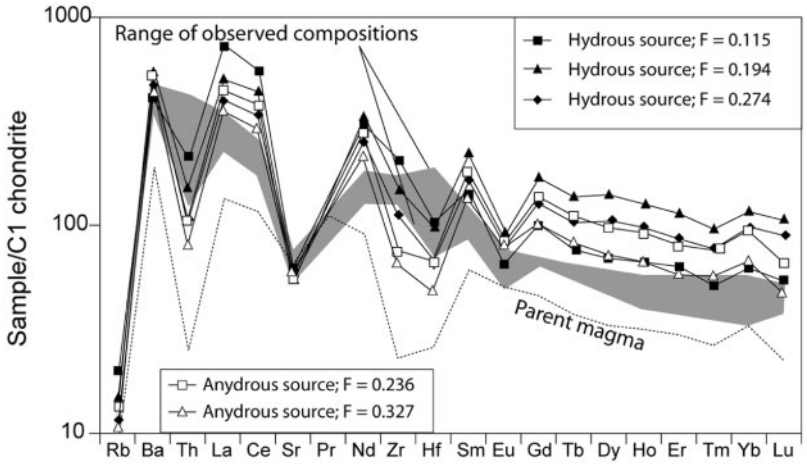

Fig. 15. Chondrite-normalized trace element variation diagram comparing the composition of the least evolved monzonitic liquids (*c.* 60 wt % SiO_2) of the Upper Series (grey field indicates lowest to highest values for each element) with melts calculated using a non-modal batch melting model for a hydrous source (with incongruent melting of amphibole) in the lower crust and an anhydrous source in the upper crust. Three fractions of liquid (F) are shown for the lower crust ($F = 0{\cdot}12$; $0{\cdot}19$; $0{\cdot}27$) and two fractions are shown for the upper crust ($F = 0{\cdot}24$; $0{\cdot}33$). Average of the parent magmas (Table 1) was used as the starting composition.

with a FeO/Fe_2O_3 of 15/85 at FMQ conditions and 1160°C (liquidus temperature of SC1; Toplis & Carroll, 1995). Calculations were performed for two amounts of equilibrium non-modal batch melting ($F = 0{\cdot}236$ and $F = 0{\cdot}327$), corresponding to the runs Fe-49 and Fe-52 that produce melts with 60–64 wt % SiO_2 (Table 13, Fig. 15). For $F = 0{\cdot}236$, the calculated HREE contents and, to a lesser extent, the calculated LREE contents are higher than those observed in the Sept Iles samples. In contrast, for $F = 0{\cdot}327$, the modeling more adequately reproduces the REE content of the natural samples. The major element composition of the liquid experimentally observed by Toplis & Carroll (1995) for a liquid fraction of 0·327 also closely matches the composition of monzonites observed in the SIIS.

Discriminating fractional crystallization vs partial melting

Results of geochemical modeling indicate that SIIS silicic magmas could result either from the extreme fractional crystallization of the Sept Iles parent magma or from the low-pressure equilibrium partial melting of a source of basaltic composition. The hypothesis of fractional crystallization is preferred here for the following reasons.

(1) No trace of silicic rocks was observed in apatite-free stratigraphic levels of the Layered Series, suggesting that silicic magmas are residual after significant troctolite and gabbro fractionation. This is in perfect agreement with least-squares calculations indicating that silicic liquids represent *c.* 10 wt % of the intrusion.
(2) Amphibole is a major phase in the Sept Iles granites. Liquids resulting from the partial melting of a basaltic source in the upper crust should be anhydrous (Sisson *et al.*, 2005), in clear contrast to the presence of amphibole in the Sept Iles granites, suggesting that they contain at least 4 wt % H_2O (Dall'Agnol *et al.*, 1999; Klimm *et al.*, 2003; Bogaerts *et al.*, 2006). This argument might of course be erroneous if water in the granites results from the interaction between the magma and meteoric water (e.g. Friedman *et al.*, 1974; Taylor, 1977) or from devolatilization and melting of hydrated blocks (e.g. Taylor, 1986; Bindeman *et al.*, 2007, 2008*a*, 2008*b*).
(3) The origin of the silicic rocks by partial melting would imply that evolved residual liquids from the Layered Series are missing.

ASSIMILATION AND FRACTIONAL CRYSTALLIZATION (AFC)

The potential influence of crustal assimilation in the genesis of Sept Iles silicic liquids has been tested using the AFC equations of DePaolo (1981). The average Sr concentration of the Sept Iles parent magma (511 ppm, Table 1) was used for modeling. The initial Sr isotopic composition of the parent magma is from sample 07-01 (0·70353), from a dyke in the Layered Series, where the least contamination is expected. With progressive differentiation, Sr contents first cluster around 500 ppm and then decrease continuously to *c.* 50 ppm (Fig. 9). Sr thus appears to be compatible for most of the differentiation path. Using mineral proportions obtained from the mass-balance calculations (Table 10) and appropriate values of D_{Sr} (Table 11),

Downloaded from petrology.oxfordjournals.org at Bibliotheque Fac de Medecine on January 12, 2011

D_{Sr}^{Bulk} values of 1·6 (for $F = 1·0–0·7$) and 2·1 (for $F = 0·7$ to 0·0) were calculated, and used in AFC modeling. The composition of the contaminant is traditionally constrained by the composition of the surrounding country-rocks (e.g. Stewart & DePaolo, 1990). Three types of country-rocks have been recognized around the Sept Iles intrusion: (1) altered gabbro [Sr 260 ppm; $(^{87}Sr/^{86}Sr)_{564}$ 0·7094]; (2) gneissic monzonite [Sr 230 ppm; $(^{87}Sr/^{86}Sr)_{564}$ 0·7189]; (3) cordierite-bearing leucocratic gneiss [Sr 97 ppm; $(^{87}Sr/^{86}Sr)_{564}$ 0·7746]. However, the geographical distribution and the relative proportions of these rocks are mostly unknown. The average composition of the three distinct types of country-rock has thus been taken as the contaminant component [Sr 195·7 ppm; $(^{87}Sr/^{86}Sr)_{564}$ 0·73431]. Results of AFC modeling (Fig. 16) indicate that the Sr isotopic compositions of the Sept Iles silicic rocks require only a very small amount of crustal contamination. A ratio (r) between 0·01 and 0·025 (1–2·5%) of assimilated to crystallized material is sufficient to match adequately the observed isotopic compositions and suggests that crustal assimilation does not play a significant role in the genesis of the silicic melts. The amount of contamination that is necessary to match the observed isotopic compositions ranges from 1%, when using the most radiogenic country-rock (cordierite-bearing gneiss), to 5% when using the least radiogenic country-rock (gneissic monzonite).

Reiners *et al.* (1995) have shown that the 'r' parameter used in the equations of DePaolo (1981) may be not constant during AFC processes. In addition, it has been demonstrated that modeling AFC processes without taking into account the energy constraint is physically unrealistic (Spera & Bohrson, 2001). Consequently, more consistent models for AFC (EC-AFC and subsequent developments; Spera & Bohrson, 2001, 2002, 2004; Bohrson & Spera, 2007) have been developed to constrain this parameter self-consistently. These models cannot be used accurately in the Sept Iles setting, as many of the required input data (e.g. magma liquidus temperature, country-rock temperature at the timing of magma injection) are not well constrained. However, Bohrson & Spera (2001) presented theoretical simulations for intrusion of basaltic magma into the upper continental crust and showed that the amount of assimilation calculated with EC-AFC is lower than that calculated with the equations of DePaolo (1981). It can thus be qualitatively suggested

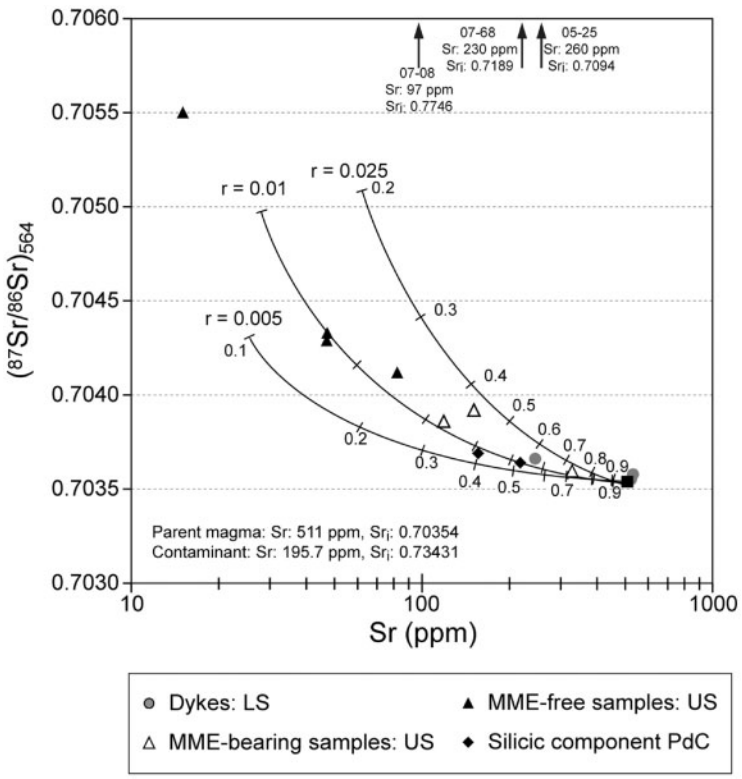

Fig. 16. $^{87}Sr/^{86}Sr$ (calculated at 564 Ma) vs Sr ppm for the Sept Iles liquids. The curves are AFC models calculated following DePaolo (1981) and showing compositional variations of a Sept Iles primitive tholeiitic basalt (Sr 511 ppm: $^{87}Sr/^{86}Sr$ 0·70354), assuming average Grenvillian gneiss as the contaminant (Sr 195·7 ppm, $^{87}Sr/^{86}Sr$ 0·73431). Ratios between mass of assimilated material and fractionated material (r) of 0·005, 0·01 and 0·025 are shown. Numbers along the line represent fractions of residual liquid. Arrows are directed toward the compositions (given values) of country-rock samples. Sr_i is $(^{87}Sr/^{86}Sr)_{564}$.

Downloaded from petrology.oxfordjournals.org at Bibliotheque Fac de Medecine on January 12, 2011

that our estimation of 1–2·5% crustal assimilation in the most evolved Sept Iles granites is an upper limit.

INTERMEDIATE COMPOSITIONS

Evidence for magma mixing

Intermediate rocks containing magmatic mafic enclaves (MME) may be considered as hybrid compositions because partial equilibration is known to occur between mingled mafic and silicic magmas (Didier & Barbarin, 1991; Barbarin, 2005). Moreover, although much effort has been made to remove any mafic enclaves during sample preparation, some small enclaves may have been included. The effect of magma mixing is difficult to assess using Harker diagrams showing a linear evolutionary trend with progressive differentiation (e.g. K_2O, CaO, MgO and the main part of the TiO_2 and FeO_t trends). However, for strongly curved distributions magma mixing will produce compositions that plot away from the crystallization trend. This is shown in the evolution of the Ba concentration (Fig. 9). In the range of *c.* 55–65 wt % SiO_2, two trends are observed, one with high Ba concentrations (950–1300 ppm) and another one with low Ba concentrations (250–800 ppm) displaying significant scatter. The latter trend is composed only of MME-bearing rocks, whereas geochemical modeling indicates that fractional crystallization of the parent magma produced the trend with high Ba concentrations. The low-Ba trend and its scatter are interpreted as resulting from mixing between silicic melts of various compositions (65–75 wt % SiO_2; 1000–300 ppm Ba) and primitive basalts (*c.* 50 wt % SiO_2; 500–600 ppm Ba; Fig. 17a).

Daly Gap

MME-bearing rocks, considered to represent hybrid magmas of bulk intermediate composition, create an artificial continuous differentiation trend between evolved basalts at 57 wt % SiO_2 and the most primitive MME-free granitoids at 67 wt % SiO_2. When whole-rock compositions are plotted without MME-bearing samples, a very low proportion of intermediate compositions are observed along the Sept Iles liquid line of descent (Fig. 17b and c). This paucity of intermediate compositions, commonly referred to as a 'Daly gap' (Daly, 1910; Chayes, 1963), is observed in many tholeiitic (Hildreth *et al.*, 1991; Geist *et al.*, 1995) and alkaline suites (Peccerillo *et al.*, 2003; Ferla & Meli, 2006; Macdonald *et al.*, 2008). In volcanic settings, this gap has been traditionally interpreted as resulting from density and viscosity barriers that preclude eruption (Marsh, 1981; Petford *et al.*, 1994; Mungall & Martin, 1995). However, this hypothesis cannot be applied to the plutonic setting of the Sept Iles layered intrusion.

Based on thermodynamic modeling, Peccerillo *et al.* (2003) investigated the evolution of the mass of residual liquid as a function of temperature during fractional crystallization from basalt to rhyolite. The decrease in the proportion of liquid per unit temperature is low during the early and late stages of fractionation but this drops abruptly during the intermediate stage of fractionation. Consequently, magma passes through all the intermediate compositions (intermediate liquid SiO_2 contents) for only a relatively small decrease in temperature, and only a small proportion of intermediate liquid is thus produced

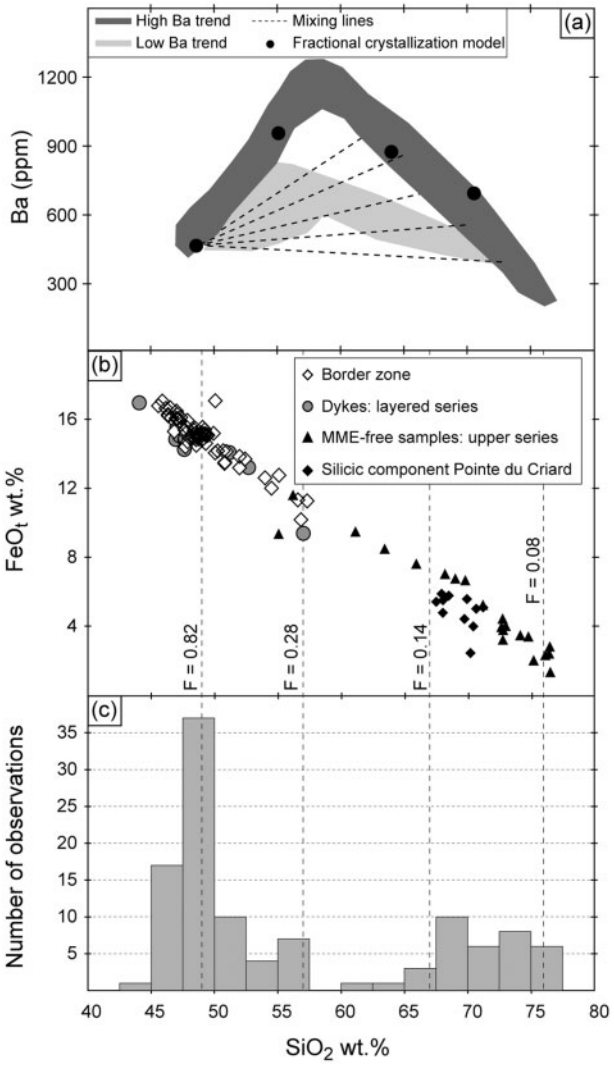

Fig. 17. (a) Ba vs SiO_2 diagram showing two different evolutionary trends: one high in Ba and the other low in Ba. (b) FeO_t vs SiO_2 diagram for samples representative of liquids. MME-bearing samples have not been plotted. Vertical lines represent the percentage of residual liquid (*F*) at different stages of fractionation [calculated by interpolation between the results of the fractional crystallization model (Table 10); the *F* value (0·28) for 57 wt % SiO_2 was interpolated between the M1 and S1 steps and the F value (0·14) for 67 wt % SiO_2 was interpolated between the S1 and G1 steps]. (c) Histogram of the SiO_2 content of the Sept Iles samples. MME-bearing samples are not included.

Downloaded from petrology.oxfordjournals.org at Bibliotheque Fac de Medecine on January 12, 2011

by fractional crystallization. A drop of residual liquid mass at intermediate stages of fractionation was also observed by Toplis & Carroll (1996) and Tegner *et al.* (2006) using forward modeling for Skaergaard and Bushveld liquid lines of descent, and was considered to explain the dearth of intermediate compositions in calc-alkaline lavas of the Medicine Lake Volcano, California (Grove & Donnelly-Nolan, 1986) and the bimodality of the basalt–trachyte association commonly observed in volcanic islands (Clague, 1978). Mass-balance calculations for Sept Iles liquids effectively indicate that only 15% of fractionation is required to cover all the range of compositions where samples are scarce (57–67 wt % SiO_2; Fig. 17c). However, in opposition to the calculations by Peccerillo *et al.* (2003), our model also shows that less than 10% fractionation is required to drive residual liquids from 67 to 77 wt % SiO_2 (Fig. 17c). In contrast to intermediate compositions, highly silicic rocks (65–75 wt % SiO_2) are abundant in the Upper Series. This dissimilarity in the volumes of intermediate and highly silicic rocks, while fractionation rates driving liquids from 57 to 67 wt % SiO_2 and from 67 to 77 wt % SiO_2 are relatively similar (Fig. 17b and c), suggests that the low proportion of intermediate compositions observed at Sept Iles cannot be related to a low volume of intermediate melts produced by the fractional crystallization process.

Apatite-bearing gabbros from the MCU II of the Sept Iles layered intrusion are in equilibrium with intermediate monzonitic melt compositions. Contrasting types of melt inclusions trapped in apatite with Fe-rich (ferrobasalt) and Si-rich (granite) compositions have been described by Charlier *et al.* (2009) and interpreted as a result of silicate liquid immiscibility just after the saturation of apatite. Although data on complex natural systems are missing, experiments by Visser & Koster van Groos (1979) on phase relations in the system K_2O–FeO–Al_2O_3–SiO_2 indicate that the miscibility gap may close at low temperatures. Consequently, although the Sept Iles silicic rocks may be entirely modeled by fractional crystallization, liquid immiscibility could be responsible for the absence of intermediate melt compositions along the liquid line of descent. It is worth noting that immiscibility has frequently been invoked as a furtive differentiation process in tholeiitic magma series in both volcanic (e.g. Philpotts, 1979) and plutonic settings (Longhi, 1998; Jakobsen *et al.*, 2005; Veksler *et al.*, 2007; Veksler, 2009).

Estimates of liquid compositions acquired in this study do not unambiguously allow us to determine of the origin of the Sept Iles Daly gap, which could thus result from at least two processes: (1) the low volume of intermediate melts produced during fractional crystallization (e.g. Peccerillo *et al.*, 2003) or (2) silicate liquid immiscibility (e.g. Charlier *et al.*, 2009).

SUMMARY OF THE CRYSTALLIZATION HISTORY OF THE SEPT ILES INTRUSIVE SUITE

Taken overall, our data may be used to propose a six-stage emplacement mechanism for the crystallization history of the Sept Iles intrusion, which ultimately leads to the formation of silicic rocks (Fig. 18).

(1) The parental tholeiitic basalt was emplaced in the upper crust at 564 Ma (Higgins & van Breemen, 1998; Higgins, 2005) and crystallized cumulate rocks to form the MCU I of the Layered Series (Fig. 18a and b). The anorthositic Upper Border Series was probably formed at this stage by flotation of plagioclase to the top of the magma chamber (Higgins, 2005; Fig. 18b).

(2) *In situ* crystallization of troctolites and gabbros from MCU I drives the residual liquid to a monzonitic composition (*c.* 55 wt % SiO_2; 10 wt % FeO_t) that lies between the top of the cumulates and the base of the Upper Border Series (Fig. 18c). At a temperature of *c.* 1050°C and with an H_2O content of *c.* 1·5 wt %, this liquid has a density close to 2·57 g cm^{-3} (considering $F = 0{\cdot}32$; see Table 10; and 0·4 wt % H_2O in the parent magma; Hunter & Sparks, 1987; Botcharnikov *et al.*, 2008), as calculated from the expression of Bottinga & Weill (1970), using partial molar volume and thermal expansion data from Lange & Carmichael (1987) and Toplis *et al.* (1994), and the compressibility data of Kress & Carmichael (1991). This density is lower than that of a typical anorthosite (*c.* 2·7 g cm^{-3}; Cawthorn & Ashwal, 2009). Part of the monzonitic liquid thus ascended through the anorthosite to form cupolas at the top of the magma chamber, where it continued to differentiate. The passage of silicic material through the Upper Border Series anorthosite is recorded by (a) a matrix of monzonitic to syenitic material surrounding plagioclase grains (Fig. 3b), (b) centimetre- to decimetre-scale pods of granophyric material and (c) centimetre- to decimetre thick dykes of monzonitic composition.

(3) During the crystallization of apatite gabbros from MCU I, a major event of undifferentiated basalt replenishment occurred (see Fig. 2b). Many dolerite feeder dykes are observed in the Layered Series, the Upper Border Series and the Upper Series (Fig. 18d) and have compositions very similar to the primitive dolerites of the Sept Iles chilled margin (Table 8). Newly injected basalts and residual monzonitic melts from the main magma body mixed thoroughly owing to vigorous convection, producing homogeneous hybrid melts in the main magma chamber. In the cupolas above the anorthosite where silicic melts had

Downloaded from petrology.oxfordjournals.org at Bibliotheque Fac de Medecine on January 12, 2011

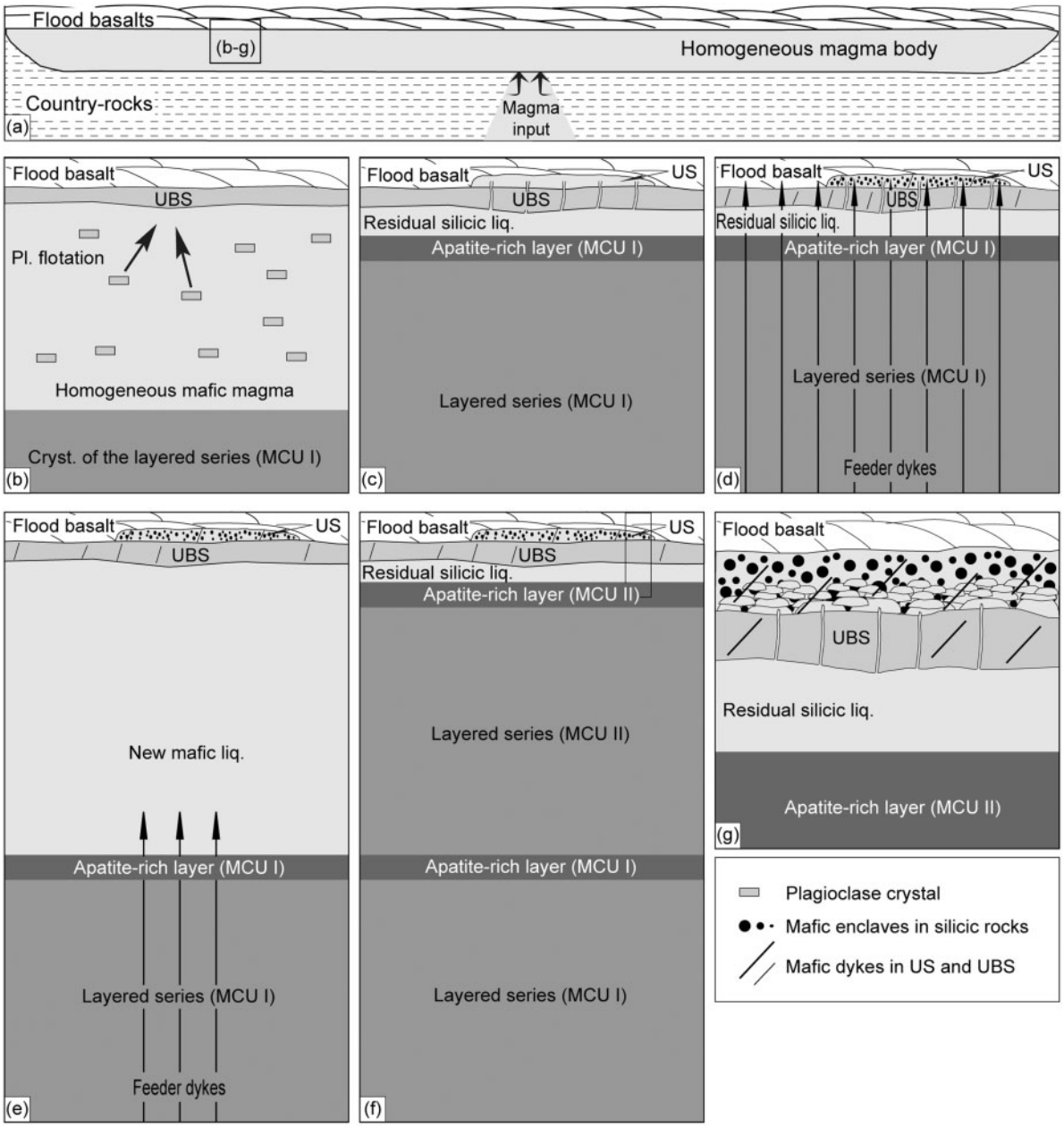

Fig. 18. Schematic model for the crystallization of the Sept Iles layered intrusion until the end of MCU II. (a) Filling of the magma chamber. (b) Crystallization of MCU I and simultaneous formation of the Upper Border Series (UBS) by plagioclase flotation. (c) The monzonitic residual liquid of MCU I partly ascends through the Upper Border Series to form a pocket of silicic melt at the top of the magma chamber (Upper Series; US). (d) Injection of basaltic (dolerite) dykes and hybridization with residual melt in the main magma chamber. Basaltic dykes are responsible for magma mingling and the formation of mafic enclaves in the silicic liquids of the Upper Series. (e) Crystallization of MCU II. (f) Part of the residual monzonitic liquids of MCU II ascends through the Upper Border Series. (g) These liquids stay at the base of the MME-bearing silicic rocks and form the MME-free silicic rock unit of the Upper Series.

migrated, viscosity contrasts between basaltic and silicic melts hampered magma mixing (Barbarin, 1988, 2005). Injection of basaltic dykes into the silicic magma was thus responsible for the formation of the mafic enclaves.

(4) The injection of undifferentiated tholeiitic basalt enlarged the magma chamber (Fig. 18e) and produced the gabbros now observed in the MCU II (Fig. 18f). The residual silicic liquid left after the crystallization of MCU II migrated through the

Downloaded from petrology.oxfordjournals.org at Bibliotheque Fac de Medecine on January 12, 2011

anorthosite to collect at the bottom of the mostly solidified MME-bearing granite (Fig. 18g). It is worth noting that MME-free silicic liquids are more radiogenic than those of the MME-rich granite, which is in agreement with the Sr isotope ratios of plagioclase from apatite layers in MCU I and MCU II (Namur *et al.*, 2010; see Table 2).

(5) The Pointe du Criard sill is dominated by a silicic component with a composition located on the Sept Iles liquid line of descent. The silicic melts that form the bulk of this sill could either be residual liquids left after the crystallization of MCU III or residual liquids of MCU II that were injected into a basaltic sill during magma chamber replenishment at the base of MCU III. However, the isotopic composition of the silicic component of the Pointe du Criard sill is clearly less radiogenic than that of MME-free silicic rocks. The hypothesis of residual liquids from MCU III is thus preferred; however, the absence of mineral composition and isotopic data from the evolved cumulates of MCU III, hidden under the St Lawrence River, makes this hypothesis unconstrained.

(6) Finally, rejuvenation of mafic magmatism could have occurred and might be responsible for the intrusion of a series of dolerite dykes that cut the Upper Series. These dykes were described by Higgins (2005) as forming the Late Gabbro intrusion.

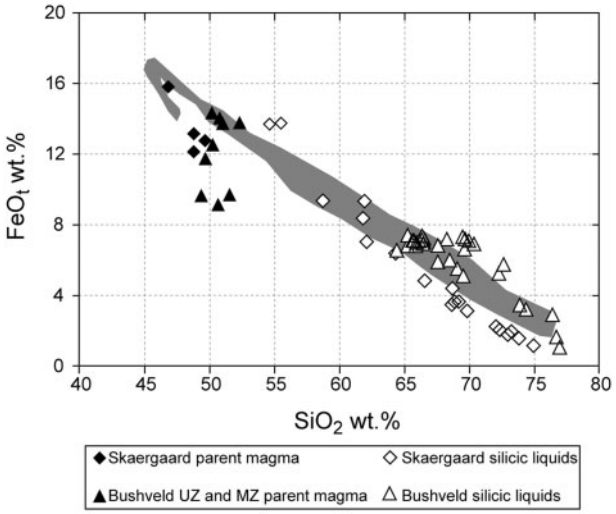

Fig. 19. FeO_t vs SiO_2 (wt %) diagram showing proposed compositions for the ferrobasaltic parent magma of the Skaergaard intrusion and the Bushveld Upper and Main Zones (filled symbols; data from Cawthorn *et al.*, 1981; Sharpe, 1981; Hatton, 1988; Hoover, 1989; Toplis & Carroll, 1995; Maier *et al.*, 2000; Nielsen, 2004; Jakobsen *et al.*, 2010; VanTongeren *et al.*, 2010) and the compositions of associated silicic liquids (open symbols; Twist, 1985; McBirney, 1989; Hischmann, 1992; Larsen & Brooks, 1994; Schweitzer *et al.*, 1997; Buchanan *et al.*, 2002). The liquid line of descent of the Sept Iles intrusive suite is represented by the grey field. UZ, Upper Zone; MZ, Main Zone.

IMPLICATIONS FOR SILICIC MELTS IN LAYERED INTRUSIONS

Although the evolution of tholeiitic magmas in layered intrusions during the first stages of differentiation is well understood, the differentiation path that occurs after Fe–Ti oxide minerals saturation is highly debated. Two of the most well-studied tholeiitic layered intrusions, the Skaergaard and the Bushveld Upper and Main Zones, display very similar cumulate sequences (troctolite or gabbronorite followed by Fe–Ti oxide gabbros and finally apatite-gabbro) and mineral compositions (McBirney, 1996; Tegner *et al.*, 2006) to those of the Sept Iles intrusion (Table 2). The Bushveld intrusion is topped by a large unit of rhyolitic rocks (VanTongeren *et al.*, 2010) whereas the Skaergaard intrusion does not contain a significant exposed volume of silicic rocks, although the occurrence of SiO_2-rich melts in pods has been noted (McBirney, 1989; Hirschmann, 1992; Larsen & Brooks, 1994). On the basis of FeO_t contents in plagioclase and mass-balance calculations based on the geochemistry of cumulate rocks, Tegner *et al.* (2006) and Tegner & Cawthorn (2010) suggested that Bushveld Fe–Ti oxide saturated melts evolved toward SiO_2 enrichment and FeO_t depletion through crystal–liquid differentiation. In contrast, on the basis of the FeO_t contents of plagioclase, Tegner (1997) suggested that Skaergaard Fe–Ti oxide saturated melts evolved toward strong FeO_t enrichment with only weak SiO_2 enrichment, in contrast to the experimental results of Toplis & Carroll (1995). Tegner & Cawthorn (2010) attributed the contrasted Skaergaard and Bushveld liquid lines of descent to differences in fO_2 conditions during crystallization.

The Sept Iles intrusion provides an unambiguous example of a tholeiitic layered intrusion that evolved toward SiO_2 enrichment and FeO_t depletion through protracted fractional crystallization. It is worth noting that the silicic melts of the Skaergaard and the Bushveld intrusions have remarkably similar compositions to those of the Sept Iles intrusion (Fig. 19).

The timing of Fe–Ti oxide saturation in tholeiitic melts is mainly controlled by the fO_2 conditions. Based on Sept Iles modeling, the saturation of Fe–Ti oxides occurs when the melt reaches 17 wt % FeO_t, a value in good agreement with the experimental results of Toplis & Carroll (1995) but lower than the 20 wt % obtained by Thy *et al.* (2009) by mass-balance calculations. The similarity between the Fe–Ti oxide-bearing gabbros of Skaergaard (average composition 26 wt % FeO_t for Lower Zone c, which corresponds to the first zone in the Layered Series with cumulus Fe–Ti oxide minerals, FeO_t compositions based on eight samples at depth of 875–784 m; Tegner *et al.*, 2009) and

Downloaded from petrology.oxfordjournals.org at Bibliotheque Fac de Medecine on January 12, 2011

Sept Iles (average composition 21 wt % FeO_t; Namur *et al.*, 2010) indicates that Skaergaard silicic liquids might also result from protracted fractionation of a tholeiitic basalt parent magma.

CONCLUSIONS

Rocks from the Sept Iles chilled margin, dykes cross-cutting the entire intrusion and silicic rocks from the Upper Series are interpreted to represent liquid compositions associated with the Sept Iles intrusive suite. They define a continuous trend from basalt to A-type granite. Melt compositions from basalt to monzonite (55 wt % SiO_2) are in equilibrium with the cumulates of the Layered Series, which range from troctolite ($An_{67–61}$, $Fo_{72–66}$) to gabbro ($An_{61–51}$; $Fo_{66–60}$) and apatite-bearing gabbro ($An_{51–34}$; $Fo_{60–21}$). Major and trace element modeling shows that fractional crystallization with minor assimilation of Grenvillian country-rocks (<2%) may explain the compositional trend from 47 to 76 wt % SiO_2. The maximum FeO_t content reached by the magma is about 17 wt %, corresponding to the magma composition at Fe–Ti oxide saturation. Fractionation of Fe–Ti oxide-bearing gabbros (*c.* 21 wt % FeO_t) is then responsible for SiO_2 enrichment and FeO_t depletion in the residual liquids.

The tholeiitic nature of the Sept Iles liquid line of descent is well supported by the following broadly accepted views on the evolution of tholeiitic liquids: (1) the most primitive liquid compositions are basaltic, have high concentrations of FeO_t and TiO_2, and mostly plot within the sub-alkaline field of the total alkalis–silica (TAS) diagram (Yoder & Tilley, 1962); (2) during the early stages of magmatic differentiation, corresponding to the crystallization of troctolite in the Layered series, the FeO_t and TiO_2 contents of the residual liquids increase (Grove & Baker, 1984); (3) the appearance of liquidus magnetite and ilmenite is responsible for the evolution of residual liquids towards SiO_2 enrichment; (4) the increase of silica activity with differentiation is responsible for the olivine hiatus observed in the Layered Series (Namur *et al.*, 2010). The strong geochemical similarity between the cumulates and liquids of Sept Iles and those of the well-known tholeiitic Skaergaard and Bushveld (Upper and Main Zones) intrusions leads us to suggest that the liquid lines of descent of the latter two intrusions might have evolved toward residual liquids of A-type silicic affinity.

Intermediate compositions within the Sept Iles liquid line of descent (57–67 wt % SiO_2) are essentially represented by MME-bearing rocks, interpreted as mingled hybrids. Following Peccerillo *et al.* (2003) and Charlier *et al.* (2009), we suggest that the scarcity of true intermediate liquid compositions (Daly gap) could be the result of the fractional crystallization process itself or of a silicate–liquid immiscibility process that occurs when the magma reached a monzonitic composition (*c.* 57 wt % SiO_2). Whatever the origin of the Daly gap, our calculations clearly indicate that the formation of metaluminous ferroan A-type granites from a tholeiitic basalt parent magma is globally the result of protracted fractional crystallization. The amount of fractionation (*c.* 90%) required to produce the granitic composition is moreover in good agreement with the relative proportions of mafic cumulates and silicic rocks as observed in the field.

ACKNOWLEDGEMENTS

G. Bologne and C. Gilson are thanked for the assistance with X-ray fluorescence and Sr-isotopic analyses. Comments by J. C. Duchesne, discussions with J. Hermann and H. O'Neill, reviews by E. Mathez, S. Morse and B. O'Driscoll, and careful editorial handling by W. Bohrson and M. Wilson were highly appreciated and significantly improved the quality of this paper.

FUNDING

This work was financed by the Belgian Fund for Joint Research (FNRS) and the Fund for Research in Industry and Agriculture (FRIA). M.D.H. would like to thank NSERC (Canada) for continuing Discovery grants.

REFERENCES

Andersen, D., Lindsley, D. & Davidson, P. (1993). QUILF—a Pascal program to assess equilibria among Fe–Mg–Mn–Ti oxides, pyroxenes, olivine, and quartz. *Computers and Geosciences* **19**, 1333–1350.

Anderson, C. I., Frost, C. D. & Frost, B. R. (2003). Petrogenesis of the Red Mountain pluton, Laramie anorthosite complex, Wyoming: Implications for the origin of A-type granite. *Precambrian Research* **124**, 243–267.

Andrews, G. D., Branney, M. J., Bonnichsen, B. & McCurry, M. (2008). Rhyolitic ignimbrites in the Rogerson Graben, southern Snake River Plain volcanic province: Volcanic stratigraphy, eruption history and basin evolution. *Bulletin of Volcanology* **70**, 269–291.

Ashwal, L. D., Wooden, J. L. & Emslie, R. F. (1986). Sr, Nd, and Pb isotopes in Proterozoic intrusives astride the Grenville Front in Labrador: Implications for crustal contamination and basement mapping. *Geochimica et Cosmochimica Acta* **50**, 2571–2585.

Bacon, C. R. & Druitt, T. H. (1988). Compositional evolution of the zoned calcalkaline magma chamber of Mount Mazama, Crater Lake, Oregon. *Contributions to Mineralogy and Petrology* **98**, 224–256.

Barbarin, B. (1988). Field evidence for successive mixing and mingling between the Piolard diorite and the Saint Julien-la-Vetre monzogranite (Nord Forez, Massif Central, France). *Canadian Journal of Earth Sciences* **25**, 49–59.

Barbarin, B. (2005). Mafic magmatic enclaves and mafic rocks associated with some granitoids of the central Sierra Nevada batolith, California: Nature, origin, and relations with the hosts. *Lithos* **80**, 155–177.

Barbey, P. (2009). Layering and schlieren in granitoids: A record of interaction between magma emplacement, crystallization and deformation in growing plutons. *Geologica Belgica* **12**, 109–133.

Bea, F., Pereira, M. D. & Stroh, A. (1994). Mineral/leucosome trace-element partitioning in a peraluminous migmatite (a laser ablation-ICP-MS study). *Chemical Geology* **117**, 291–312.

Downloaded from petrology.oxfordjournals.org at Bibliotheque Fac de Medecine on January 12, 2011

Beard, J. S. & Lofgren, G. E. (1991). Dehydration melting and water-saturated melting of basaltic and andesitic greenstones and amphibolites at 1, 3 and 6·9 kb. *Journal of Petrology* **32**, 365–401.

Bindeman, I. N., Watts, K. E., Schmitt, A. K., Morgan, L. A. & Shanks, P. W. (2007). Voluminous low $\delta^{18}O$ magmas in the late Miocene Heise volcanic field, Idaho: Implications for the fate of Yellowstone hotspot calderas. *Geology* **35**, 1019–1022.

Bindeman, I. N., Brooks, C. K., McBirney, A. R. & Taylor, H. P. (2008*a*). The low-$\delta^{18}O$ late-stage ferrodiorite magmas in the Skaergaard intrusion: Result of liquid immiscibility, thermal metamorphism, or meteoric water incorporation into magma? *Journal of Geology* **116**, 571–586.

Bindeman, I. N., Fu, B., Kita, N. T. & Valley, J. W. (2008*b*). Origin and evolution of silicic magmatism at Yellowstone based on ion microprobe analysis of isotopically zoned zircons. *Journal of Petrology* **49**, 163–193.

Bogaerts, M., Scaillet, Liegeois, J. P. & Vander Auwera, J. (2003). Petrology and geochemistry of the Lyngdal granodiorite (Souther Norway) and the role of fractional crystallization in the genesis of the Proterozoic ferro-potassic A-type granites. *Precambrian Research* **124**, 149–184.

Bogaerts, M., Scaillet, B. & Vander Auwera, J. (2006). Phase equilibria of the Lyngdal granodiorite (Norway): Implications for the origin of metaluminous ferroan granitoids. *Journal of Petrology* **47**, 2405–2431.

Bohrson, W. A. & Spera, F. J. (2001). Energy-constrained open-system magmatic processes II: Application of energy-constrained assimilation–fractional crystallization (EC-AFC) model to magmatic systems. *Journal of Petrology* **42**, 1019–1041.

Bohrson, W. A. & Spera, F. J. (2007). Energy-constrained recharge, assimilation, and fractional-crystallization (EC-RA_XFC): A visual basic computer code for calculating trace element and isotope variations of open-system magmatic systems. *Geochemistry, Geophysics, Geosystems* **8**, Q11003, doi:10.1029/2007GC0011781.

Bonin, B. (2007). A-type granites and related rocks: Evolution of a concept, problems and prospects. *Lithos* **97**, 1–29.

Bonnichsen, B., Leeman, W. P., Honjo, N., McIntosh, W. C. & Godchaux, M. M. (2008). Miocene silicic volcanism in southwestern Idaho: Geochronology and evolution of the central Snake River Plain. *Bulletin of Volcanology* **70**, 315–342.

Botcharnikov, R. E., Almeev, R. R., Koepke, J. & Holtz, F. (2008). Phase relations and liquid lines of descent in hydrous ferrobasalt–implications for the Skaergaard intrusion and Columbia River flood basalts. *Journal of Petrology* **49**, 1687–1727.

Bottinga, Y. & Weill, D. F. (1970). Densities of liquid silicate systems calculated from partial molar volumes of oxide components. *American Journal of Science* **269**, 169–182.

Bougault, H. & Hekinian, R. (1974). Rift valley in the Atlantic Ocean near 36°50'N: Petrology and geochemistry of basalt rocks. *Earth and Planetary Science Letters* **24**, 249–261.

Brooks, C. K. & Nielsen, T. F. (1990). The differentiation of the Skaergaard intrusion: A discussion of Hunter and Sparks (*Contributions to Mineralogy and Petrology* **95**, 451–461). *Contributions to Mineralogy and Petrology* **104**, 244–247.

Brueseke, M. E., Hart, W. K. & Heizler, M. T. (2008). Diverse mid-Miocene silicic volcanism associated with the Yellowstone–Newberry thermal anomaly. *Bulletin of Volcanology* **70**, 343–360.

Buchanan, P. C., Reimold, W. U., Koeberl, C. & Kruger, F. J. (2002). Geochemistry of intermediate to siliceous volcanic rocks of the Rooiberg Group, Bushveld Magmatic Province, South Africa. *Contributions to Mineralogy and Petrology* **144**, 131–143.

Byerly, G. R. (1980). The nature of differentiation trends in some volcanic rocks from the Galapagos Spreading Center. *Journal of Geophysical Research* **85**, 3797–3810.

Byerly, G. R., Melson, W. G. & Vogt, P. R. (1976). Rhyodacites, andesites, ferro-basalts and ocean tholeiites from the Galapagos Spreading Cente. *Earth and Planetary Science Letters* **30**, 215–221.

Carmichael, I. S. (1964). The petrology of the Thingmuli, a tertiary volcano in eastern Iceland. *Journal of Petrology* **5**, 435–460.

Carmichael, I. S. (1991). The redox states of basic and silicic magmas: A reflection of their source region? *Contributions to Mineralogy and Petrology* **106**, 129–141.

Caroff, M., Maury, R. C., Leterrier, J., Joron, J. L. & Cotten, J. (1993). Trace element behavior in the alkalic basalt comenditic trachyte series from Mururoa atoll, French Polynesia. *Lithos* **30**, 1–22.

Cawthorn, I. S., Davies, G., Clubley-Amstrong, A. & McCarthy, T. S. (1981). Sills associated with the Bushveld Complex, South Africa: An estimate of the parental magma composition. *Lithos* **14**, 1–14.

Cawthorn, R. G. & Ashwal, L. D. (2009). Origin of anorthosite and magnetitite layers in the Bushveld Complex, constrained by major element compositions of plagioclase. *Journal of Petrology* **50**, 1607–1637.

Charlier, B., Namur, O., Schiano, P. & Vander Auwera, J. (2009). A-type granite of the ferrobasaltic Sept Iles layered intrusion: a product of large-scale immiscibility? *EOS Transactions American Geophysical Union* **90**, AGU Fall Meeting Supplement, abstract v14a-06.

Chayes, F. (1963). Relative abundance of intermediate members of the oceanic basalt–trachyte association. *Journal of Geophysical Research* **68**, 1519–1534.

Chazot, G., Menzies, M. A. & Harte, B. (1996). Determination of partition coefficients between apatite, clinopyroxene, amphibole, and melt in natural spinel lherzolites from Yemen: Implications for wet melting of the lithospheric mantle. *Geochimica et Cosmochimica Acta* **60**, 423–437.

Cimon, J. (1998). *Le complexe de Sept-Îles: I—L'Unité à apatite de Rivière des Rapides, Complexe de Sept-Îles: localisation stratigraphique et facteurs à l'origine de sa formation*. Québec: Ministère de l'Energie et des Ressources du Québec, , ET-97-05, 33.

Civetta, L., D'Antonio, M., Orsi, G. & Tilton, G. R. (1998). The geochemistry of volcanic rocks from the Pantelleria Island, Sicily Channel: Petrogenesis and characteristics of the mantle source region. *Journal of Petrology* **39**, 1453–1491.

Clague, D. A. (1978). The oceanic basalt–trachyte association: An explanation of the Daly gap. *Journal of Geology*, **86**, 739–743.

Clemens, J. D., Holloway, J. R. & White, A. J. (1986). Origin of an A-type granite: Experimental constraints. *American Mineralogist* **71**, 317–324.

Cox, K. G., Bell, J. D. & Pankhurst, R. J. (1979). *The Interpretation of Igneous Rocks*. London: George Allen & Unwin, 450.

Dall'Agnol, R., Scaillet, B. & Pichavant, M. (1999). An experimental study of a lower Proterozoic A-type granite from the Eastern Amazonian Craton, Brazil. *Journal of Petrology* **40**, 1673–1698.

Daly, R. A. (1910). Origin of alkaline rocks. *Geological Society of America Bulletin* **21**, 87–118.

Davidson, A. (1995). A review of the Grenville orogen in its North American type area. *Journal of Australian Geology and Geophysics* **16**, 3–24.

Demaiffe, D. & Hertogen, J. (1981). Rare earth geochemistry and strontium isotopic composition of a massif-type anorthositic–charnockitic body: The Hidra massif (Rogaland, SW Norway). *Geochimica et Cosmochimica Acta* **45**, 1545–1561.

DePaolo, D. J. (1981). Trace element and isotopic effects of combined wallrock assimilation and fractional crystallization. *Earth and Planetary Science Letters* **53**, 189–202.

Downloaded from petrology.oxfordjournals.org at Bibliotheque Fac de Medecine on January 12, 2011

Dickin, A. P. (2000). Crustal formation in the Grenville Province: Nd-isotope evidence. *Canadian Journal of Earth Sciences* **37**, 165–181.

Didier, J. & Barbarin, B. (1991). *Enclaves and Granite Petrology. Development in Petrology 3*. Amsterdam: Elsevier.

Dickin, A. P. & Higgins, M. D. (1992). Sm/Nd evidence for a major 1·5 Ga crust-forming event in the central Grenville province. *Geology* **20**, 137–140.

Duchesne, J. C., Roelandts, I., Demaiffe, D., Hertogen, J., Gijbels, R. & de Winter, J. (1974). Rare-earth data on monzonoritic rocks related to anorthosites and their bearing on the nature of the parental magma of the anorthositic series. *Earth and Planetary Science Letters* **24**, 325–335.

Duke, J. M. (1976). Distribution of the period four transition elements among olivine, calcic clinopyroxene and mafic silicate liquid: Experimental results. *Journal of Petrology* **17**, 499–521.

Eby, G. N. (1990). The A-type granitoids: A review of their occurrence and chemical characteristics and speculations on their petrogenesis. *Lithos* **26**, 115–134.

Ewart, A. & Griffin, W. L. (1994). Application of proton-microprobe data to trace-element partitioning in volcanic rocks. *Chemical Geology* **117**, 251–284.

Ferla, P. & Meli, C. (2006). Evidence of magma mixing in the Daly gap of alkaline suites: A case study from the enclaves of Pantelleria (Italy). *Journal of Petrology* **47**, 1467–1507.

Frey, F. A. (1969). Rare earth abundances in a high-temperature peridotite intrusion. *Geochimica et Cosmochimica Acta* **33**, 1429–1447.

Friedman, I., Lipman, P. W., Obradovich, J. D., Gleason, J. D. & Christiansen, R. L. (1974). Meteoric water in magmas. *Science* **184**, 1069–1072.

Frost, B. R., Lindsley, D. H. & Anderson, D. J. (1988). Fe–Ti oxide–silicate equilibria: Assemblages with fayalitic olivine. *American Mineralogist* **73**, 727–740.

Frost, C. D., Frost, B. R., Chamberlain, K. R. & Edwards, B. R. (1999). Petrogenesis of the 1·43 Ga Sherman batholith SE Wyoming, USA: A reduced rapakivi-type anorogenic granite. *Journal of Petrology* **40**, 1771–1802.

Frost, B. R., Barnes, C. G., Collins, W. J., Arculus, R. J., Ellis, D. J. & Frost, C. D. (2001). A geochemical classification for granitic rocks. *Journal of Petrology* **42**, 2033–2048.

Frost, C. D., Frost, B. R., Bell, J. M. & Chamberlain, K. R. (2002). The relationship between A-type granites and residual magmas from anorthosite: Evidence from the northern Sherman batholith, Laramie Mountains, Wyoming, USA. *Precambrian Research* **119**, 45–71.

Geist, D., Howard, K. A. & Larson, P. (1995). The generation of oceanic rhyolites by crystal fractionation: the basalt–rhyolite association at Volcán Alcedo, Galápagos Archipelago. *Journal of Petrology* **36**, 965–982.

Ghiorso, M. S. & Sack, R. O. (1995). Chemical mass transfer in magmatic processes. IV. A revised and internally consistent thermodynamic model for the interpolation and extrapolation of liquid–solid equilibria in magmatic systems at elevated temperatures and pressures. *Contributions to Mineralogy and Petrology* **119**, 197–212.

Grove, T. L. & Baker, M. B. (1984). Phase equilibrium controls on the tholeiitic versus calc-alkaline differentiation trends. *Journal of Geophysical Research* **89**, 3253–3274.

Grove, T. L. & Donnelly-Nolan, J. M. (1986). The evolution of young silicic lavas at Medicine Lake Volcano, California: Implications for the origin of compositional gaps in calc-alkaline series lavas. *Contributions to Mineralogy and Petrology* **92**, 281–302.

Hart, S. & Dunn, T. (1993). Experimental cpx melt partitioning of 24 trace-elements. *Contributions to Mineralogy and Petrology* **113**, 1–8.

Hatton, C. J. (1988). Densities and liquidus temperatures of Bushveld parental magmas as constraints on the formation of the Merensky Reef in the Bushveld Complex, South Africa. In: Prendergast, M. D. & Jones, M. J. (eds) *Magmatic Sulphides—The Zimbabwe Volume*. London: Institution of Mining and Metallurgy, pp. 87–94.

Hauri, E. H., Wagner, T. P. & Grove, T. L. (1994). Experimental and natural partitioning of Th, U, Pb and other trace elements between garnet, clinopyroxene and basaltic melts. *Chemical Geology* **117**, 149–166.

Henderson, P. (1982). *Inorganic Geochemistry*. Oxford: Pergamon Press.

Hertogen, J. & Gijbels, R. (1976). Calculation of trace element fractionation during partial melting. *Geochimica et Cosmochimica Acta* **40**, 313–322.

Higgins, M. D. (1990). A three-component composite dyke and its associated intrusion, Pointe du Criard, Quebec, Canada. In: Parker, A. J., Rickwood, P. C. & Tucker, D. H. (eds) *Mafic Dykes and Emplacement Mechanism*. Rotterdam: Balkema, pp. 63–68.

Higgins, M. D. (2005). A new model for the structure of the Sept Iles Intrusive suite, Canada. *Lithos* **83**, 199–213.

Higgins, M. D. & Doig, R. (1981). The Sept Iles anorthosite complex: field relationships, geochronology, and petrology. *Canadian Journal of Earth Sciences* **18**, 561–573.

Higgins, M. D. & Doig, R. (1986). Geochemical constraints on the differentiation processes that were active in the Sept Iles complex. *Canadian Journal of Earth Sciences* **23**, 670–681.

Higgins, M. D. & van Breemen, O. (1998). The age of the Sept Iles layered mafic intrusion, Canada: Implications for the late Neoproterozoic/Cambrian history of Southeastern Canada. *Journal of Geology* **106**, 421–431.

Hildreth, W., Halliday, A. N. & Christiansen, R. L. (1991). Isotopic and chemical evidence concerning the genesis and contamination of basaltic and rhyolitic magma beneath the Yellowstone plateau volcanic field. *Journal of Petrology* **32**, 63–138.

Hirschmann, M. (1992). Origin of transgressive granophyres from the layered series of the Skaergaard intrusion, East Greenland. *Journal of Volcanology and Geothermal Research* **52**, 185–207.

Honjo, M. & Leeman, W. P. (1987). Origin of hybrid ferrolatite lavas from Magic Reservoir eruptive center, Snake River Plain, Idaho. *Contributions to Mineralogy and Petrology* **96**, 163–177.

Hoover, J. D. (1989). The chilled marginal gabbro and other contact rocks of the Skaergaard intrusion. *Journal of Petrology* **30**, 441–476.

Horn, I., Foley, S. F., Jackson, S. E. & Jenner, G. A. (1994). Experimentally determined partitioning of high field strength- and selected transition elements between spinel and basaltic melt. *Chemical Geology* **117**, 193–218.

Hunter, R. H. & Sparks, R. S. (1987). The differentiation of the Skaergaard intrusion. *Contributions to Mineralogy and Petrology* **95**, 451–461.

Irvine, T.N. (1982). Terminology for layered intrusions. *Journal of Petrology* **23**, 127–162.

Irvine, T. N. & Baragar, W. R. (1971). A guide to chemical classification of common volcanic rocks. *Canadian Journal of Earth Sciences* **8**, 315–341.

Jakobsen, J. K., Veksler, I. V., Tegner, C. & Brooks, C. K. (2005). Immiscible iron- and silica-rich melts in basalt petrogenesis documented in the Skaergaard intrusion. *Geology* **33**, 885–888.

Jakobsen, J. K., Tegner, C., Brooks, C. K., Kent, A. J., Lesher, C. E., Nielsen, T. F. & Wiedenbeck, M. (2010). Parental magma of the Skaergaard intrusion: Constraints from melt inclusions in primitive troctolite blocks and FG-1 dykes. *Contributions to Mineralogy and Petrology* **159**, 61–79.

Jensen, J. C., Nielsen, F. M., Duchesne, J. C., Demaiffe, D. & Wilson, J. R. (1993). Magma influx and mixing in the Bjerkreim–

Downloaded from petrology.oxfordjournals.org at Bibliotheque Fac de Medecine on January 12, 2011

Sokndal layered intrusion, South Norway: Evidence from the boundary between two megacyclic units at Storeknuten. *Lithos* **29**, 311–325.

Johnson, K. T. & Kinzler, R. J. (1989). Partitioning of REE, Ti, Zr, Hf, and Nb between clinopyroxene and basaltic liquid: An ion microprobe study. *EOS Transactions, American Geophysical Union* **70**, 1388.

Juster, T. C., Grove, T. L. & Perfit, M. R. (1989). Experimental constraints on the generation of FeTi basalts, andesites, and rhyodacites at the Galapagos Spreading Center, 85°W and 95°W. *Journal of Geophysical Research* **94**, 9251–9274.

Kerr, A. C., Kent, R. W., Thomson, B. A., Seedhouse, J. K. & Donaldson, C. H. (1999). Geochemical evolution of the Tertiary Mull volcano, Western Scotland. *Journal of Petrology* **40**, 873–908.

Kilinc, A., Carmichael, I. S., Rivers, M. L. & Sack, R. O. (1983). The ferric–ferrous ratio of natural silicate liquids equilibrated in air. *Contributions to Mineralogy and Petrology* **83**, 136–140.

Klimm, K., Holtz, F., Johannes, W. & King, P. L. (2003). Fractionation of metaluminous A-type granites: An experimental study of the Wangrah Suite, Lachlan Fold Belt, Australia. *Precambrian Research* **124**, 327–341.

Kress, V. C. & Carmichael, I. S. E. (1991). The compressibility of silicate liquids containing Fe_2O_3 and the effect of composition, temperature, oxygen fugacity and pressure on their redox states. *Contributions to Mineralogy and Petrology* **108**, 82–92.

Kumarapeli, P. S. & Saull, V. A. (1966). The St Lawrence Valley system: A North American equivalent of the East African rift system. *Canadian Journal of Earth Sciences* **3**, 639–657.

Kuno, H. (1966). Lateral variations of basalt magma types across continental margins and island arcs. *Bulletin of Volcanology* **29**, 195–222.

Lange, R. A. & Carmichael, I. S. (1987). Densities of Na_2O–K_2O–CaO–MgO–FeO–Fe_2O_3–Al_2O_3–TiO_2–SiO_2 liquids: New measurements and derived partial molar properties. *Geochimica et Cosmochimica Acta* **53**, 2195–2204.

Larsen, R. B. & Brooks, C. K. (1994). Origin and evolution of gabbroic pegmatites in the Skaergaard intrusion, East Greenland. *Journal of Petrology* **35**, 1651–1679.

Leake, B. E., Woolley, A. R., Arps, *et al*. (1997). Nomenclature of amphiboles: Report of the subcommittee on amphiboles of the International Mineralogical Association, Commission on new minerals and mineral series. *Canadian Mineralogist* **35**, 219–246.

Leeman, W. P. & Vitaliano, C. J. (1976). Petrology of McKinney basalt, Snake River Plain, Idaho. *Geological Society of America Bulletin* **87**, 1777–1792.

Leeman, W. P., Vitaliano, C. J. & Prinz, M. (1976). Evolved lavas from the Snake River Plain: Craters of the Moon National Monument, Idaho. *Contributions to Mineralogy and Petrology* **56**, 35–60.

Liégeois, J. P. & Black, R. (1987). Alkaline magmatism subsequent to collision in the Pan-African belt of Adrar des Iforas. In: Fitton, J. G. & Upton, B. G. (eds) *Alkaline Igneous Rocks*. London: Geological Society, pp. 381–401.

Lightfoot, P. C., Hawkesworth, C. J. & Sethna, S. F. (1987). Petrogenesis of rhyolites and trachytes from the Deccan trap: Sr, Nd and Pb isotope and trace element evidence. *Contributions to Mineralogy and Petrology* **95**, 44–54.

Loiselle, M. C. & Wones, D. (1979). Characteristics and origin of anorogenic granites. *Geological Society of America, Abstracts with Program* **11**, 468.

Loncarevic, B. D., Feininger, T. & Lefebvre, D. (1990). The Sept-Iles layered mafic intrusion: geophysical expression. *Canadian Journal of Earth Sciences* **27**, 501–512.

Longhi, J. (1998). Silicate liquid immiscibility: A furtive agent of fractionation. *Proceedings of the 29th Lunar and Planetary Science Conference*, Lunar and Planetary Institute, Houston, p. 1903.

Lowenstern, J. B. & Mahood, G. A. (1991). New data on magmatic H_2O contents of pantellerites, with implications for the petrogenesis and eruption dynamics at Pantelleria. *Bulletin of Volcanology* **54**, 78–83.

Ludwig, K. R. (2001). *User's manual for Isoplot/Ex version 2.49, a geochronological toolkit for Microsoft Excel*. Berkeley Geochronology Center Special Publications No. 1a.

Lugmair, G. W. & Marti, K. (1978). Lunar initial $^{143}Nd/^{144}Nd$: Differential evolution of the lunar crust and mantle. *Earth and Planetary Science Letters* **39**, 349–357.

Luhr, J. F. & Carmichael, I. S. (1980). The Colima volcanic complex, Mexico. I: Post-caldera andesites from Volcan Colima. *Contributions to Mineralogy and Petrology* **71**, 343–372.

Macdonald, R., Belkin, H. E., Fitton, J. G., Rogers, N. W., Nejbert, K., Tindle, A. G. & Marshall, A. S. (2008). The roles of fractional crystallization, magma mixing, crystal mush remobilization and volatile–melt interactions in the genesis of a young basalt–peralkaline rhyolite suite, the Greater Olkaria volcanic complex, Kenya Rift Valley. *Journal of Petrology* **49**, 1515–1547.

Mahood, G. A. & Hildreth, E. W. (1983). Large partition coefficients for trace elements in high-silica rhyolites. *Geochimica et Cosmochimica Acta* **47**, 11–30.

Mahood, G. A. & Stimac, J. A. (1990). Trace-element partitioning in pantellerites and trachytes. *Geochimica et Cosmochimica Acta* **54**, 2257–2276.

Maier, W. D., Arndt, N. T. & Curl, E. A. (2000). Progressive crustal contamination of the Bushveld Complex: evidence from Nd isotopic analysis of the cumulate rocks. *Contributions to Mineralogy and Petrology* **140**, 316–327.

Marsh, B. D. (1981). On the crystallinity, probability of occurrence, and rheology of lava and magma. *Contributions to Mineralogy and Petrology* **78**, 85–98.

McBirney, A. R. (1989). The Skaergaard layered series: I. Average compositions. *Journal of Petrology* **30**, 363–397.

McBirney, A. R. (1996). The Skaergaard intrusion. In: Cawthorn, R. G. (ed.) *Layered Intrusions. Developments in Petrology*, Vol. 15. Amsterdam: Elsevier, pp. 147–180.

McBirney, A. R. (2002). The Skaergaard layered series. Part VI. Excluded trace elements. *Journal of Petrology* **43**, 535–556.

McBirney, A. R. & Naslund, H. R. (1990). The differentiation of the Skaergaard intrusion: A discussion of Hunter and Sparks (*Contributions to Mineralogy and Petrology* **95**, 451–461). *Contributions to Mineralogy and Petrology* **104**, 235–240.

McCurry, M., Hayden, K. P., Morse, L. H. & Mertzman, S. (2008). Genesis of post-hotspot, A-type rhyolite of the Eastern Snake River Plain volcanic field by extreme fractional crystallization of olivine tholeiite. *Bulletin of Volcanology* **70**, 361–383.

McKay, G. A. (1989). Partitioning of rare earth elements between major silicate minerals and basaltic melts. In: Lipin, B. R. & McKay, G. A. (eds) *Geochemistry and Mineralogy of Rare Earth Elements. Mineralogical Society of America, Reviews in Mineralogy* **21**, 45–78.

McKay, G. A., Wagstaff, J. & Yang, S. R. (1986). Zirconium, hafnium, and rare earth partition coefficients for ilmenite and other minerals in high-Ti lunar mare basalts: An experimental study. *Journal of Geophysical Research* **91**, 229–237.

McKenzie, D. & O'Nions, R. K. (1991). Partial melt distributions from inversion of rare earth element concentrations. *Journal of Petrology* **32**, 1021–1091.

Downloaded from petrology.oxfordjournals.org at Bibliotheque Fac de Medecine on January 12, 2011

Morse, S. A. (1990). The differentiation of the Skaergaard intrusion: A discussion of Hunter and Sparks (*Contributions to Mineralogy and Petrology* **95**, 451–461). *Contributions to Mineralogy and Petrology* **104**, 240–244.

Mungall, J. E. & Martin, R. F. (1995). Petrogenesis of basalt–comendite and basalt–pantellerite suites, Terceira, Azores, and some implications for the origin of ocean-island rhyolites. *Contributions to Mineralogy and Petrology* **119**, 43–55.

Namur, O., Charlier, B., Toplis, M. J., Higgins, M. D., Liégeois, J. P. & Vander Auwera, J. (2010). Crystallization sequence and magma chamber processes in the ferrobasaltic Sept Iles layered intrusion, Canada. *Journal of Petrology* **51**, 1203–1236.

Naumann, T., Geist, D. & Kurz, M. (2002). Petrology and geochemistry of Volcan Cerro Azul: Petrologic diversity among the western Galapagos volcanoes. *Journal of Petrology* **43**, 859–883.

Nielsen, R. L., Forsythe, L. M., Gallahan, W. E. & Fisk, M. R. (1994). Major- and trace-element magnetite–melt equilibria. *Chemical Geology* **117**, 167–191.

Nielsen, T. F. (2004). The shape and volume of the Skaergaard intrusion, Greenland: Implications for mass balance and bulk composition. *Journal of Petrology* **45**, 507–530.

Olive, V., Hébert, R., Vermette, D. & Loubet, M. (1997). Geochemistry of Iapetus volcanic rocks, Quebec Appalachians: Nd, Sr isotopic compositions. *American Journal of Science* **297**, 418–439.

Paster, T. P., Schauwecker, D. S. & Haskin, L. A. (1974). The behavior of some trace elements during solidification of the Skaergaard layered series. *Geochimica et Cosmochimica Acta* **38**, 1549–1577.

Patiño Douce, A. E. (1997). Generation of metaluminous A-type granites by low-pressure melting of calc-alkaline granitoids. *Geology* **25**, 743–746.

Peccerillo, A. & Taylor, S. R. (1976). Geochemistry of Eocene volcanic rocks from the Kastamonu area, Northern Turkey. *Contributions to Mineralogy and Petrology* **58**, 63–81.

Peccerillo, A., Barberio, M. R., Yirgu, G., Ayalew, D., Barbieri, M. & Wu, T. W. (2003). Relationships between mafic and peralkaline silicic magmatism in continental rift settings: A petrological, geochemical and isotopic study of the Gedemsa Volcano, Central Ethiopian Rift. *Journal of Petrology* **44**, 2003–2032.

Petford, N., Lister, J. R. & Kerr, R. C. (1994). The ascent of felsic magmas in dykes. *Lithos* **32**, 161–168.

Philpotts, A. R. (1979). Silicate liquid immiscibility in tholeiitic basalts. *Journal of Petrology* **20**, 99–118.

Phinney, W. C. & Morrison, D. A. (1990). Partition coefficient for calcic plagioclase: Implications for Archean anorthosites. *Geochimica et Cosmochimica Acta* **54**, 1639–1654.

Rapp, R. P. & Watson, E. B. (1995). Dehydration melting of metabasalt at 8–32 kbar: Implications for continental growth and crust–mantle recycling. *Journal of Petrology* **36**, 891–931.

Rapp, R. P., Watson, E. B. & Miller, C. F. (1991). Partial melting of amphibolite/eclogite and the origin of Archean trondhjemites and tonalites. *Precambrian Research* **51**, 1–25.

Ray, G. L., Shimizu, N. & Hart, S. R. (1983). An ion microprobe study of the partitioning of trace elements between clinopyroxene and liquid in the system diopside–albite–anorthite. *Geochimica et Cosmochimica Acta* **47**, 2131–2140.

Reiners, P. W., Nelson, B. K. & Ghiorso, M. S. (1995). Assimilation of felsic crust by basaltic magma: Thermal limits and extents of crustal contamination of mantle-derived magmas. *Geology* **23**, 563–566.

Rivers, T. (2008). Assembly and preservation of lower, mid, and upper orogenic crust in the Grenville Province: implications for the evolution of large hot long-duration orogens. *Precambrian Research* **167**, 237–259.

Rushmer, T. (1991). Partial melting of two amphibolites: Contrasting results under fluid-absent conditions. *Contributions to Mineralogy and Petrology* **107**, 41–59.

Schweitzer, J. K., Hatton, C. J. & De Wall, S. A. (1997). Link between the granitic and volcanic rocks of the Bushveld Complex, South Africa. *Journal of African Earth Sciences* **24**, 95–104.

Seifert, S., O'Neill, H. S. & Brey, G. (1988). The partitioning of Fe, Ni and Co between olivine, metal, and basaltic liquid: An experimental and thermodynamic investigation, with application to the composition of the lunar core. *Geochimica et Cosmochimica Acta* **52**, 603–616.

Sharpe, M. R. (1981). The chronology of magma influxes to the eastern compartment of the Bushveld Complex as exemplified by its marginal border groups. *Journal of the Geological Society, London* **138**, 307–326.

Shaw, D. M., Cramer, J. J., Higgins, M. D. & Truscott, M. G. (1986). Composition of the Canadian Precambrian shield and the continental crust of the earth. In: Dawson, J. B., Carswell, D. A., Hall, J. & Wedepohl, K. H. (eds) *The Nature of the Lower Continental Crust*. Geological Society, London, Special Publications **24**, 275–282.

Sisson, T. W. (1994). Hornblende–melt trace-element partitioning measured by ion microprobe. *Chemical Geology* **117**, 331–344.

Sisson, T. W., Ratajeski, K., Hankins, W. & Glazner, A. F. (2005). Voluminous granitic magmas from common basaltic sources. *Contributions to Mineralogy and Petrology* **148**, 635–661.

Snyder, D., Carmichael, I. S. & Wiebe, R. A. (1993). Experimental study of liquid evolution in an Fe-rich layered mafic intrusion: constraints of Fe–Ti oxide precipitation on the T–fO_2 and T–ρ paths of tholeiitic magmas. *Contributions to Mineralogy and Petrology* **113**, 73–86.

Spera, F. J. & Bohrson, W. A. (2001). Energy-constrained open-system magmatic processes I: General model and energy-constrained assimilation and fractional crystallization (EC-AFC) formulation. *Journal of Petrology* **42**, 999–1018.

Spera, F. J. & Bohrson, W. A. (2002). Energy-constrained open-system magmatic processes 3. Energy-constrained recharge, assimilation, and fractional crystallization (EC-RAFC). *Geochemistry, Geophysics, Geosystems* **3**, 8001, doi:10.1029/2002GC000315.

Spera, F. J. & Bohrson, W. A. (2004). Open-system magma chamber evolution: An energy-constrained geochemical model incorporating the effects of concurrent eruption, recharge, variable assimilation and fractional crystallization (EC-E'RA_XFC). *Journal of Petrology* **45**, 2459–2480.

Springer, W. & Seck, H. A. (1997). Partial fusion of basic granulites at 5 to 15 kbar: Implications for the origin of TTG magmas. *Contributions to Mineralogy and Petrology* **127**, 30–45.

Steiger, R. H. & Jäger, E. (1977). Subcommission on geochronology: convention of the use of decay constants in geo- and cosmochronology. *Earth and Planetary Science Letters* **36**, 359–362.

Stewart, B. W. & DePaolo, D. J. (1990). Isotopic studies of processes in mafic magma chambers: II. The Skaergaard Intrusion, East Greenland. *Contributions to Mineralogy and Petrology* **104**, 125–141.

Stormer, J. C. & Nicholls, J. (1978). XLFRAC: A program for the interactive testing of magmatic differentiation models. *Computers and Geosciences* **4**, 143–159.

Stout, M. Z. & Nicholls, J. (1977). Mineralogy and petrology of Quaternary lavas from the Snake River Plain, Idaho. *Canadian Journal of Earth Sciences* **14**, 2140–2156.

Sun, S. S. & McDonough, W. F. (1989). Chemical and isotopic systematics of oceanic basalts: implication for mantle composition and process. In: Saunders, A. D. & Norry, M. J. (eds) *Magmatism in the*

Downloaded from petrology.oxfordjournals.org at Bibliotheque Fac de Medecine on January 12, 2011

Ocean Basins. Geological Society, London, Special Publications **42**, 313–345.

Tamura, Y. & Tatsumi, Y. (2002). Remelting of an andesitic crust as a possible origin for rhyolitic magma in oceanic arcs: An example from the Izu–Bonin Arc. *Journal of Petrology* **43**, 1029–1047.

Taylor, H. P. (1977). Water/rock interaction and the origin of H_2O in granitic batholiths. *Journal of the Geological Society, London* **133**, 509–558.

Taylor, H. P. (1986). Igneous rocks. II. Isotopic case studies of circum-Pacific magmatism. In: Valley, J. W., Taylor, H. P. & O'Neill, J. R. (eds) *Stable Isotopes in High-temperature Geological Processes*. Mineralogical Society of America, Reviews in Mineralogy **16**, 217–317.

Tegner, C. (1997). Iron in plagioclase as a monitor of the differentiation of the Skaergaard intrusion. *Contributions to Mineralogy and Petrology* **128**, 45–51.

Tegner, C. & Cawthorn, R.G. (2010). Iron in plagioclase in the Bushveld and Skaergaard intrusions: Implications for iron contents in evolving basic magmas. *Contributions to Mineralogy and Petrology* **159**, 719–730.

Tegner, C., Cawthorn, R. G. & Kruger, F. J. (2006). Cyclicity in the Main and Upper Zones of the Bushveld Complex, South Africa: Crystallization from a Zoned Magma Sheet. *Journal of Petrology* **47**, 2257–2279.

Tegner, C., Thy, P., Holness, M., Jakobsen, J. K. & Lesher, C. E. (2009). Differentiation and compaction in the Skaergaard intrusion. *Journal of Petrology* **50**, 813–840.

Thy, P., Lesher, C. E., Nielsen, T. F. & Brooks, C. K. (2006). Experimental constraints on the Skaergaard liquid line of descent. *Lithos* **92**, 154–180.

Thy, P., Lesher, C. E. & Tegner, C. (2009). The Skaergaard liquid line of descent revisited. *Contributions to Mineralogy and Petrology* **157**, 735–747.

Tilley, C. E. & Thompson, R. N. (1970). Melting and crystallization relations of the Snake River basalts of southern Idaho. *Earth and Planetary Science Letters* **8**, 79–92.

Toplis, M. J. & Carroll, M. R. (1995). An experimental study of the influence of oxygen fugacity on Fe–Ti oxide stability, phase relations, and mineral–melt equilibria in ferro-basaltic systems. *Journal of Petrology* **36**, 1137–1170.

Toplis, M. J. & Carroll, M. R. (1996). Differentiation of ferro-basaltic magmas under conditions closed and open to oxygen: Implications for the Skaergaard intrusion and other natural systems. *Journal of Petrology* **37**, 837–858.

Toplis, M. J., Dingwell, D. B. & Libourel, G. (1994). The effect of phosphorus on the iron redox ratio, viscosity, and density of an evolved ferro-basalt. *Contributions to Mineralogy and Petrology* **117**, 293–304.

Trua, T., Deniel, C. & Mazzuoli, R. (1999). Crustal control in the genesis of Plio-Quaternary bimodal magmatism of the Main Ethiopian Rift (MER): Geochemical and isotopic (Sr, Nd, Pb) evidence. *Chemical Geology* **155**, 201–231.

Turner, S. P., Foden, J. D. & Morrison, R. S. (1992). Derivation of some A-type magmas by fractionation of basaltic magma: An example from the Padthaway Ridge, South Australia. *Lithos* **28**, 151–179.

Twist, D. (1985). Geochemical evolution of the Rooiberg silicic lavas in the Loskop Dam Area, Southeastern Bushveld. *Economic Geology* **80**, 1153–1165.

Vander Auwera, J., Bologne, G., Roelandts, I. & Duchesne, J. C. (1998*a*). Inductively coupled plasma-mass spectrometric (ICP-MS) analysis of silicate rocks and minerals. *Geologica Belgica* **1**, 49–53.

Vander Auwera, J., Longhi, J. & Duchesne, J. C. (1998*b*). A liquid line of descent of the jotunite (hypersthene monzodiorite) suite. *Journal of Petrology* **39**, 439–468.

Vander Auwera, J., Bogaerts, M., Liegeois, J. P., Demaiffe, D., Wilmart, E., Bolle, O. & Duchesne, J. C. (2003). Derivation of the 1·0–0·9 Ga ferro-potassic A-type granitoids of southern Norway by extreme differentiation from basic magmas. *Precambrian Research* **124**, 107–148.

Vander Auwera, J., Bogaerts, M., Bolle, O. & Longhi, J. (2008). Genesis of intermediate igneous rocks at the end of the Sveconorwegian (Grenvillian) orogeny (S Norway) and their contribution to intracrustal differentiation. *Contributions to Mineralogy and Petrology* **156**, 721–743.

VanTongeren, J. A., Mathez, E. A. & Kelemen, P.B. (2010). A felsic end to Bushveld differentiation. *Journal of Petrology* **51**, 1891–1912.

Veksler, I. V. (2009). Extreme iron enrichment and liquid immiscibility in mafic intrusions: Experimental evidence revisited. *Lithos* **111**, 72–82.

Veksler, I. V., Dorfman, A. M., Borisov, A. A., Wirth, R. & Dingwell, D. B. (2007). Liquid immiscibility and the evolution of basaltic magma. *Journal of Petrology* **48**, 2187–2210.

Villemant, B. (1988). Trace-element evolution in the Phlegrean Fields (Central Italy): Fractional crystallization and selective enrichment. *Contributions to Mineralogy and Petrology* **98**, 169–183.

Villemant, B., Jaffrezic, H., Joron, J. L. & Treuil, M. (1981). Distribution coefficients of major and trace-elements: fractional crystallization in the alkali basalt series of Chaîne-des-Puys (Massif Central, France). *Geochimica et Cosmochimica Acta* **45**, 1997–2016.

Visser, W. & Koster van Groos, A. F. (1979). Phase relations in the system K_2O–FeO–Al_2O_3–SiO_2 at 1 atmosphere with special emphasis on low temperature liquid immiscibility. *American Journal of Science* **279**, 70–91.

Wadleigh, M. A., Veizer, J. & Brooks, C. (1985). Strontium and its isotope in Canadian rivers: fluxes and global implications. *Geochimica et Cosmochimica Acta* **49**, 1727–1736.

Wager, L. R. & Brown, G. M. (1968). *Layered Igneous Rocks*. Edinburgh: Oliver & Boyd, 558 p.

Wager, L. R. & Deer, W. A. (1939). Geological investigations in East Greenland. Part III. The petrology of the Skaergaard intrusion, Kangerrdlugssuaq, East Greenland. *Meddelelser om Gronland* **105**, 1–352.

Walsh, J. N., Beckinsale, R. D., Skelhorn, R. R. & Thorpe, R. S. (1979). Geochemistry and petrogenesis of Tertiary granitic rocks from the Island of Mull, Northwest Scotland. *Contributions to Mineralogy and Petrology* **71**, 99–116.

Watson, E. B. & Green, T. H. (1981). Apatite/liquid partition coefficients for REE and Sr. *Earth and Planetary Science Letters* **56**, 405–421.

Whalen, J. B., Currie, K. L. & Chappell, B. W. (1987). A-type granites: Geochemical characteristics, discrimination and petrogenesis. *Contributions to Mineralogy and Petrology* **95**, 407–419.

Wiebe, R. A. & Collins, W. J. (1998). Depositional features and stratigraphic sections in granitic plutons: Implications for the emplacement and crystallization of granitic magma. *Journal of Structural Geology* **20**, 1273–1289.

Wolf, M. B. & Wyllie, P. J. (1994). Dehydration melting of solid amphibolite at 10 kbar: The effects of temperature and time. *Contributions to Mineralogy and Petrology* **115**, 369–383.

Yoder, H. S. & Tilley, C. E. (1962). Origin of basaltic magmas: an experimental study of natural and synthetic rock systems. *Journal of Petrology* **3**, 342–532.

Zack, T. & Brumm, R. (1998). Ilmenite/liquid partition coefficients of 26 trace elements determined through ilmenite/clinopyroxene partitioning in garnet pyroxene. In: Gurney, J. J., Gurney, J. L., Pascoe, M. D. & Richardson, S. H. (eds) *Proceedings of the 7th International Kimberlite Conference*. Cape Town: Red Roof Design, pp. 986–988.

Downloaded from petrology.oxfordjournals.org at Bibliotheque Fac de Medecine on January 12, 2011

APPENDIX

Sample preparation and analytical methods

All rock samples (1–4 kg) were carefully cleaned prior to further treatment. They were then manually crushed with a hammer and milled in agate mortars. Whole-rock compositions were obtained for major and some trace elements (Rb, Sr, Y, Zr, Nb, Pb, Co, Cu, Ni, Zn, Ba, Cr, V, Ga) using an ARL 9400 XP X-ray fluorescence system at the Université de Liège (Belgium). Major elements (except P) were measured on lithium tetra- and meta-borate fused glass discs, with matrix corrections following the Traill–Lachance algorithm. Phosphorus and trace elements were measured on pressed powder pellets and the data were corrected for matrix effects by Compton peak monitoring (except for V, Cr and Ba). Accuracy is estimated as better than 1% for major elements and 5% for trace elements and was controlled using 40 international and in-house standards.

Ninety-two whole-rock samples were analysed for REE, Ta, W, U, Th and Hf by inductively coupled plasma mass spectrometry (ICP-MS) with a VG Plasma Quad PQ2 at the Université de Liège (Belgium) and a VG Plasma Quad PQ2 at the Royal Museum for Central Africa of Tervuren (Belgium). Precision is better than 10% for all elements (Vander Auwera *et al.*, 1998*a*). Sample 05-45 was analysed in the two laboratories (Liège and Tervuren) and also with a Perkin–Elmer Elan 6000 at the Centre de Recherches Pétrographiques et Géochimiques (CRPG), Nancy (France). Results were found to be very similar in the three sets of analyses.

Strontium and Nd isotopic compositions were measured in 32 and 19 whole-rock samples, respectively, by thermal ionization mass spectrometry (TIMS) at the Royal Museum for Central Africa, Tervuren (Belgium). After dissolution of the sample and Sr and Nd separation on ion-exchange resin, Sr isotopic compositions were measured on Ta simple filaments and Nd isotopic compositions on triple Ta–Re–Ta filaments on a VG Sector 54 mass spectrometer. Repeated measurements of Sr and Nd isotope ratios agreed at better than 0·000015. The standard NBS987 was used for Sr and gave a value of $0{\cdot}710297 \pm 0{\cdot}000005$ for $^{87}Sr/^{86}Sr$, with a normalization value of 0·1194 for $^{86}Sr/^{88}Sr$. The Rennes Nd standard was used for Nd and gave a value of $0{\cdot}511958 \pm 0{\cdot}000006$ for $^{143}Nd/^{144}Nd$, with a normalization value of 0·7219 for $^{146}Nd/^{144}Nd$. The decay constants used were $1{\cdot}42 \times 10^{-11}$ a^{-1} for ^{87}Rb (Steiger & Jäger, 1977) and $6{\cdot}54 \times 10^{-12}$ a^{-1} for ^{147}Sm (Lugmair & Marti, 1978). Initial ratios were calculated for an age of 564 Ma (Higgins & van Breemen, 1998). Rb and Sr concentrations were determined by repeated XRF measurements ($n = 8$) on pressed powder pellets. Accuracy is estimated as better than 5% for Rb and 2% for Sr. Sm and Nd were analysed by ICP-MS with the VG Plasma Quad PQ2 at the Université de Liège (Belgium). Accuracy is estimated as better than 5% (Vander Auwera *et al.*, 1998*a*).

Eleven representative samples of felsic rocks from the Upper Series and the Pointe du Criard sill were selected for mineral analyses. Feldspars (11 samples), amphiboles (10 samples) and Ca-rich pyroxenes (four samples) were analysed with a Cameca SX 100 electron microprobe at Laval University (Canada). Analytical conditions were 15 kV for the accelerating voltage and 15 nA for the beam current. A defocused beam of 10 μm in diameter was used. The following standards were used for Kα X-ray line calibrations: albite for Na and Al; orthoclase for Si and K; hematite for Fe; wollastonite for Ca; $MnTiO_3$ for

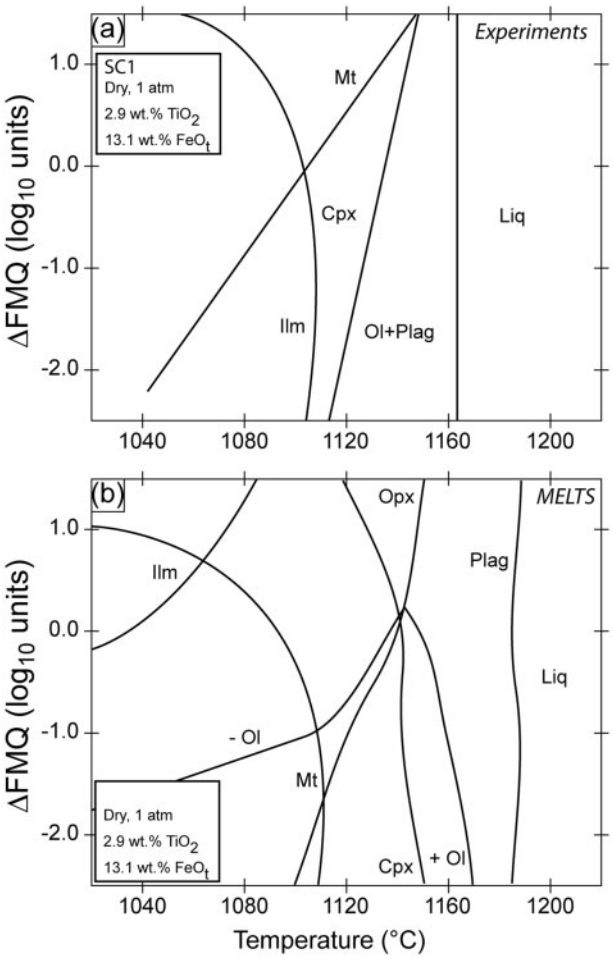

Fig. A1. Phase equilibria for composition SC1 (Toplis & Carroll, 1995) as a function of temperature and oxygen fugacity (log fO_2 relative to FMQ buffer). Continuous lines mark inferred phase boundaries. (a). Experimentally determined phase diagram. All experiments contain liquid (Liq) in addition to crystalline phases (plagioclase: Plag; olivine: Ol; Ca-rich pyroxene: Cpx; magnetite–ulvöspinel solid solution: Mt; ilmenite–hematite solid solution: Ilm). The diagram was drawn after Toplis *et al.* (1994) and Toplis & Carroll (1995). (b). MELTS-predicted SC1 phase diagram for equilibrium equilibrium crystallization.

Downloaded from petrology.oxfordjournals.org at Bibliotheque Fac de Medecine on January 12, 2011

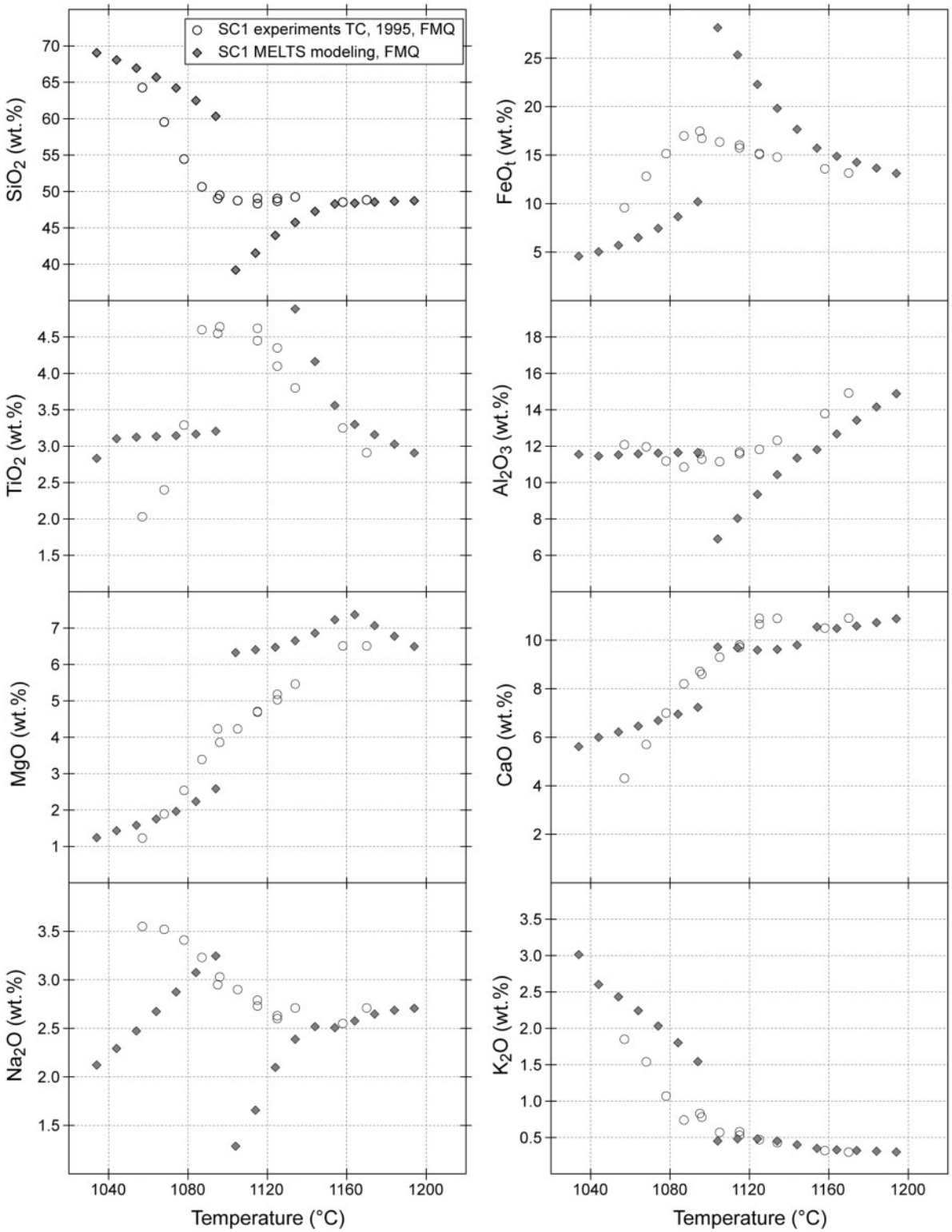

Fig. A2. Comparison between experimentally determined (at FMQ) and MELTS-predicted SC1 [Toplis & Carroll, 1995 (TC, 1995)] liquid line of descent of major elements as a function of temperature.

Downloaded from petrology.oxfordjournals.org at Bibliotheque Fac de Medecine on January 12, 2011

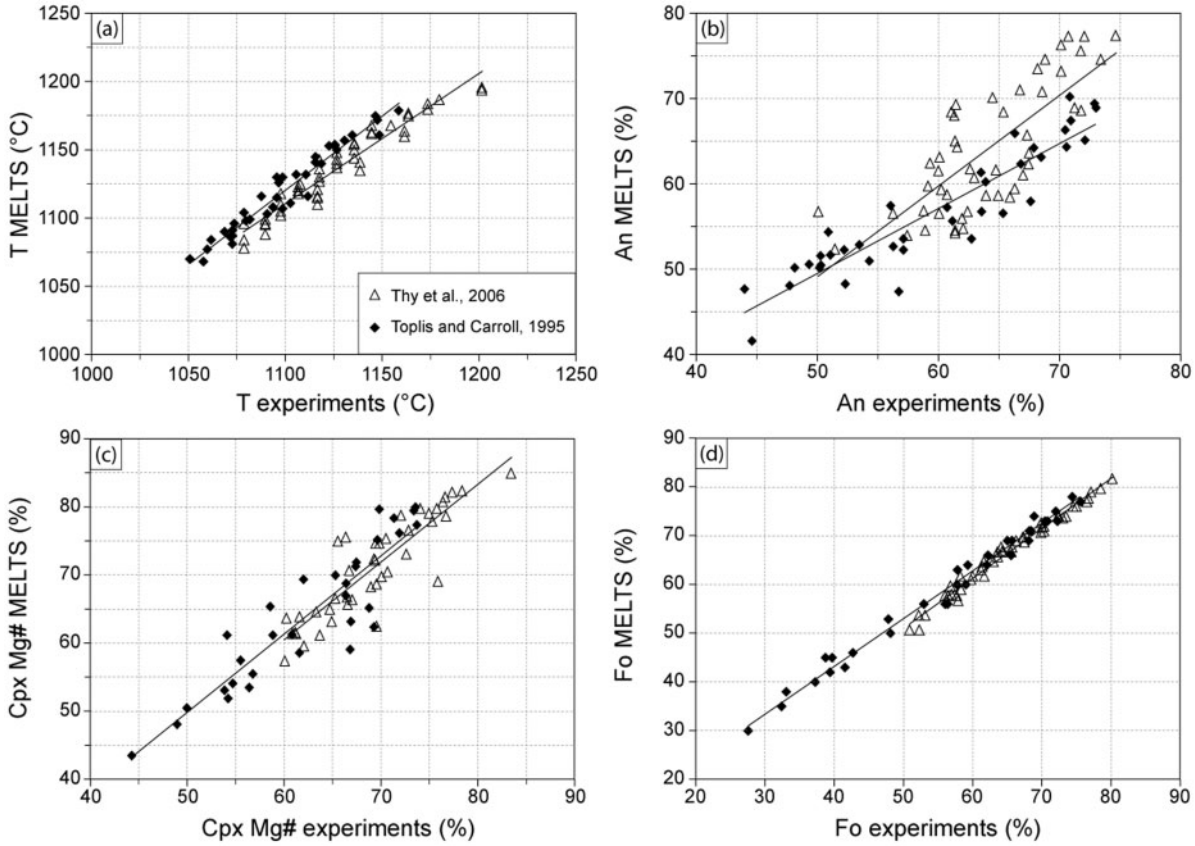

Fig. A3. Comparison between experimentally determined and MELTS predicted liquidus temperatures and mineral compositions for silicate minerals. (a) Liquidus temperatures. (b) Plagioclase compositions (anorthite content). (c) by Ca-rich pyroxene compositions (Mg-number) and replace the caption. (d) by Olivine compositions (Fo content).

Ti and Mn; forsterite for Mg. Counting times were 20 s on the peak and 10 s for the background. Raw data were corrected with the CATZAF software.

Modeling the liquid line of descent of the Layered Series

Calculations of mineral compositions crystallized by Sept Iles liquids were carried out using experimentally derived mineral–melt equilibria equations presented by Thy *et al.* (2006). These equations involve the temperature and the FeO/Fe_2O_3 ratio of the liquids. Temperatures used in Sept Iles calculations are liquidus temperatures predicted by MELTS (Ghiorso & Sack, 1995); FeO/Fe_2O_3 ratios were calculated from the equations of Kress & Carmichael (1991) for fO_2 conditions of FMQ − 1 and FMQ

Downloaded from petrology.oxfordjournals.org at Bibliotheque Fac de Medecine on January 12, 2011